Surface Circulation in Dixon Entrance Results from Lagrangian and Eulerian Measurements

by
Paul Greisman
Dobrocky Seatech Ltd.
Sidney, B.C. V8L 4M7

Published by
Institute of Ocean Sciences
P.O. Box 6000
Sidney, B.C. V8L 4B2

1986

Canadian Contractor Report of Hydrography and Ocean Sciences No. 23

Fisheries and Oceans Pêches et Océans

Canada

Canadian Contractor Report of Hydrography and Ocean Sciences

Contractor reports are unedited final reports from scientific and technical projects contracted by the Ocean Science and Surveys (OSS) sector of the Department of Fisheries and Oceans.

The contents of the reports are the responsibility of the contractor and do not necessarily reflect the official policies of the Department of Fisheries and Oceans.

If warranted, contractor reports may be rewritten for other publications of the Department, or for publication outside the government.

Contractor reports are abstracted in *Aquatic Sciences and Fisheries Abstracts* and indexed in the Department's annual index to scientific and technical publications.

Contractor reports are produced regionally but are numbered nationally. Requests for individual reports will be filled by the issuing establishment listed on the front cover and title page. Out of stock reports will be supplied for a fee by commercial agents.

Regional and headquarters establishments of Ocean Science and Surveys ceased publication of their various report series as of December 1981. A complete listing of these publications is published in the *Canadian Journal of Fisheries and Aquatic Sciences*, Volume 39: Index to Publications 1982. The current series, which begins with report number 1, was initiated in January 1982.

Rapport canadien des entrepreneurs sur l'hydrographie et les sciences océaniques

Cette série se compose des rapports finals non révisés préparés dans le cadre des projets scientifiques et techniques réalisés par des entrepreneurs travaillant pour le service des Sciences et levés océaniques (SLO) du ministère des Pêches et des Océans.

Le contenu des rapports traduit les opinions de l'entrepreneur et ne reflète pas nécessairement la politique officielle du ministère des Pêches et des Océans.

Le cas échéant, certains rapports peuvent être rédigés à nouveau de façon à être publiés dans une autre série du Ministère, ou à l'extérieur du gouvernement.

Les rapports des entrepreneurs sont résumés dans la publication *Résumés des sciences halieutiques et aquatiques* et ils sont classés dans l'index annuel des publications scientifiques et techniques du Ministère.

Les rapports des entrepreneurs sont produits à l'échelon régional, mais numérotés à l'échelon national. Les demandes de rapports seront satisfaites par l'établissement auteur dont le nom figure sur la couverture et la page du titre. Les rapports épuisés seront fournis contre rétribution par des agents commerciaux.

Les établissements des Sciences et levés océaniques dans les régions et à l'administration centrale ont cessé de publier leurs diverses séries de rapports en décembre 1981. Une liste complète de ces publications figure dans le volume 39, Index des publications 1982 du *Journal canadien des sciences halieutiques et aquatiques*. La série actuelle a commencé avec la publication du rapport numéro 1 en janvier 1982.

Canadian Contractor Report of
Hydrography and Ocean Sciences No. 23

1986

SURFACE CIRCULATION IN DIXON ENTRANCE

Results from Lagrangian and Eulerian Measurements

by

Paul Greisman
Dobrocky Seatech Ltd.
Sidney, B.C. V8L 4M7

Published by

Institute of Ocean Sciences
P.O. Box 6000
Sidney, B.C. V8L 4B2

Prepared Under Contract 08SB.FP941-3-1273
for the Institute of Ocean Sciences.

Cat. No. Fs 97-17/23E ISSN 0711-6748

Correct citation for this publication:

Greisman, P. 1986. Surface Circulation in Dixon Entrance: Results from Lagrangian and Eulerian Measurements. Can. Contract Rep. Hydrogr. Ocean Sci. 23: x + 112 p.

ABSTRACT

Greisman, P. 1986. Surface Circulation in Dixon Entrance: Results from Lagrangian and Eulerian Measurements. Can. Contract. Rep. Hydrogr. Ocean Sci. 23: x + 112 p.

Drifting buoys with on-board LORAN-C navigator's and radios coupled with "holey sock" drogues were developed and used to determine the near-surface circulation in Dixon Entrance. These measurements along with data from moored current meters and a CTD survey are analysed and provide insight into the driving mechanisms in the region.

In addition to wind stress and runoff, tidal rectification appears to be important in determing the mean flow patterns. In particular, the cyclonic eddy north of Rose Spit and the anti-cyclonic flow around Learmonth Bank are driven by tidal rectifications.

Keywords: surface currents, Lagrangian measurements, Dixon Entrance, Tidal Rectification, LORAN-C buoys.

RÉSUMÉ

Greisman, P. 1986. Surface Circulation in Dixon Entrance: Results from Lagrangian and Eulerian Measurements. Can. Contract. Rep. Hydrogr. Ocean Sci. 23: x + 112 p.

On a mis au point et utilisé des bouées dérivantes, avec appareils de navigation Loran-C et radios, reliées à des drogues "holey sock" afin de déterminer la circulation près de la surface dans l'entrée Dixon. Les mesures obtenues et des données provenant de courantomètres amarrés et d'un relevé du MTC ont été analysées et fournissent un aperçu des mécanismes entraînant la circulation dans la région.

En plus de l'effect du vent et du ruissellement, la rectification par les marées semble importante pour la détermination des configurations moyennes de l'écoulement. En particulier le tourbillon cyclonique au nord de la flèche Rose et l'écoulement anti-cyclonique autour du banc de Learmonth sont entraînés par des rectifications par les marées.

Mots clés: courants de surface, mesures lagrangiennes, entrée Dixon, rectification par les marées, bouées Loran-C.

ACKNOWLEDGEMENTS

Bill Crawford was the scientific authority for the project. He provided great encouragement during its course and sympathetically shared the usual alternating triumphs and defeats. Without his trust the project would never have been undertaken.

The work reported here was performed over a period of two years and involved dozens of people. Those mentioned below are only some of them.

The design, construction and testing of the Loran-C buoys were accomplished with the aid of:

G. Antonovich, D. Gregson, P. Breen, J. Harrington, Canadian Coast Guard, Parksville and Campbell River and the Canadian Hydrographic Service.

The field measurements were made by the author, assisted by:

C. Olafson, D. Olafson, K. Miners, J. Harrington and G. Miskulin.

Data analysis was performed principally by A. Blaskovich and K. Lee.

TABLE OF CONTENTS

	Page
TITLE PAGE	ii
ABSTRACT	iii
ACKNOWLEDGEMENTS	iv
TABLE OF CONTENTS	v
LIST OF TABLES	vii
LIST OF FIGURES	viii
1.0 INTRODUCTION	1
1.1 Project History	1
1.2 Geographical Setting	2
1.3 Background Physical Oceanography	2
2.0 THE DATA	8
2.1 Eulerian Current Data	8
2.2 Lagrangian Current Data	8
2.3 CTD Data	14
2.4 Wind Data	14
3.0 RESULTS	16
3.1 Mean Flows	16
3.1.1 Lagrangian Circulation	16
3.1.2 Eulerian Circulation	19
3.1.3 Distribution of Variables	23
3.2 Tidal Oscillations	32
3.2.1 Lagrangian Measurements of Tidal Currents	32
3.2.2 Eulerian Measurements of Tidal Currents	32
3.2.3 Comparison of Eulerian & Lagrangian Tidal Analyses	33
3.2.4 Internal Tides	36

TABLE OF CONTENTS

(Continued)

	Page
4.0 DISCUSSION	39
4.1 Tidal Rectification	39
4.1.1 Theory	40
4.1.2 R and ϕ From Tidal Ellipses	44
4.1.3 Application to Dixon Entrance	46
4.2 Thermohaline Flow	47
4.3 Wind-driven Flow	49
4.4 Analysis of the Components of Flow	50
5.0 CONCLUSIONS	56
6.0 REFERENCES	57
APPENDIX 1: Cross Sections S, T, σ_t June 1984	59
APPENDIX 2: Tidal Stream Analyses, Drifters	89
APPENDIX 3: Tidal Stream Analyses, Current Meters	101

LIST OF TABLES

	Page
Table 1.1 - Summary of Crean's (1967) Findings	5
Table 2.1 - Specifics of the Eulerian Current Data Collected in Dixon Entrance 1983 - 1984	10
Table 3.1 - Comparison of 1-day Average Velocities Derived from Drift Tracks and From Near-surface Current Meters	22
Table 3.2 - Comparison of Tidal Oscillations Computed with Lagrangian and Eulerian Data	35
Table 3.3 - Height of Internal Tide Waves Computed from Temperature Time Series and Local Vertical Temperature Gradient	37
Table 4.1 - Rectified Flows Predicted by Theory	48

LIST OF FIGURES

	Page
Figure 1.1 - Location of Dixon entrance	3
Figure 1.2 - Bathymetry of Dixon entrance	4
Figure 2.1 - Mooring locations. Subsurface current meter moorings at all locations except D7s which is a surface anemometer	9
Figure 2.2 - Composite of four drifter trajectories in Western Dixon Entrance. The numbers along the tracks indicate hours after deployment	12
Figure 2.3 - Composite of seven drifter trajectories in Eastern Dixon Entrance. The numbers along the tracks indicate hours after deployment	13
Figure 2.4 - Locations of CTD stations	15
Figure 3.1 - Smoothed Drifter trajectories	17
Figure 3.2 - Daily realizations of the Eulerian flow field. Mean daily currents from instruments at 50 m depth are contoured	20
Figure 3.3 - Dynamic height topography 0/100 decibars	24
Figure 3.4 - Salinity field at 10 m depth in Dixon Entrance, June 1984	26
Figure 3.5 - Salinity field at 30 m depth in Dixon Entrance, June 1984	27
Figure 3.6 - Salinity field at 50 m depth in Dixon Entrance, June 1984	28
Figure 3.7 - Salinity field at 150 m depth in Dixon Entrance, June 1984	29

LIST OF FIGURES

(Continued)

	Page
Figure 3.8 - Average salinity in the upper 50 m of the water column. The region where the average salinity is less than 31.4 is shaded	30
Figure 3.9 - Average salinity in the upper 100 m of the water column. The region where the average salinity is less than 31.8 is shaded	31
Figure 3.10- M_2 tidal ellipse axes from instruments for the period 12-24 June 1984	34
Figure 4.1 - Schematic of the approximate contribution to the total near-surface flow due to tidal rectification (numbers indicate speeds in cm s^{-1})	51
Figure 4.2 - Schematic of the approximate contribution of freshwater discharge	52
Figure 4.3 - Schematic of the approximate contribution of moderate northwest wind stress	53
Figure 4.4 - The sum of the effects shown in Figures 4.1, 4.2 and 4.3: tidal rectification + freshwater discharge + wind stress	54

1.0 INTRODUCTION

1.1 PROJECT HISTORY

In August 1983 Dobrocky Seatech Ltd. was awarded a contract, as the result of an unsolicited proposal, to design and develop drifting buoys in order to describe the surface circulation in Dixon Entrance. Surface trajectories were to be measured concurrently with an intensive program of moored current measurements during the summer of 1984.

The drifters were to incorporate Loran-C navigators to determine their positions and a VHF radio link to telemeter the position every half hour to a vessel in attendance up to 100 km distant.

Design of the buoys began immediately and initial testing began in winter 1983/84. From the outset we viewed our major technical problem as achieving the 100 km range of transmission by VHF. The range of reliable transmission was successfully demonstrated in the spring of 1984 when tests between Parksville and Campbell River, B.C. were performed.

Parallel with the development of the buoy, hydrodynamic drag and stability studies were performed for various buoy hull configurations and for various drogue designs. A flat elliptical hull was chosen and a "holey sock" drogue configuration adopted.

In June 1984 drift trajectory data as well as conductivity-temperature-depth profile data were collected in Dixon Entrance utilising the seiner M/V Ocean Island.

Details of the design of the Loran-C drifter and of the field program can be found in the data report (Greisman, 1985).

1.2 GEOGRAPHICAL SETTING

Dixon Entrance is located between the Queen Charlotte Islands and Southeast Alaska between 54° 00' N and 54° 40' N (Figure 1.1). On the west, Dixon Entrance is in free communication with the Pacific Ocean. On the east, Hecate Strait forms a southern approach while Clarence Strait extends to the north. Hecate Strait opens to the Pacific through Queen Charlotte Sound but Clarence Strait is virtually clossed off at its northern end.

The freedom with which the waters communicate among regions is greatly affected by the bottom topography. Figure 1.2 shows the bathymetry of Dixon Entrance. The remarkable change in depth between northern Hecate Strait (generally less than 50 m) and Dixon Entrance (up to 400 m deep) is immediately apparent. Learmonth Bank, which is situated at the western end of Dixon Entrance, rises from about 400 m depth to within 35 m of the surface. Very steep bottom slopes are present north of Langara Island and near both shores of Clarence Strait.

The very important influence of bottom topography, particularly the slope, on the circulation in Dixon Entrance is explained in Section 4.

1.3 BACKGROUND PHYSICAL OCEANOGRAPHY

The oceanography of Dixon Entrance was thoroughly reviewed by Crean (1967). At the time of that writing (and, in fact, until 1984) no long time series of direct current measurements were available from the region. Crean's discussion was based upon measurements of water properties, the wind field and runoff. In addition he used the results of a physical model constructed at the Pacific Biological Station, Nanaimo, (Bell and Boston, 1962, 1963; Bell, 1963) to draw comparisons between inferred and modelled circulation. A summary of Crean's conclusion is presented in Table 1.1.

The overall impression given of the Dixon Entrance system is of dramatic seasonal variability. Between about September and March strong southeast winds drive a northward flow through Hecate Strait, into Clarence Strait

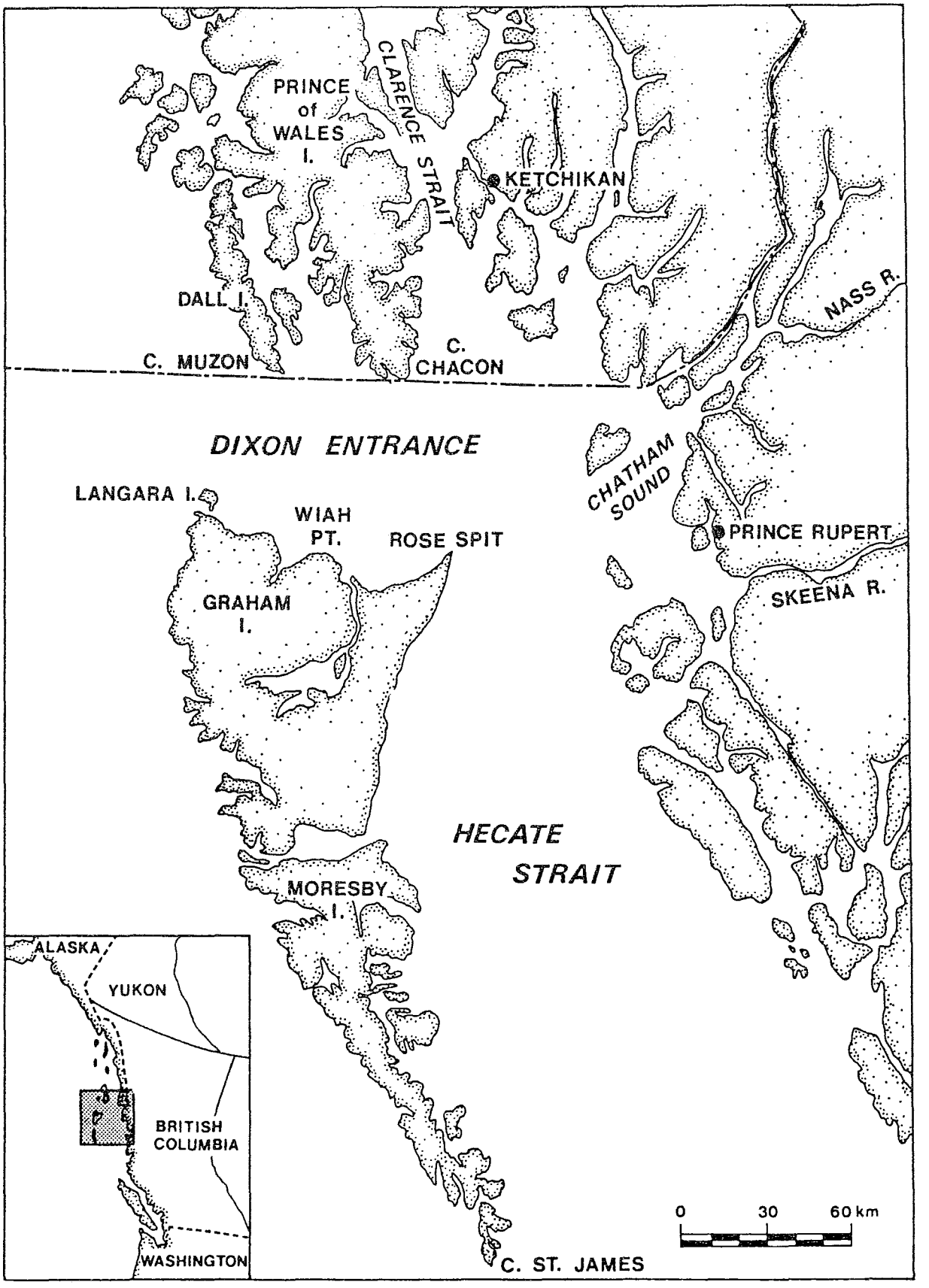

Figure 1.1 Location of Dixon entrance

DOBROCKY SEATECH

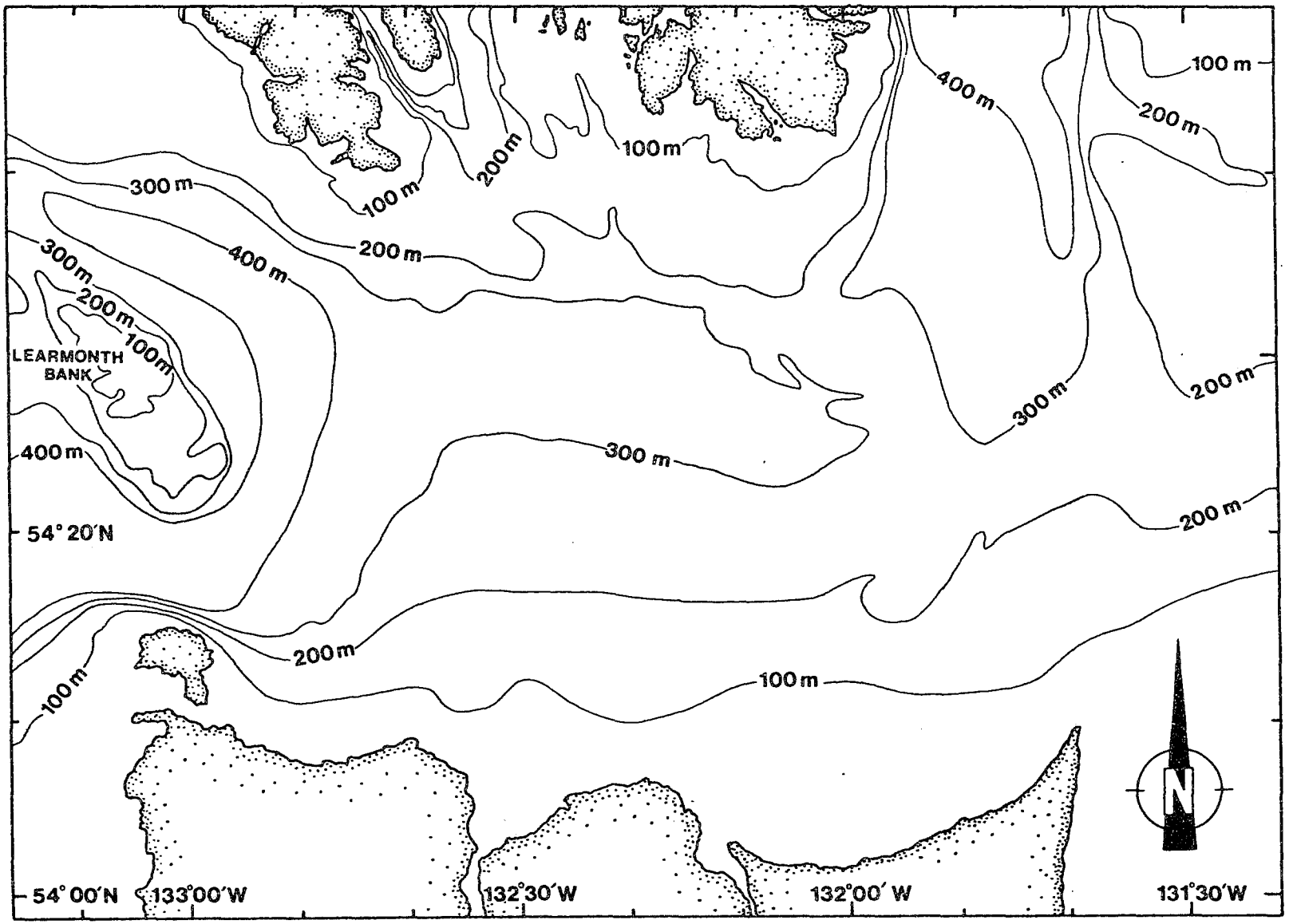

Figure 1.2 Bathymetry of Dixon entrance

Table 1.1 Summary of Crean's (1967) Findings

	Atmospheric Forcing			
Season	Winds	Ekman Transport	River Discharge	Resulting Flows
Spring (Apr. - May)	decreasing from SE	beginning of relaxation of onshore convergence	increasing rapidly	Net northward flow through Hecate Strait is reduced, most of it continues northward through Clarence Strait. Net cyclonic circulation dominates Dixon Entrance.
Summer (June - Aug.)		complete relaxation of onshore convergence		
(a) early summer	influence of SE winds minimal		peak discharge (snow melt)	Net northward flow through Hecate Strait negligible. Early summer: major flushing of brackish water and a strong intrusion of cold, saline oceanic water at depth.
(b) late summer	some W winds		minimum discharge	Late summer: seaward flow of fresh water decreases, and is confined to Clarence Strait and northern shores and west-central part of Dixon Entrance, cyclonic circulation extends to seaward approaches
Autumn (Sept-Oct.)	marked increase in SE winds	beginning of a general onshore convergence of surface waters	secondary maximum (local precipitation) generally confined to Clarence Strait	Northward flow through Hecate Strait increases. The net tidal cyclonic circulation dominates the central part of Dixon Entrance. The seaward flushing of brackish water is weak.

Table 1.1 (continued)

Season	Atmospheric Forcing: Winds	Ekman Transport	River Discharge	Resulting Flows
Winter (Nov.-March)				
(a) early winter	maximum SE winds	a marked onshore flow of oceanic surface water	relatively small	A well developed northward flow through Hecate and Clarence Straits enhanced by direct wind forcing. A marked movement of water seaward through Dixon Entrance, then northward along the SE Alaskan Coast.
(b) late winter	SE winds begin to decrease	intensity of onshore convergence diminishes	small discharge	In Dixon Entrance a basically conservative situation obtains, dominated by the net cyclonic circulation. The seaward flushing of brackish water is weak.

and westward through Dixon Entrance. During the late spring and summer, on the other hand, southeast winds weaken and fresh water discharge and tidal flows dominate the region. The peak river discharge occurs during June and July causing a major flushing of brackish water through Dixon Entrance. In late summer (August, early September) the circulation is dominated by a "net tidal cyclonic" eddy in the central part of Dixon Entrance.

Crean's work served as a background for the investigations undertaken in 1984. Quantification of the circulation described by Crean as well as a dynamical description was sought. In particular, direct measurements of the circulation using both Lagrangian and Eulerian techniques were undertaken in order to explain the presence of the apparently permanent eddy in Dixon Entrance.

2.0 THE DATA

The data set used in the present report is comprised of four subsets:

- moored current meter data
- drifting buoy data
- CTD data
- wind data

2.1 EULERIAN CURRENT DATA (MOORED CURRENT METERS)

Aanderra current meters were deployed in Dixon Entrance during April 1984 by the Institute of Ocean Sciences. The instruments were recovered during October 1984. Figure 2.1 shows the locations of the successfully recovered moorings and Table 2.1 displays the mooring specifics.

Data processing and tidal stream analyses were performed by K. Lee of the Tides and Currents group of IOS and by A. Blaskovich of Dobrocky Seatech Ltd. In general, only current data from meters within 50 m of the surface are used here.

2.2 LAGRANGIAN CURRENT DATA (DRIFTING BUOY TRAJECTORIES)

During June 1984 the trajectories of drifting buoys with on-board Loran-C and VHF radios were measured in Dixon Entrance. The buoys were drogued at 10 m depth with "holey socks" 5 m long.

The position data were edited to eliminate Loran-C lane "skip" and plotted. The buoy trajectories are presented in Figures 2.2 and 2.3. It is apparent from these figures that both tidal oscillations and substantial mean flows were resolved.

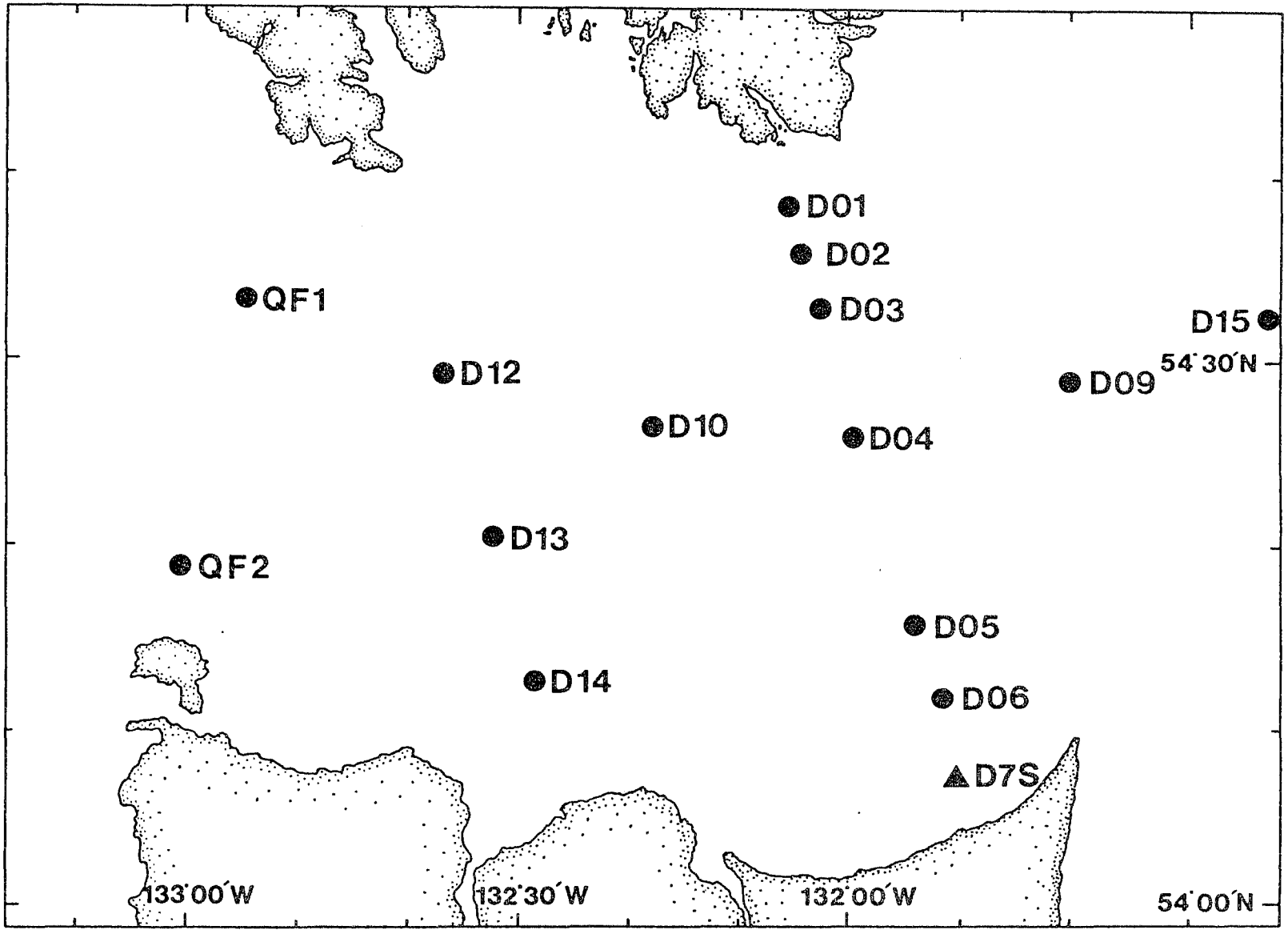

Figure 2.1 Mooring locations. Subsurface current meter moorings at all locations except D7s which is a surface anemometer.

Table 2.1 Specifics of the Eulerian Current Data Collected by IOS in Dixon Entrance - 1984.

Mooring	Location Latitude	Location Longitude	Water Depth	Instrument Depth	Dates of Measurement
QF1	54°33.8'	132°55.0'	383	57	21 Apr 84 - 15 Oct 84
				156	21 Apr 84 - 15 Oct 84
				307	21 Apr 84 - 15 Oct 84
				357	21 Apr 84 - 15 Oct 84
QF2	54°19.3'	133°02.2'	475	70	21 Apr 84 - 15 Oct 84
				170	21 Apr 84 - 15 Oct 84
				320	21 Apr 84 - 15 Oct 84
				420	21 Apr 84 - 15 Oct 84
D01	54°38.4'	132°05.7'	135	18	16 Apr 84 - 23 Aug 84
				48	16 Apr 84 - 20 Aug 84
				98	16 Apr 84 - 19 Aug 84
D02	54°35.2'	132°07.8'	169	146	16 Apr 84 - 29 Aug 84
D03	54°32.8'	132°03.9'	295	150	18 Apr 84 - 18 Sep 84
D04	54°26.7'	132°00.5'	294	52	18 Apr 84 - 20 Oct 84
				152	18 Apr 84 - 20 Oct 84
				279	21 Apr 84 - 20 Oct 84
D05	54°16.3'	131°55.0'	208	50	18 Apr 84 - 20 Oct 84
				150	18 Apr 84 - 20 Oct 84
D06	54°12.1'	131°57.0'	118	53	19 Apr 84 - 20 Oct 84
				103	19 Apr 84 - 20 Oct 84
D09	54°29.0'	131°40.2'	305	152	16 Apr 84 - 21 Oct 84
D10	54°27.0'	132°17.0'	356	50	18 Apr 84 - 19 Oct 84

Table 2.1 (Continued)

Mooring	Location Latitude	Location Longitude	Water Depth	Instrument Depth	Dates of Measurement
D11	54°36.6'	132°41.6'	136	50	18 Apr 84 - 22 Apr 84
				100	18 Apr 84 - 22 Apr 84
D12	54°29.4'	132°38.1'	371	150	18 Apr 84 - 11 Oct 84
				356	18 Apr 84 - 11 Oct 84
D13	54°21.9'	132°34.6'	263	45	18 Apr 84 - 19 Oct 84
				145	18 Apr 84 - 19 Oct 84
D14	54°13.0'	132°30.0'	124	59	21 Apr 84 - 19 Oct 84
				109	21 Apr 84 - 19 Oct 84
D15	54°33.1'	131°21.3'	110	22	16 Apr 84 - 21 Oct 84
				52	16 Apr 84 - 29 Jul 84

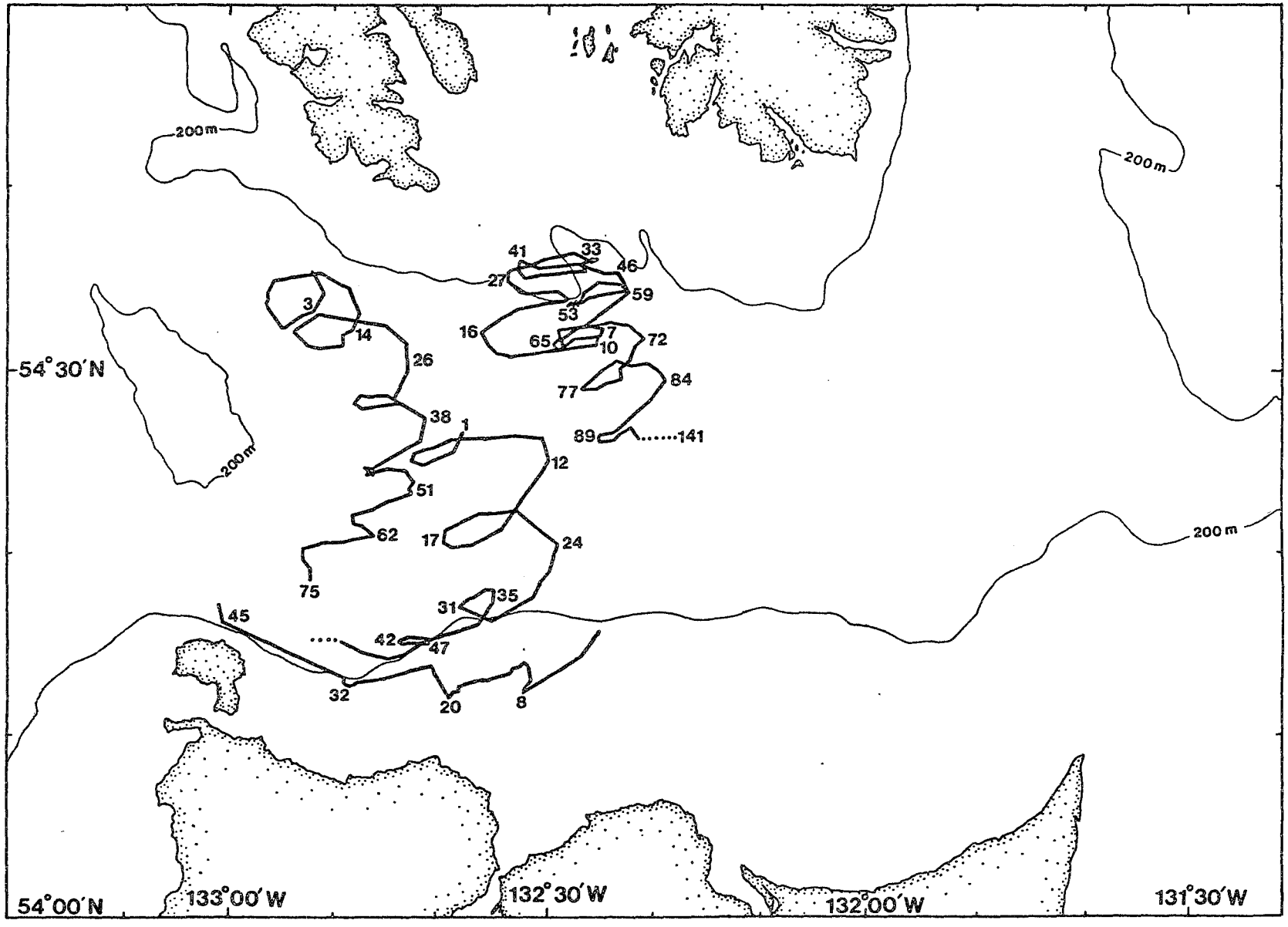

Figure 2.2 Composite of four drifter trajectories in Western Dixon Entrance. The numbers along the tracks indicate hours after deployment.

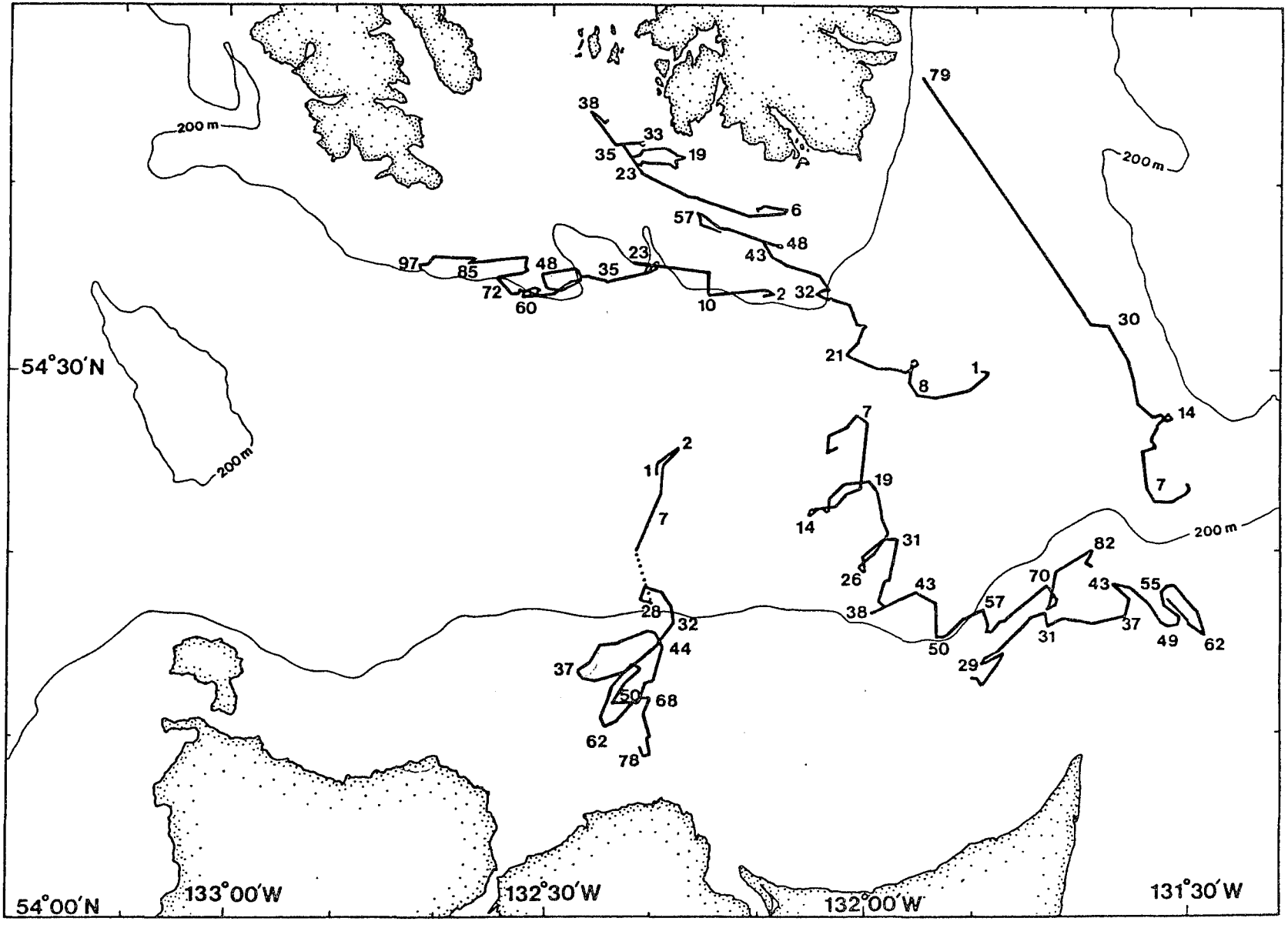

Figure 2.3 Composite of seven drifter trajectories in Eastern Dixon Entrance. The numbers along the tracks indicate hours after deployment.

The position data were differentiated to produce time series of velocities. These time series were then smoothed to eliminate spuriously high velocities (generally due to overlooked lane skips). For tidal stream analysis a cubic spline interpolation was applied to the time series to obtain hourly values of velocity. The computer programs of Foreman (1978) were utilised to obtain tidal ellipse parameters over the period of deployment for each drift track.

Individual drift tracks and tabulated positions are provided in the data report (Greisman, 1985).

2.3 CONDUCTIVITY-TEMPERATURE-DEPTH DATA

CTD data were collected in a non-synoptic fashion between 12 June and 23 June 1984. A Guildline Model 8706 probe was employed. The instrument was calibrated both at Aanderaa Instruments in Victoria and in situ in the field with salinity samples collected with a Niskin bottle. Our calibrations show that the temperatures measured are within $\pm$ .02° of the actual value and the salinities are within $\pm$ .05 parts per thousand. The reason for this rather poor accuracy was our in situ calibration performed in a water column in which vertical gradients were present throughout. Combined with the rolling of the vessel we could not be certain that our Niskin bottle and our CTD were sampling the same water parcel.

Figure 2.4 shows the location of the CTD stations occupied during June 1984. Individual CTD profile and listings are presented in the data report (Greisman, 1985).

2.4 WIND DATA

Wind data for the period of the buoy tracking were obtained from an IOS instrument mounted on a surface buoy (denoted D7S in Figure 2.1) just west of Rose Spit and from the Langara Island Light.

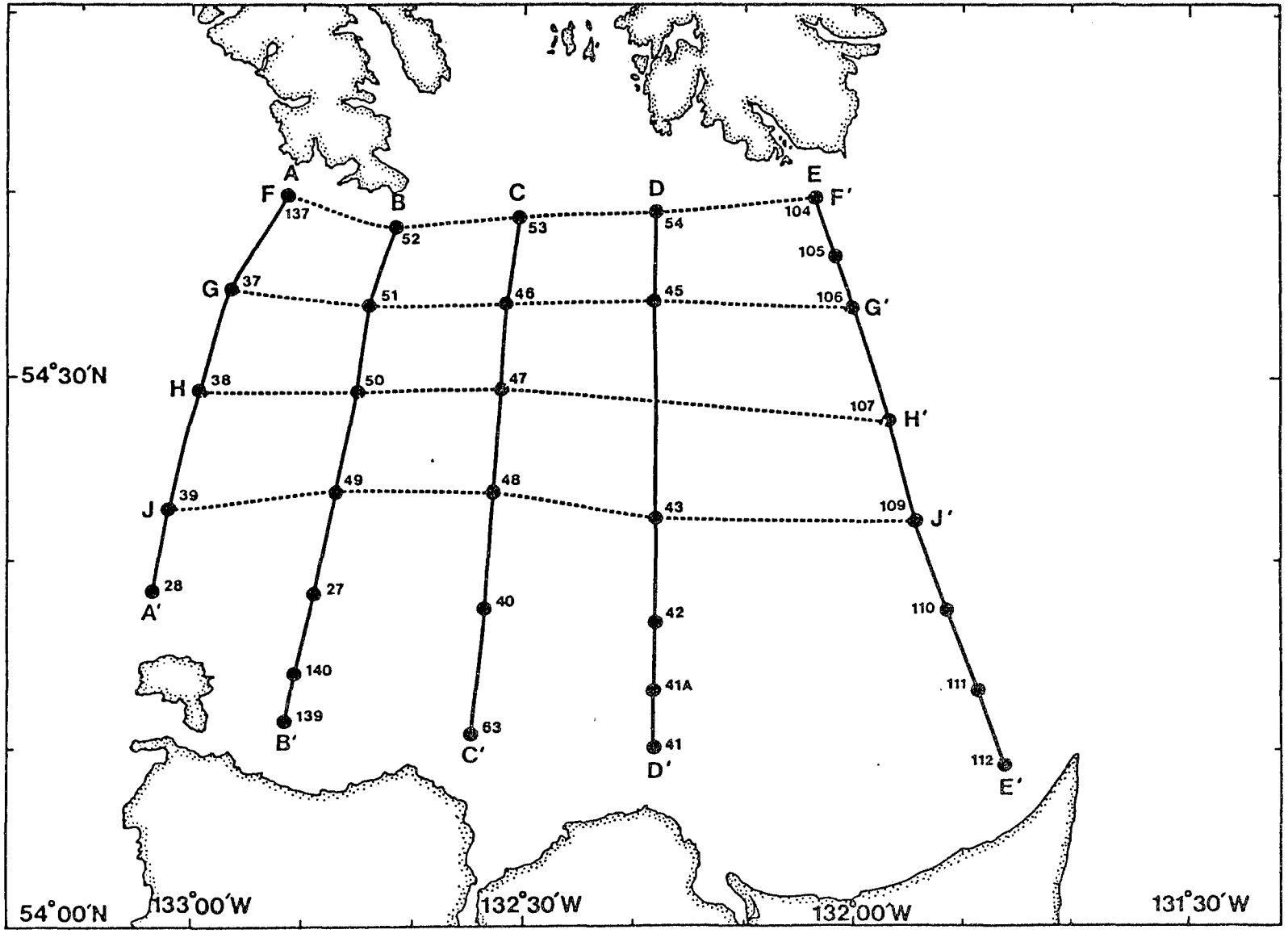

Figure 2.4 Locations of CTD stations

3.0 RESULTS

3.1 MEAN FLOWS

3.1.1 Lagrangian Circulation

With the tidal oscillations removed, the drifter trajectories immediately present a view of the surface circulation in Dixon Entrance during June 1984. Figure 3.1 shows the smoothed drifter trajectories. The deployment and recovery times of each drifter are shown. Each drift track is identified by a number within a diamond while a filled black circle denotes the position along the tracks where the southeast gale of 21 to 24 June began. The average speed of each drifter is indicated along the trajectories in km/d and cm/s.

In the western part of Dixon Entrance, tracks 1, 4 and 10 indicate an inflow at the north and an outflow at the south (just north of Langara Island). This flow can be either a manifestation of anticyclonic circulation around Learmonth Bank or of an eastward intrusion by a current flowing southward along the Alaskan coast. The southeast gale which began on 21 June appears to have had little effect on track 10.

The central part of Dixon Entrance is characterized by a slow southerly drift (tracks 2 and 3) toward Wiah Point. The mean flow in this area was so slow that we doubted the buoy positions sufficiently during the field work to relocate and fix them on three occasions from the survey vessel.

At the eastern end of Dixon Entrance, tracks 5 and 6 represent the southwestern sector of the cyclonic Rose Spit eddy described by Crean (1967). Tracks 11 and 12 presumably also would have traced the eddy in the absence of the southeast gale which began almost synchronously with their deployment.

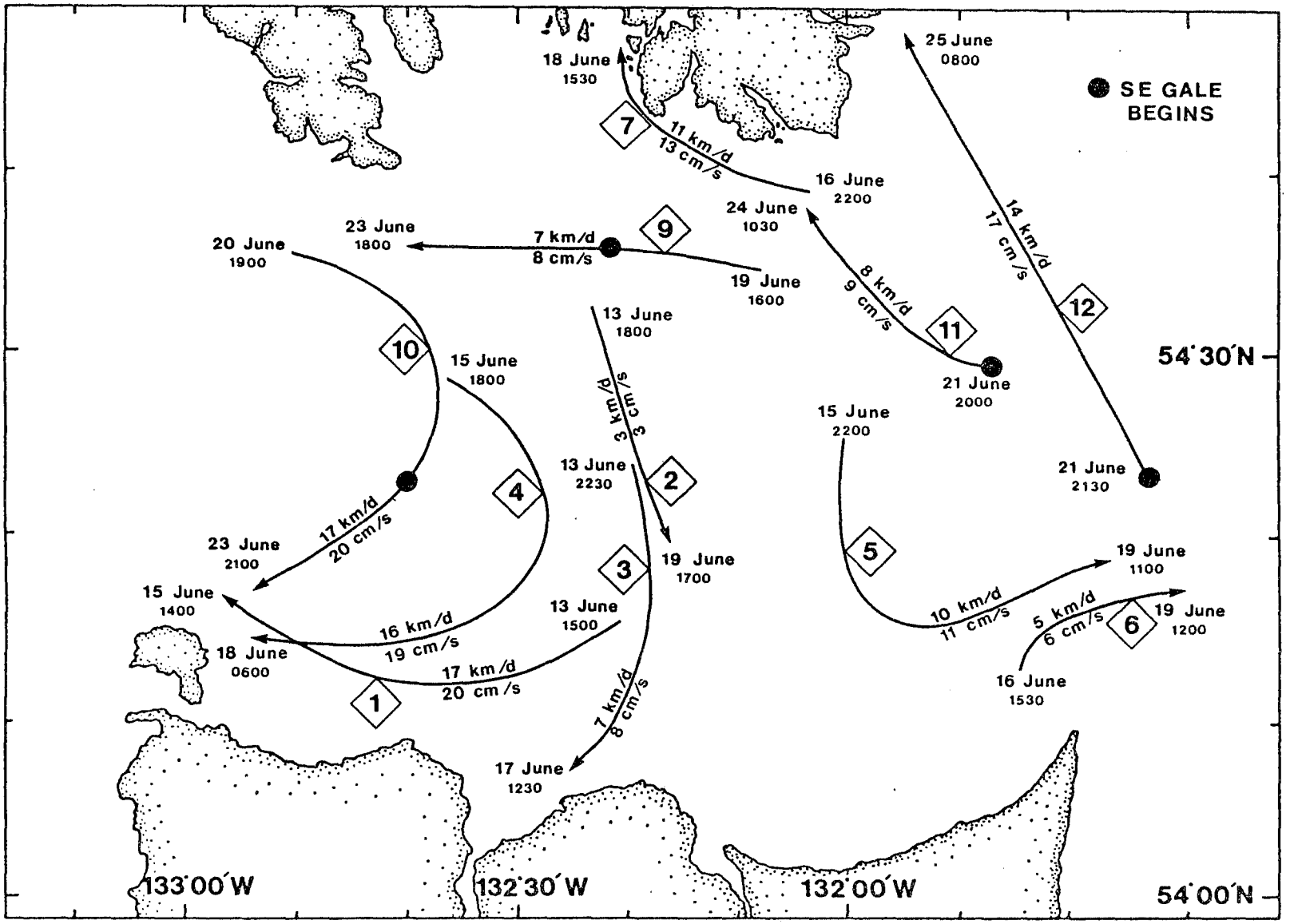

Figure 3.1 Smoothed Drifter trajectories

Track 7 closely parallels the isobaths. (This drifter was deployed in 100 m of water while the others were all deployed in depths greater than 200 m.) It slowly approached shore until it grounded on 18 June. Such shoreward motion was absent in all the other drifts.

Track 9, perhaps, most clearly shows the effect of the gale on the mean circulation. On deployment, we supposed that the drifter would turn southward and move toward Wiah Point. The gale was of sufficient strength (about 35 knots) to counteract the 3 cm s^{-1} southward drift at 10 m depth.

Tracks 11 and 12 represent the trajectory of water parcels at about 10 m depth during a southeast gale. Although the position data are very sparse along these tracks, the total mean displacement is accurate. The effect of the southeast wind was transmitted to the drogue through the agency of the surface Ekman layer and the windage on the surface buoy. The computed purely wind-driven flow at 10 m depth was approximately 10 cm s^{-1} directed about 60° to the right of the measured trajectory. Of course, the effect of the Alaskan coast is to permit the establishment of a pressure gradient which will, to some degree, balance the Ekman flow. One can only estimate that the velocities which would have been measured in the absence of the southeast gale would have been directed more toward the west; in agreement with the sense of the cyclonic gyre.

The impression given by the trajectories is that of a cyclonic gyre centred north of Rose Spit and an anticyclonic circulation at the western end of Dixon Entrance. In the central region the flow is weak and southward.

In the absence of southeast winds, a strong outflow between Langara Island and Learmonth Bank is present. Southeasterly winds appear to modify the flow of the Rose Spit gyre and, due to the setup along the Alaskan coast, cause a westerly flow along the northern shore of Dixon Entrance.

3.1.2 Eulerian Circulation

The picture of the circulation obtained with drifter trajectories (Lagrangian data) can be compared with average currents measured at the mooring locations (Eulerian data). Figure 3.2 shows the approximate isotachs for each day of the experiment (contours represent constant speed not streamlines). Individual mean current vectors were obtained from the low-passed filtered data ($A_{24}{}^2$ A_{25} filters of Godin). Average daily currents from instruments at depths less than about 50 m were used. The major characteristics of the circulation are similar to those obtained with the drifters. The Eulerian data, however, provide a better view of the time dependence of the flow while sacrificing spatial detail.

At the beginning of the period, both the anticyclonic gyre around Learmonth Bank and the cyclonic Rose Spit gyre are well developed. Weak southerly flow dominates the central part of Dixon Entrance. The current meter moored just off Cape Chacon indicates a strong westerly flow which may be interpreted as continuing along the Alaskan shore and exiting at Cape Muzon. However, the measurements lack the spatial resolution necessary to confirm this outflow.

The contouring of the Eulerian data is subjective and other interpretations are certainly possible. For example, the strong westward current south of Cape Chacon could be interpreted as veering southward in the central part of Dixon Entrance and contributing to an outflow north of Langara Island.

It should be recognized that both the Eulerian and Lagrangian measurements in mid-June 1984 indicate a southerly flow in central Dixon Entrance toward Wiah Point, and flows conforming to a two gyre system.

The daily average flows at each near-surface current meter which most closely correspond in time and space to drogue trajectories are compared in Table 3.1. In only one case do the Eulerian and Lagrangian directions differ by more than 45°; the Eulerian speeds tend to be slightly lower than the Lagrangian. There is no apparent consistent effect on direction due to an Ekman boundary layer. At the one location where a current meter was

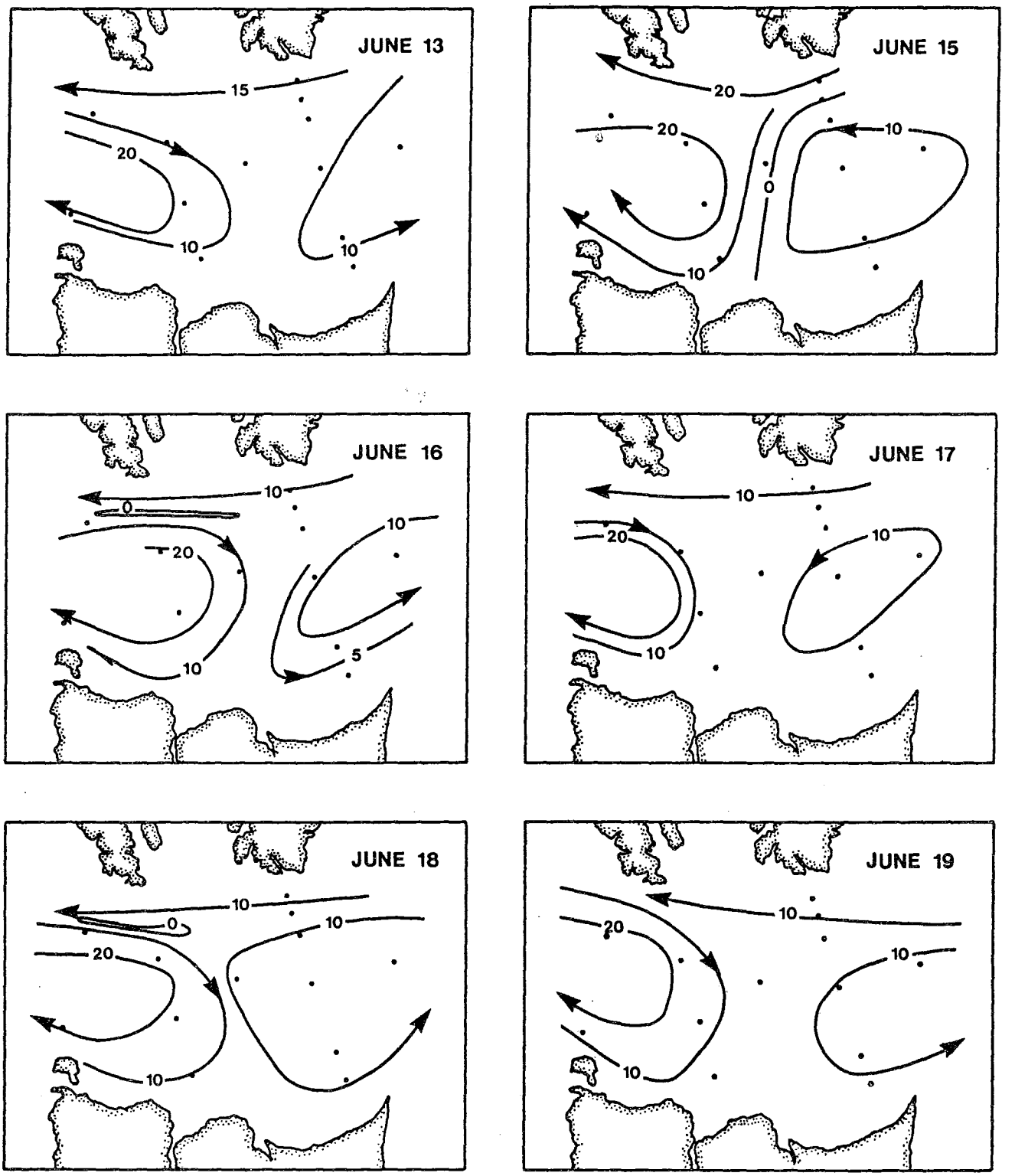

Figure 3.2 Daily realizations of the Eulerian flow field. Mean daily currents from instruments at 50 m depth are contoured in cm s^{-1}.

DOBROCKY SEATECH

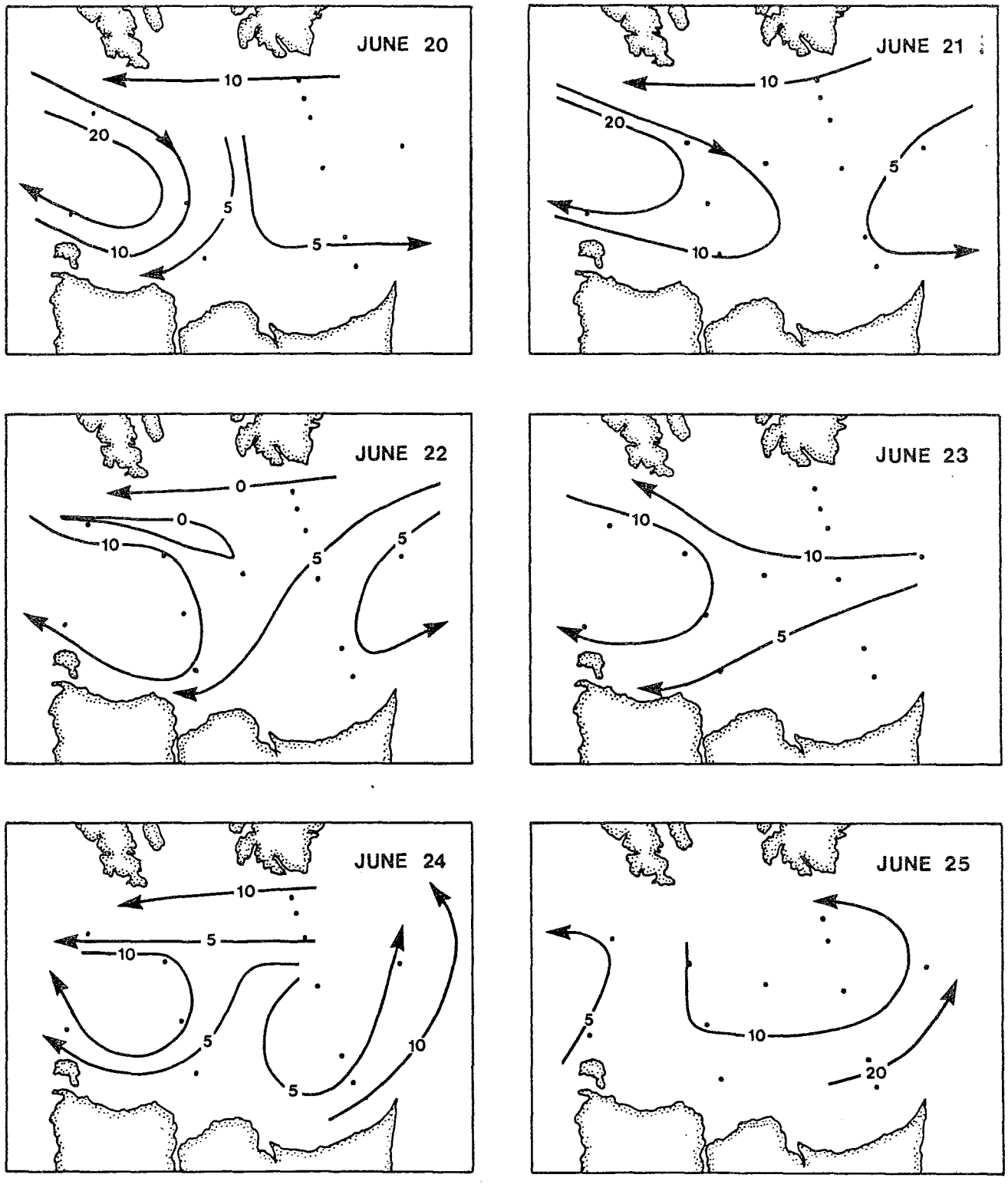

Figure 3.2 Daily realizations of the Eulerian flow field. Mean daily currents from instruments at 50 m depth are contoured in cm s^{-1} (Continued).

Table 3.1 Comparison of 1-day average velocities derived from drift tracks and from near-surface current meters

LAGRANGIAN				EULERIAN			
Date (June '84)	Drift Track No.	Speed cm s^{-1}	Direction °T	Mooring No.	Instrument Depth	Speed cm s^{-1}	Direction °T
21	10	13	135	QF1	57	9	125
15	1	31	295	QF2	70	7	309
17	7	24	285	DO1	18	25	278
16	5	17	185	DO4	52	5	230
18	5	18	065	DO5	50	6	143
18	6	18	065	DO6	53	11	086
13	3	17	185	D10	50	11	185
15	4	21	115	D12	150	18	117
16	4	19	200	D13	45	24	229
14	1	18	245	D14	59	16	218

moored 18 m below the surface (and thus, quite near the centre of effect of the holey sock drogue at about 10 m) there is excellent agreement between the two measurement techniques.

3.1.3 Distributions of Variables (Flows Inferred by Indirect Means)

The classical "dynamic method" is that most frequently used to infer oceanic flow fields from the fields of temperature, salinity and pressure. The method is so familiar that it will not be reviewed here. However, the many assumptions presupposed within the method must be borne in mind. In Dixon Entrance a major weakness of the method is the assumption of steady state included in the geostrophic approximation. The tidal flows in Dixon Entrance have both strong barotropic and baroclinic components (see Section 3.2). Local accelerations, therefore, cannot be neglected and CTD data at each station should be collected over a tidal cycle. Perhaps more importantly, the vertical excursion of isopycnal surfaces due to internal tides can be substantial and greatly affect the computations of dynamic height.

A CTD survey such as that conducted during this project which was neither synoptic nor tidally averaged will have severe shortcomings for geostrophic current computations. Only one dynamic height topography chart is presented here. Figure 3.3 shows the dynamic height of the surface relative to 100 decibars. A weak inflow on the northern shore off Cape Muzon appears to continue no farther east than Cape Chacon. A clear indication of the general westward flow crossing Dixon Entrance at about the longitude of Wiah Point and exiting north of Langara Island is present. Surface speeds relative to 100 m depth are computed to be about 30 cm s^{-1}. Despite their limitations therefore, the dynamic height data suggest a plausible circulation although it is different from that shown by the drifters and current metres. The dynamic height topography suggests a strong influence of freshwater outflow in the upper 100 m where the bulk of the flow enters Dixon Entrance on the northeast and exits on the southwest between Langara Island and Learmonth Bank.

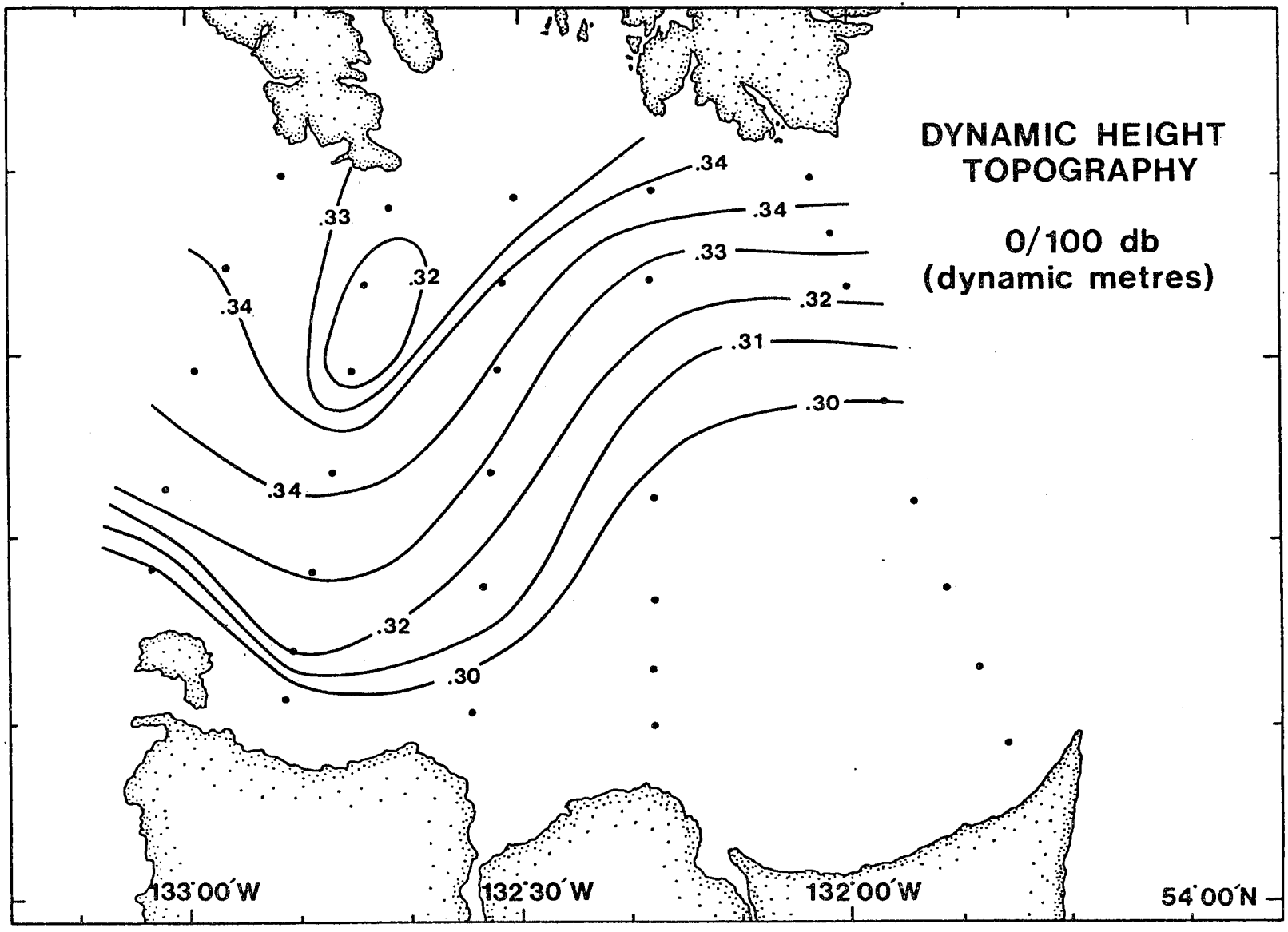

Figure 3.3 Dynamic height topography 0/100 decibars

Perhaps a more appropriate use of the CTD data is to seek the signature of the freshwater discharge from the Nass and Skeena Rivers which is generally at a maximum in June and July. (Cross sections of Temperture, Salinity and Sigma-t are presented in Appendix 1 to provide an overall impression of the CTD data.) The salinity field at 10, 30, 50 and 100 metres depth are shown in Figures 3.4 through 3.7. The main feature of the 10 m salinity field is the low values found in the northeast sector off Cape Chacon. The 30 m salinity field is confused but the continuous 31.6 isohaline which runs diagonally northeast to southwest is suggestive of a mean flow in that direction. The 50 m salinity field strengthens the impression of a flow from north to south across the Entrance and also indicates the cyclonic eddy off Rose Spit. The 150 m salinity field is of very different form. The impression of an intrusive flow penetrating from northwest far east into the entrance and exiting north of Langara Island can arise. The direction of this flow is based upon the fresher water (33.0) found at a central station and the presumably anticyclonic flow which could arise.

The salinity field, as viewed in individual horizontal sections, is ambiguous for the same basic reasons as is the field of dynamic heights: lack of synopticity and the presence of large internal oscillations. An extensive enough vertical average will effectively remove most of the spurious signal associated with internal tides. Figures 3.8 and 3.9 represent the average salinities in the upper 50 m and the upper 100 m of the water column respectively. In Figure 3.8 the region where the average layer salinity is less than 31.4 is shaded while in Figure 3.9 the region less than 31.8 is shaded. The relatively freshened regions in these figures indicate the routes by which the freshwater discharge traverses Dixon Entrance. There is a clear indication of the slightly freshened waters crossing Dixon Entrance from north to south. Outflow to the Pacific appears to be present at both the north and the south (off Cape Muzon and Langara Island) in the upper 50 m while the upper 100 m flow appears to exit between Langara Island and Learmonth Bank.

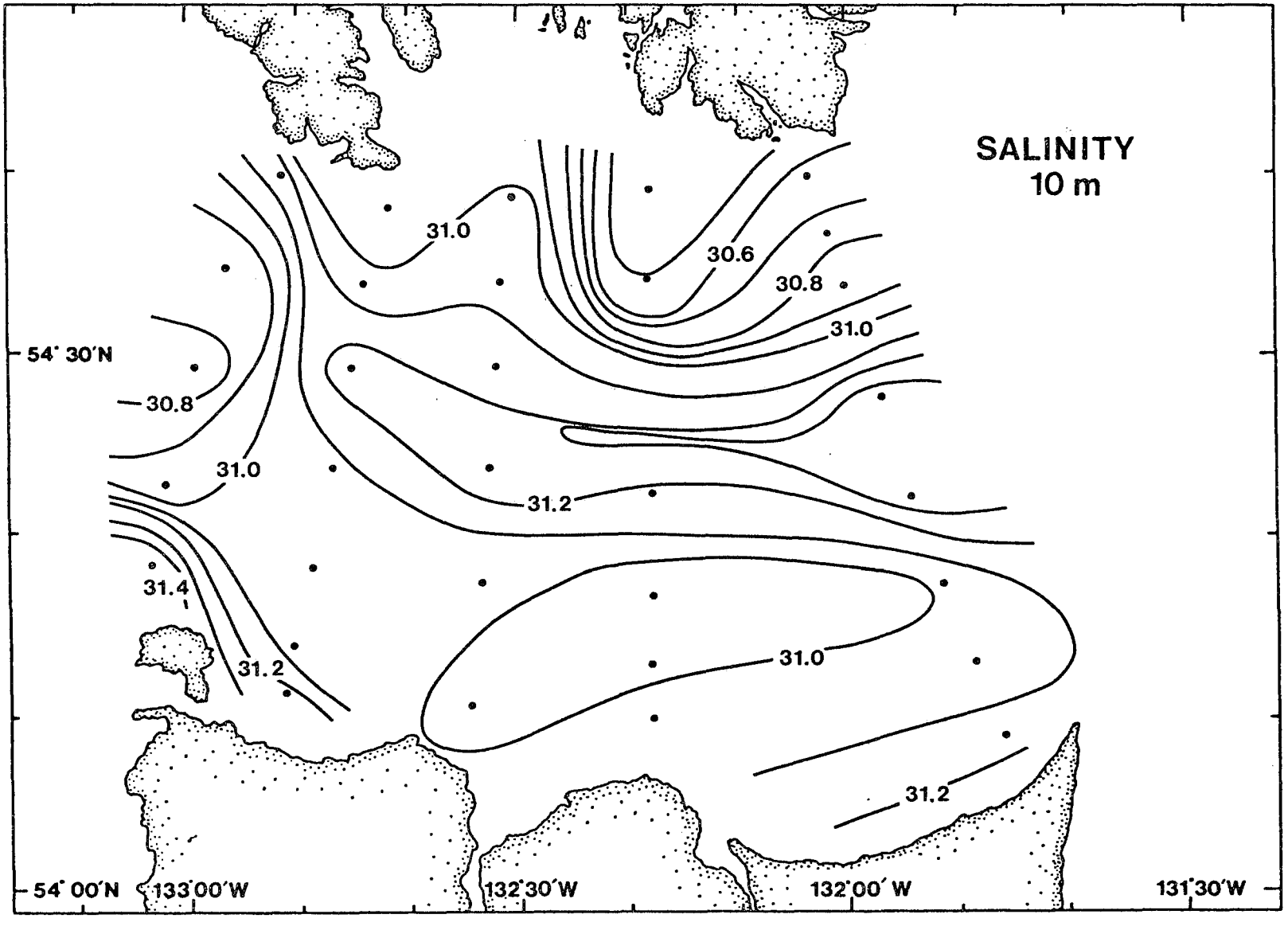

Figure 3.4 Salinity field at 10 m depth in Dixon Entrance, June 1984.

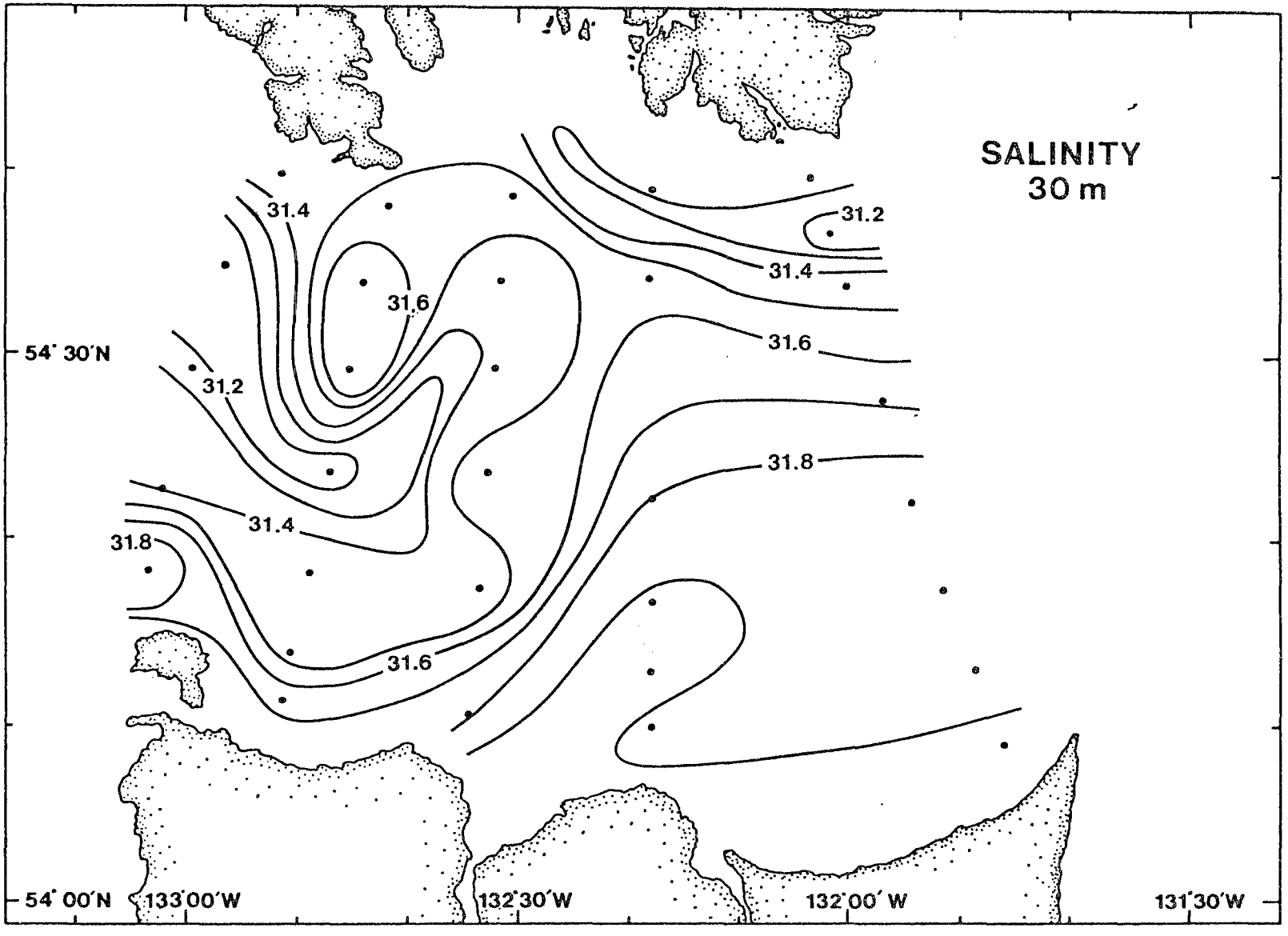

Figure 3.5 Salinity field at 30 m depth in Dixon Entrance, June 1984.

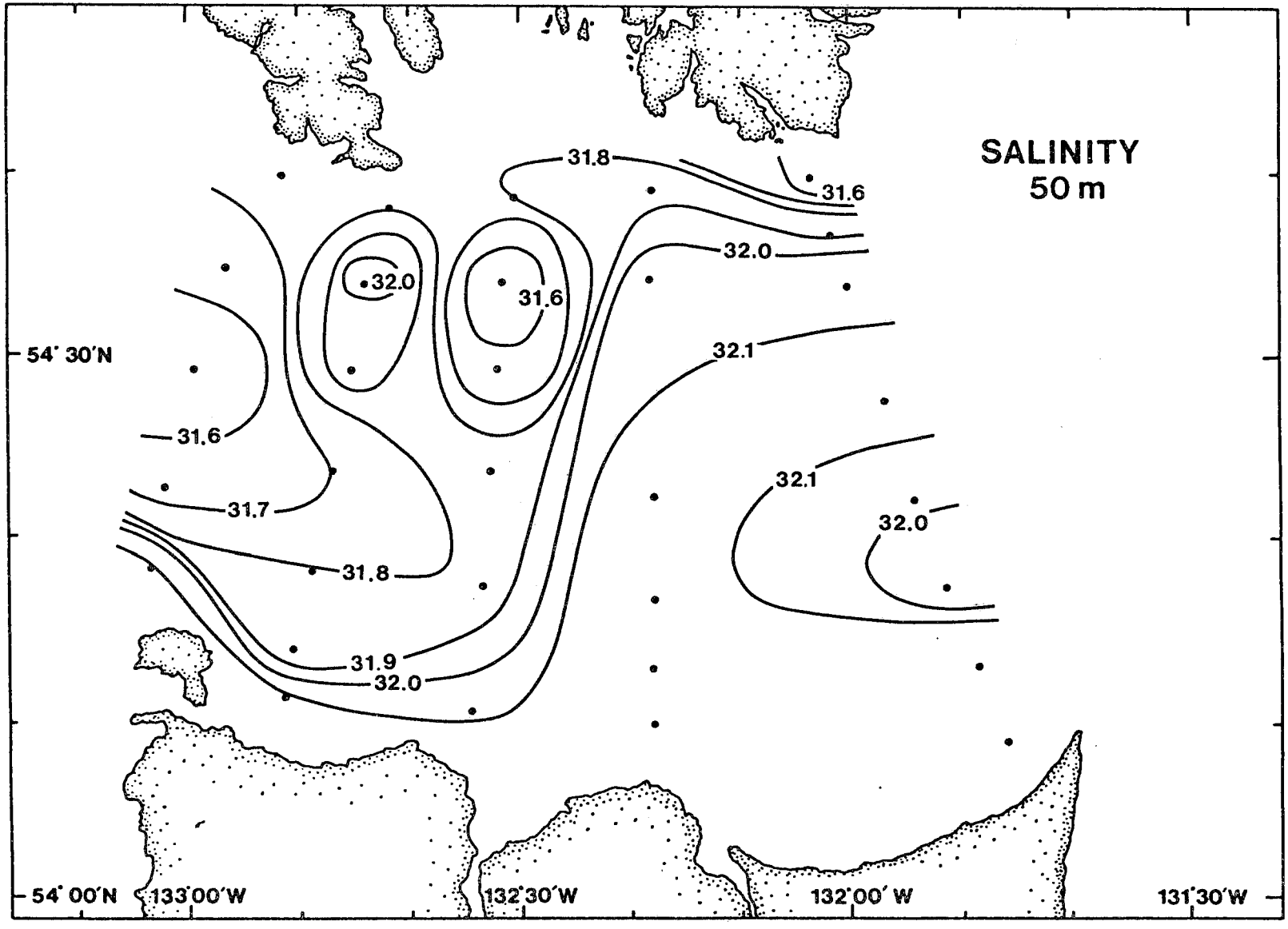

Figure 3.6 Salinity field at 50 m depth in Dixon Entrance, June 1984.

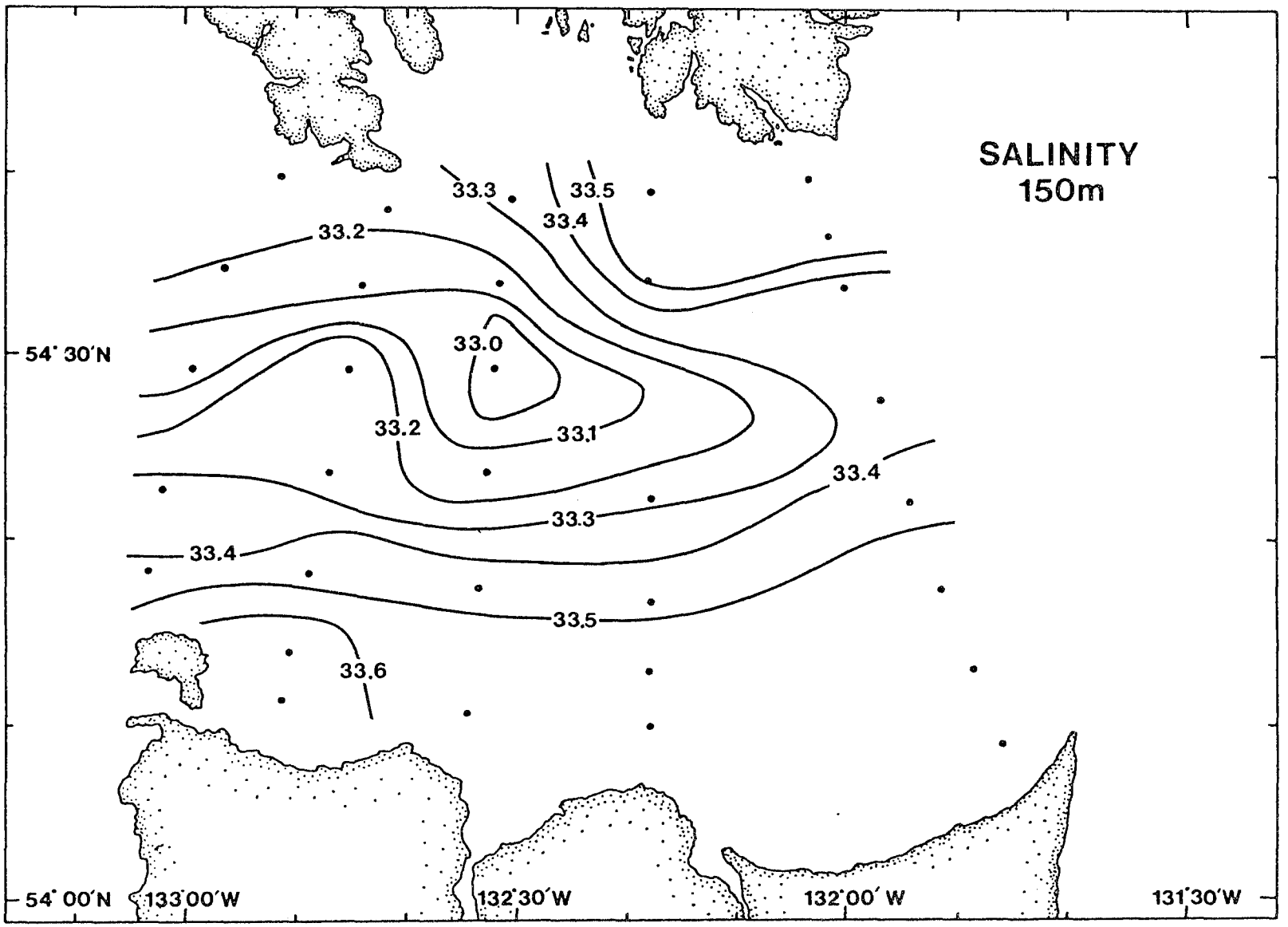

Figure 3.7 Salinity field at 150 m depth in Dixon Entrance, June 1984.

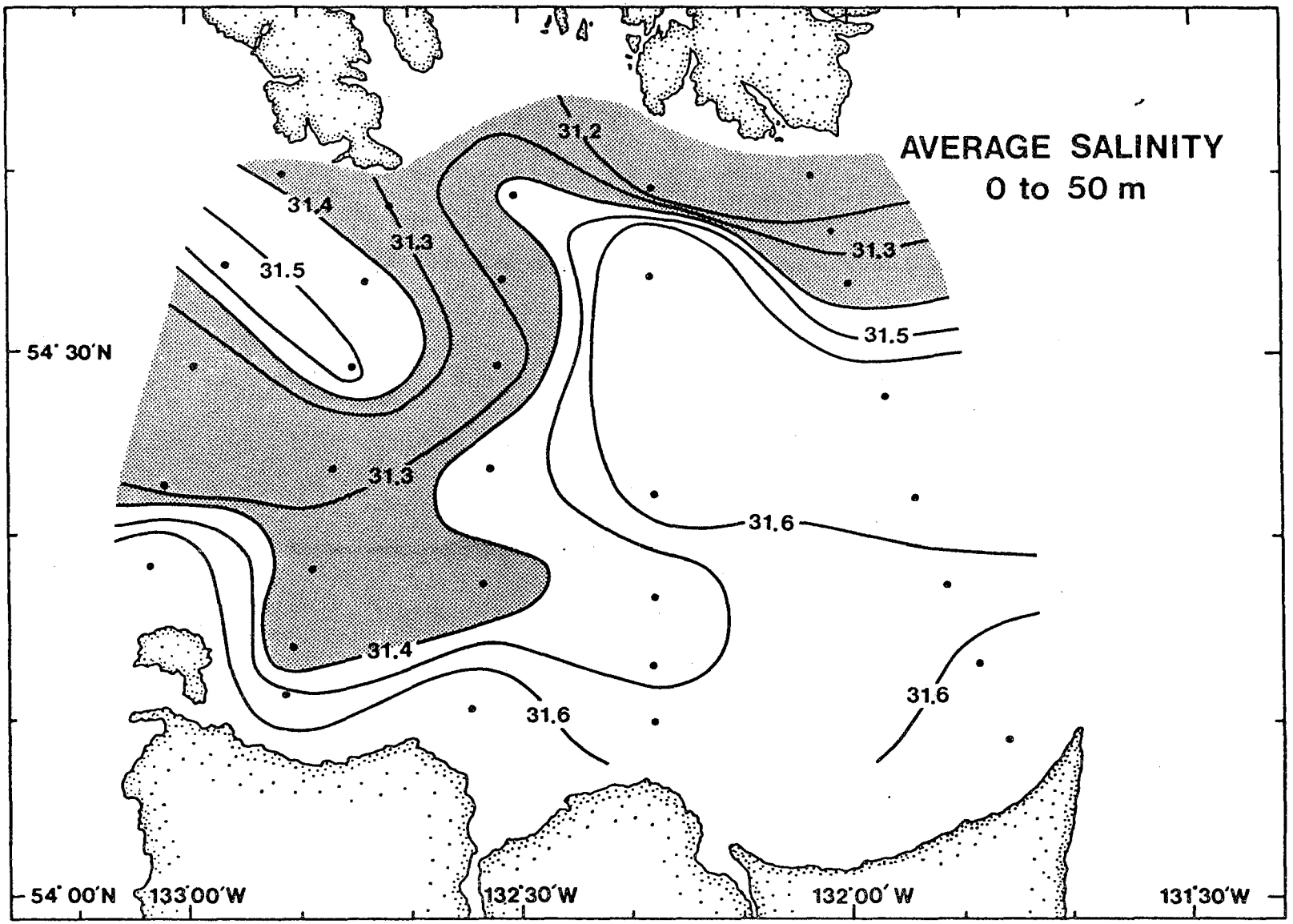

Figure 3.8 Average salinity in the upper 50 m of the water column. The region where the average salinity is less than 31.4 is shaded.

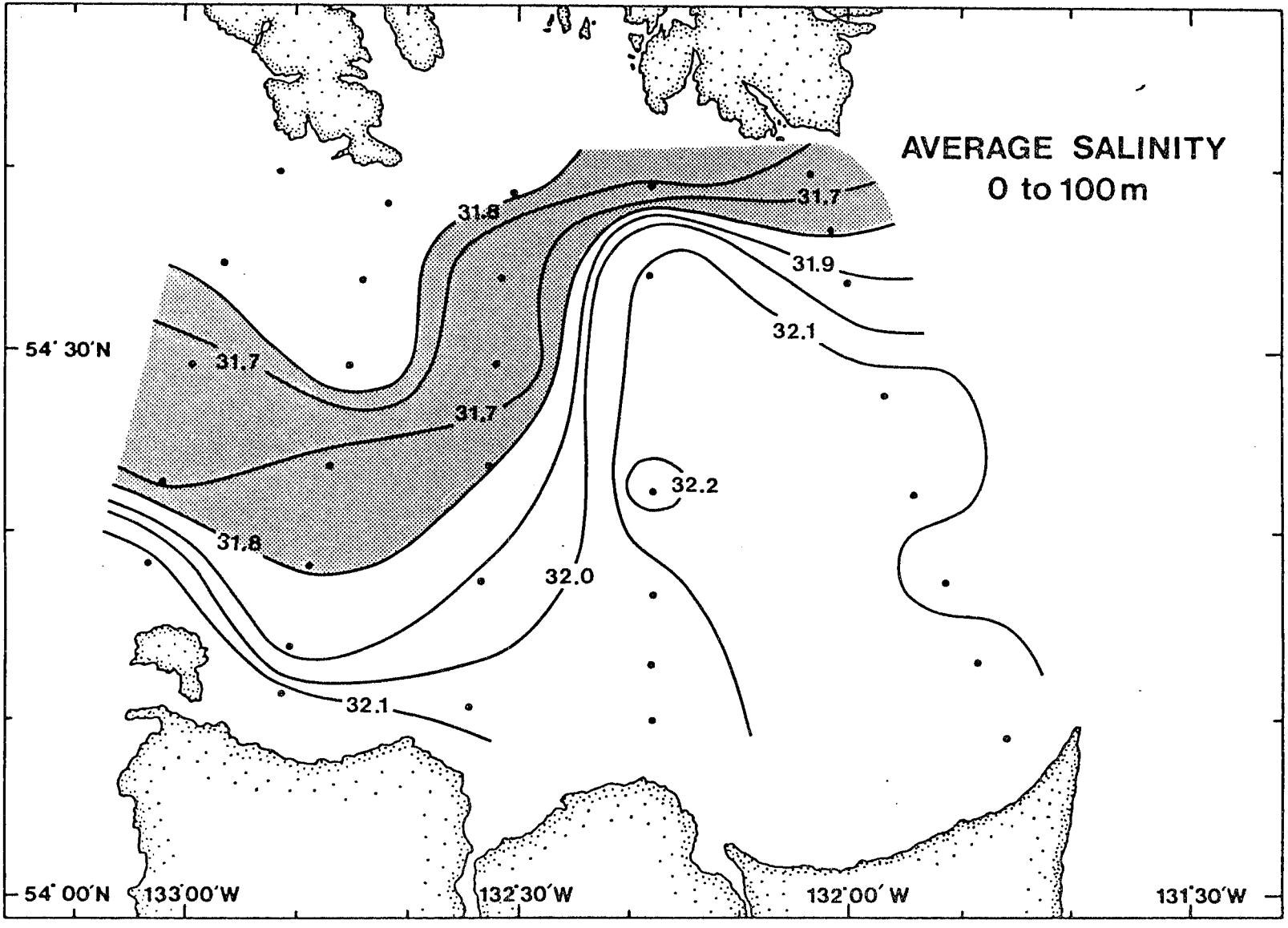

Figure 3.9 Average salinity in the upper 100 m of the water column. The region where the average salinity is less than 31.8 is shaded.

3.2 TIDAL OSCILLATIONS

It is well known that the tidal currents in Dixon Entrance can exceed 1 m s^{-1} and the tidal range can be in excess of 6 m. It is, therefore, not surprising that tidal oscillations dominate both the Lagrangian and Eulerian measurements and have a strong influence on the property distributions.

3.2.1 Lagrangian Measurements of Tidal Currents.

The drift tracks (Figure 2.2 and 2.3) are, quite dramatically, influenced by tidal oscillations. The trajectories, however, spatially average tidal oscillations over distances in which significant changes in the tidal regime occur. Comparison of such Lagrangian tidal data and the more conventional data obtained from moored current meters is, therefore, not precise particularly in the presence of strong horizontal gradients in tidal flow. Nevertheless tidal stream analyses were performed on the time derivatives of the drifter position data and are presented in Appendix 2. These indicate the average tidal ellipse parameters over each trajectory.

In computing the amplitude of the tidal constituents it was necessary, due to the shortness of the time series, to infer the characteristics of the S_2 and O_1 constituents. The inference relations were developed by performing tidal stream analyses on current meter data of several month's duration. These analyses showed that the amplitude of S_2 were 31% of M_2 and that the S_2 component lagged its astronomical potential by 24° more than M_2 lagged it. In effect, the S_2 Greenwich phase is 24° larger than the M_2 Greenwich phase. Similarly the O_1 constituent was inferred from the K_1 constituent. O_1 was taken as 60% of K_1, leading K_1 by 8°.

3.2.2 Eulerian Measurements of Tidal Currents.

In order to permit a rational comparison with the Lagrangian measurements, tidal stream analyses were performed on the shallowest current records over

the period 12 June to 25 June 1984. This abbreviated period spans the time of the drifter trajectories and is short enough so that the separate diurnal and semi-diurnal constituents are not resolved. Inference was performed using the same values of phase difference and amplitude ratio as used for the Lagrangian measurements. Each of the tidal stream analyses for the near-surface current meters is presented in Appendix 3. M_2 tidal ellipses computed for the period May 1984 to October 1985 are shown in Figure 3.10.

3.2.3 Comparison of Eulerian and Lagrangian Tidal Analyses.

Each drift track analysis has been paired with the geographically closest current meter analysis in Table 3.2. The sign of "MIN" (the amplitude of the semi-minor axis) indicates the sense of rotation of the current vector: a positive sign indicates anticlockwise, negative clockwise. (See Foreman, 1978, for an explanation of tidal current ellipses.) Thirty-two of the 36 ellipses indicate clockwise rotation. There is fair agreement between the Lagrangian and Eulerian measurements for the dominant semi-diurnal ellipses, but the smaller diurnal ellipses compare less well.

It must be borne in mind that the drifter trajectories naturally average the tidal streams over the region through which they pass while the current meter measurements are indicative of the tidal stream at one point. Thus the comparison of the two types of measurements made in Table 3.2 yields only fair agreement. On the other hand, if the amplitudes of the major axes of the M_2 ellipses are averaged, the Lagrangian data yield a mean of 37.1 cm s^{-1} and the Eulerian data yield a mean of 35.1 cm s^{-1}. Similarly good agreement is achieved between the average for the K_1 ellipses: 7.3 cm s^{-1} for the Lagrangian measurements and 6.6 cm s^{-1} for the Eulerian measurements. The mean phases agree within 11° for the M_2 and 28° for the K_1 constituent.

In general, the global agreement between the two type of measurements is gratifying and lend credence to the drifter data.

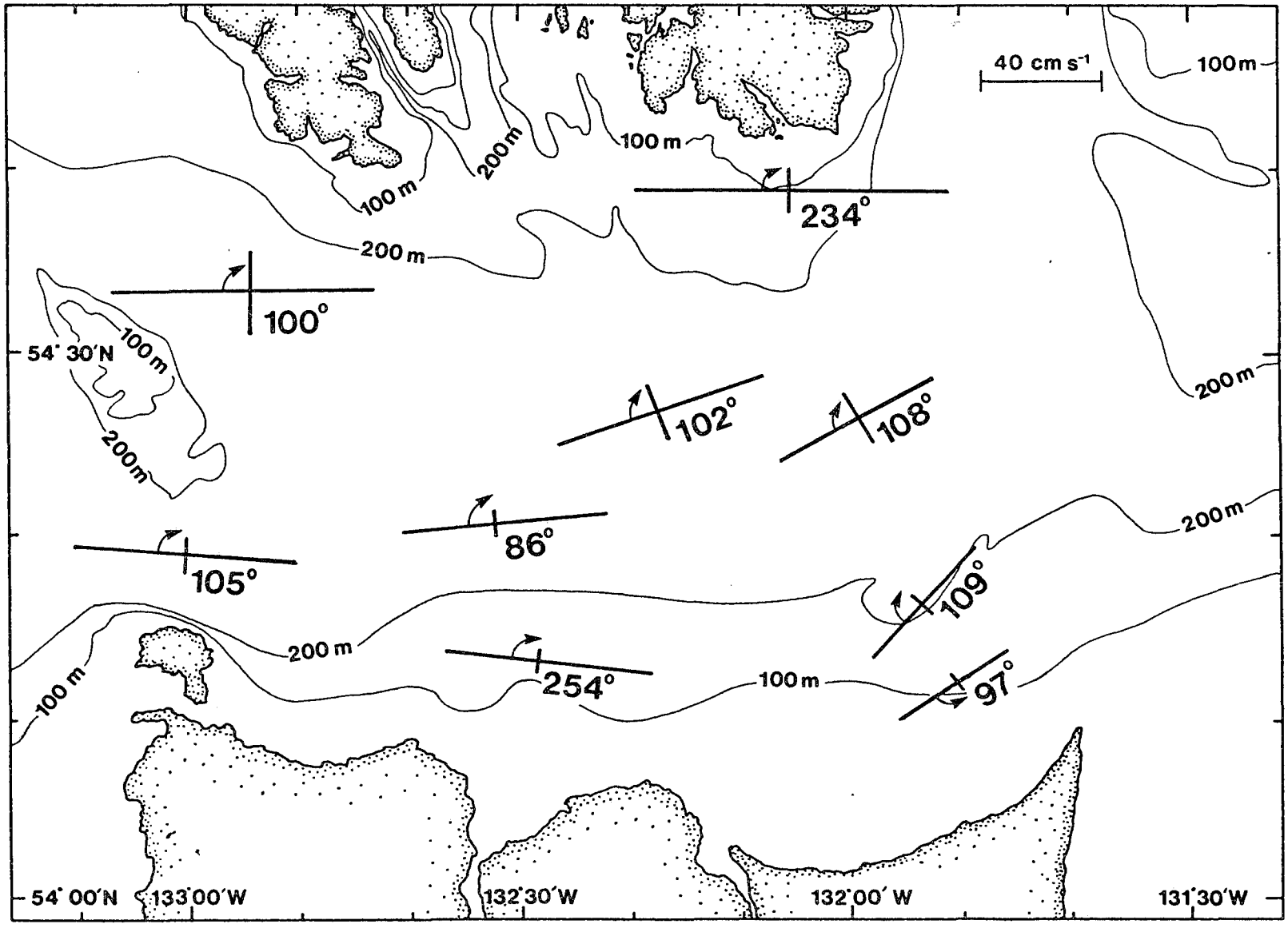

Figure 3.10 M_2 tidal ellipse axes from instruments for the period 12-24 June 1984.

Table 3.2 Comparison of Tidal Constituent Ellipses Computed with Lagrangian and Eulerian Data.

	Lagrangian				M_2		Eulerian			
Track No.	MAJ	MIN	INC	G	CM NO.	Depth (m)	MAJ	MIN	INC	G
1	30.6	5.4	30	117	D14	59	33.8	-4.2	170	254
2	52.4	-7.9	10	110	D13	45	34.0	-5.1	20	86
3	37.7	-12.3	43	131	D14	59	33.8	-4.2	170	254
4	52.0	-21.4	26	113	QF2	70	37.4	-5.7	7	105
5	27.8	-9.8	49	134	DO5	50	26.0	-5.1	47	109
6	19.2	7.4	164	256	D06	53	17.9	3.7	31	97
7	34.2	-9.5	173	263	D01	18	52.5	-7.7	179	234
9	26.3	-2.2	12	112	D10	50	36.5	-10.4	32	102
10	53.4	-26.3	4	102	QF1	57	42.8	-14.0	3	100

					K_1					
Track No.	MAJ	MIN	INC	G	CM NO.	Depth (m)	MAJ	MIN	INC	G
1	4.2	-0.7	44	179	D14	59	7.7	-1.3	134	64
2	10.6	-0.5	14	103	D13	45	6.9	-0.5	180	116
3	8.3	-1.8	178	261	D14	59	7.7	-1.3	134	64
4	5.4	2.2	122	296	QF2	70	10.0	-2.5	155	118
5	7.3	-0.4	10	122	DO5	50	3.0	-0.3	19	292
6	6.2	-1.0	169	318	DO6	53	1.8	-0.6	0	248
7	10.7	-3.8	157	285	DO1	18	11.5	-0.3	9	258
9	3.6	-0.6	29	61	D10	50	5.8	-0.4	11	300
10	9.6	-3.8	175	313	QF1	57	5.7	-0.5	166	98

MAJ = Amplitude of semi-major axis in cm s^{-1}.
MIN = Amplitude of semi-minor axis in cm s^{-1}.
INC = Inclination of northern semi-major axis anti-clockwise from east.
G = Greenwich phase.

3.2.4 Internal Tides

No attempt is made here to partition the tidal energy among the barotropic and baroclinic modes, rather the approximate vertical excursion of isopycnals is evaluated. Such vertical excursions can seriously affect the accuracy of geostrophic current computations. In addition, an estimate of the vertical excursions gives some intuitive feeling for the importance of internal tides in energy propagation.

Several time series of temperature from the moored current meters were examined visually to determine the magnitude of large temperature oscillations of approximately tidal period in June 1984. The CTD data collected in June 1984 were then used to determine the vertical temperature gradient at the geographical position and depth of each instrument. The magnitude of the tidal period internal waves could then be determined from

$$A = \left| \frac{T'}{\Delta T / \Delta Z} \right| \qquad (1)$$

where A is the vertical excursion of the internal tide, T' is the temperature excursion and $\Delta T / \Delta Z$ is the local vertical temperature gradient. Equation 1 assumes that the horizontal advection of spatially varying vertical gradients can be neglected and that a single realization of the vertical gradient is sufficient to approximate a mean vertical gradient. Also assumed is that the vertical excursions of current meters due to mooring motion is negligible.

Table 3.3 lists the results for several instruments. Vertical excursions of the instruments due to mooring motion were estimated with a simple mooring model. Only the time series from those instruments at which the vertical excursions were less than 5 m and at which temperature "waves" of clearly tidal period were present were used to compile the table.

Table 3.3 Height of Internal Tide Waves Computed from Temperature Time Series and Local Vertical Temperature Gradient.

Mooring No.	Instrument Depth	$\Delta T/\Delta Z$ (°C/m)	T'_{max} (°C)	A (m)
D1	48	1.9/50	1.5	40
	98	2.5/50	2.5	50
D4	52	2.1/50	3.0	70
D5	150	0.9/100	0.5	55
D6	53	2.4/50	1.2	25
	103	1.6/50	1.6	50
D14	59	1.8/50	1.8	50
	109	1.4/100	1.2	85

The estimated internal tide height in Dixon Entrance appears to be in the range 25 to 90 metres. Excursions approaching the depth of an instrument or the distance of an instrument above the bottom, however, are not realistic. The results of this analysis show that substantial internal tidal energy is present in the region and that the data from either non-synoptic or non-tidally averaged CTD surveys must be used with extreme caution, particularly in the computation of geostrophic currents.

4.0 DISCUSSION

4.1 TIDAL RECTIFICATION

Measurements of mean surface currents in the Hecate model (Bell, 1963) showed that the major feature in the region, the Rose Spit eddy, was well reproduced in the absence of wind stress and freshwater input. The logical implication is, therefore that the periodic forcing which was applied to the model was responsible for driving the mean anti-clockwise eddy. Such mean flows arising from purely oscillatory flows are termed rectified flows; those due to tidal oscillations are tidally-rectified flows.

There are two general situations in which tidal rectification can occur. The first, denoted as "shallow water effect", occurs when the height of the tide wave is comparable with the water depth. The tide wave is then strongly affected by non-linear dynamics, becomes non-sinusoidal through the development of higher harmonics (the shallow water constituents) and a mean flow also develops. The ratio of the tidal range to depth in Dixon Entrance is small so that the shallow water effect is unimportant.

The second situation occurs where substantial cross-isobath oscillations are present. Two mechanisms are involved in this rectification situation; one termed the "Coriolis mechanism" and the other the "bottom drag mechanism" by Huthnace (1973). He found that the two mechanisms were about equally important in tidal rectification over the Norfolk Sandbanks while Loder (1980) determined that the Coriolis mechanism dominated on the side of Georges Bank.

Any application of tidal rectification theory to Dixon Entrance must explain the fact that rectified flows measured in the non-rotating Hecate model closely resemble those found in the field.

4.1.1 Theory

The clearest development of the theory is given by Wright and Loder (1985) in which both depth independent and depth dependent solutions are given for an unstratified fluid. Although Dixon Entrance is strongly stratified in June, no theory for tidal rectification in a stratified fluid exists. Some insight can be gained, however, by scrutinizing the existing developments.

For time averaged quantities in the depth independent limit the expression for the non-dimensionalized Eulerian and Lagrangian mean velocities arising from tidal rectification are respectively

$$\bar{v} = 1/2L_{h_o}^{-1} L_e (1 + F^2)^{-1}[f/\sigma + (1 + F^2)^{1/2}(1 + L_k^{-1}L_{h_o})R \cos(\phi + \alpha)] \quad (2)$$

$$\bar{v}_L = 1/2L_{h_o}^{-1} L_e (1 + L_k^{-1} L_{h_o})R \sin\phi \quad (3)$$

where
- x is the cross-isobath direction,
- y is the along-isobath direction,
- L_{h_o} is the local value of the topographic length scale, $L_h \equiv -h/h_x$,
- L_e is the local cross-isobath tidal excursion ($= U_o/\sigma$),
- U_o is the local value of the amplitude of the cross-isobath tidal velocity,
- σ is the frequency of the tidal constituent,
- F $k/(\sigma h_o)$,
- k $C_D Q$ (a friction parameter),
- C_D is the bottom drag coefficient, (approximately 7×10^{-3}),
- Q is the mean tidal current speed just out of the bottom frictional boundary layer,
- h_o is the local depth,
- f is the Coriolis parameter,

L_k is the length scale of variation of the friction parameter ($\equiv L_{h_o} k/k_x$),

R is the ratio of along-isobath to cross-isobath amplitude of the local depth-averaged tidal current,

ϕ is the phase lead of the along-isobath over the cross-isobath current and

$\alpha = \tan^{-1}(-F^{-1})$.

The non-dimensional variables $\bar{v}$ and $\bar{v}_L$ can be re-dimensionalized by multiplying by U_o. The somewhat unwieldy expression (2) can be greatly simplified by evaluating F. In Dixon Entrance

$$k = C_D Q < (10^{-2}) \quad (.3\ ms^{-1}) \quad = \quad 3 \times 10^{-3}\ ms^{-1}$$

$$\sigma h_o > 1.4 \times 10^{-4}\ s^{-1}\ (200\ m) \quad = \quad 2.9 \times 10^{-2}\ ms^{-1}$$

so that $F < 0.1$

Therefore $F^2 << 1$, and α approaches $-\pi/2$.
(2) becomes

$$\bar{v} = 1/2 L_{h_o}^{-1} L_e [f/\sigma + (1 + L_k^{-1} L_{h_o}) R \sin \phi] \tag{4}$$

Furthermore, following Wright and Loder the approximation $L_k = L_{h_o}$ is made and (4) becomes

$$\bar{v} = 1/2 L_{h_o}^{-1} L_e [f/\sigma + 2R \sin \phi] \tag{5}$$

The expression for Lagrangian velocity (3) becomes

$$\bar{v}_L = 1/2\ L_{h_o}^{-1} L_e [2R \sin \phi] \tag{6}$$

Wright and Loder further assume that R is approximately equal to f/σ. Such an approximation is valid far from boundaries, but R can better be

evaluated from observations of currents. Expressions for R and ϕ are derived in terms of tidal ellipse parameters in Section 4.1.2. Values for R and ϕ are computed from the tidal ellipses in Section 4.1.3 where rectified currents are also calculated. The values of R and ϕ are very approximately 5 and 90° respectively in Dixon Entrance.

If the value $\phi = 90°$ is used in expressions (5) and (6) then

$$\bar{v} = 1/2\ L_{h_o}^{-1}\ L_e\left(\frac{f}{\sigma} + 2R\right) \tag{7}$$

and

$$\bar{v}_L = 1/2\ L_{h_o}^{-1}\ L_e[2R] \tag{8}$$

The ratio of the Eulerian to the Lagrangian velocity when $F \ll 1$, $L_k = L_{h_o}$ and $\phi = 90°$ is

$$\frac{v}{V_L} = \frac{f/\sigma + 2R}{2R} \tag{9}$$

According to (9), as the tidal ellipses become more elongated along the isobaths (R increases) the Lagrangian velocity approaches the Eulerian velocity.

$\bar{v}$ and $\bar{v}_L$ are non-dimensional variables scaled by U_o, the amplitude of the cross-isobath tidal flow. It is therefore, not accurate to infer that a simple increase in ellipticity implies larger rectified currents; rather when the minor (cross-isobath) axis of the tidal ellipse is constant then the larger the major axis, the larger the rectified current.

The foregoing expressions apply to the case where the rectified flows are independent of depth. Wright and Loder show that even in the absence of stratification substantial vertical structure will be present in the rectified velocity profiles in relatively deep water. However the depth independent solution will provide an approximation of the rectified flows, generally larger in magnitude at the surface than the depth dependent solutions.

Close examination of (7) and (8) reveals that the role of the Coriolis mechanism of rectification can be somewhat less important than suggested by Wright and Loder. For example the Coriolis parameter is completely absent in the expression for the Lagrangian current, while the relative importance of the Coriolis term in the expression for the Eulerian current depends upon the value of R. In Dixon Entrance observed values of 2R average about 10 while $f/\sigma = 0.84$. Therefore, from (9)

$$\frac{V}{V_L} = \frac{.84 + 10}{10} = 1.084$$

The Eulerian velocities will be only moderately larger than the Lagrangian velocities - that is, the Stokes' drift is nearly negligible.

Expressions (7) and (8) contain further implicit information on the nature of the rectification mechanism. The expression for the <u>dimensional</u> Eulerian rectified current can be written

$$v' = \frac{1}{2} U_o \frac{L_e}{L_h} \left[\frac{f}{\sigma} + 2 \frac{V_o}{U_o}\right] \qquad (10)$$

since $R = \frac{V_o}{U_o}$ by definition.

Then $$v' = \frac{1}{2} L_e \left[\frac{L_e}{L_h} f + 2 \frac{V_o}{L_h}\right] \qquad (11)$$

since $$\frac{U_o}{\sigma} = L_e.$$

Now $V = \frac{V_o h_o}{h}$, from continuity, so that

$$\frac{\partial V}{\partial x} = V_o \frac{1}{h} \frac{\partial h}{\partial x} = \frac{V_o}{L_h}$$

(11) becomes $$v' = \frac{1}{2} L_e \left[\frac{L_e}{L_h} f + 2 \frac{\partial V}{\partial x}\right] \qquad (12)$$

(12) states that the rectified current is caused by the cross-isobath excursion advectiving water columns whose vorticity is composed of both planetary and relative vorticity. The interpretation of the two mechanisms of rectification offered by Wright and Loder is, therefore, somewhat altered when $L_k = L_h$.

The second terms in both (5) and (12) are dominant in Dixon Entrance. This implies that rotational effects of planetary vorticity contribute insignificantly to the vorticity. Both the Lagrangian and Eulerian velocities measured in a non-rotating model when properly scaled would be closely representative of those present in nature. Equation (9) predicts that the drifts measured in the Hecate Model (Bell, 1963), which was a non-rotating model, would have been virtually unchanged if rotation had been introduced. The reason for the success of the Hecate Model in reproducing the Rose Spit eddy is thus evident.

Further confirmation of the dominance of non-rotational effects in tidal rectification in Dixon Entrance is available in the work of M. Bowman (pers. comm.). A numerical model of Dixon Entrance quite successfully reproduced rectified Eulerian currents around the Rose Spit eddy with the Coriolis parameter set equal to zero.

4.1.2 R and ϕ from tidal ellipses

Tidal analyses of current observations typically yield results such as those shown in Appendices 2 and 3. Each tidal constituent is described in terms of ellipse parameters. These are M and m, the amplitude of the semi-major and semi-minor axes of the ellipse; INC, the inclination of the northern semi-major axis anti-clockwise from east and G the Greenwich phase. R and ϕ can be expressed in terms of the ellipse parameters.

Let the along isobath component of flow be

$$v = V_o \sin (wt + \phi),$$

where $w = \frac{2\pi}{T}$ and T is the tidal period

and the cross isobath component of flow be

$$u = U_o \sin wt$$

to agree with Wright and Loder's formulation.

The magnitude of the flow at any time is $U^2 + V^2$, and the time at which the current vector is along the major and minor axes can be determined by differentiating the expression for the current speed, yielding

$$\tan (2\, wt_m) = \frac{-\sin 2\phi}{(\frac{V_o}{U_o})^2 + \cos 2\phi} \qquad (13)$$

In Dixon Entrance the ellipses are <u>generally</u> elongated along the isobaths (see Figure 3.10) and the maximum current can be shown to occur within 5° of phase of the maximum of the larger velocity component. For $V_o/U_o > 2.5$,

$$wt_m = (90 - \phi) \pm 5°.$$

The inclination of the ellipse anticlockwise from the along-isobath direction can be expressed as

$$\tan \theta = -\frac{U_o \sin wt_m}{V_o \sin (wt_m + \phi)} \qquad (14)$$

If it is assumed that $wt_m = 90 - \phi$, the

$$\tan \theta = -\frac{U_o}{V_o} \cos \phi \qquad (15)$$

(15) gives the value of θ to within $\pm$ 1.5°; considerably better than the accuracy of current measurements.

The maximum current amplitude occurs at $wt = wt_m$ and can be written as

$$M^2 = U_o^2 \sin^2 wt_m + V_o^2 \sin^2 (wt_m + \phi) \qquad (16)$$

Assuming, once again that $wt_m = (90° - \phi)$,

$$M^2 = U_o^2 \cos^2\phi + V_o^2 \quad (17)$$

Similarly if the minimum current m, occurs at $wt_m = -\phi$, then

$$m = -U_o \sin\phi \quad (18)$$

Expressions (15), (17) and (18) can be manipulated to yield expressions for U_o, V_o and ϕ

$$U_o^2 = M^2 \sin^2\theta + m^2 \quad (19)$$

$$V_o = M \cos\theta \quad (20)$$

$$R = V_o/U_o \quad (21)$$

$$\cot\phi = \frac{M}{m}\left|\sin\theta\right| \quad (22)$$

where ϕ is of the opposite sign as m.

The results of the tidal stream analyses through application of equations (19), (20), (21) and (22) can be used to evaluate R and ϕ in equation (5).

4.1.3 Application to Dixon Entrance

The predicted rectified tidal flows in Dixon Entrance were evaluated using equation (6). Two independent data sources were employed: the current meter data and the drifter data, both of which were subjected to tidal stream analysis. The O_1 and S_2 constituents were inferred and the resulting M_2 ellipse parameters transformed to yield values of R and ϕ. In the two cases where the cross-isobath flow component exceeded the along-isobath component, the approximations of Section 4.1.2 are not valid and R sin ϕ was taken equal to zero.

Table 4.1 shows the results of the computations. Rectified flows are directed with the shallow water to the right in all cases but one. Most significantly, the predicted rectified flows do not exceed 9 cm s^{-1} and average 2.6 cm s^{-1}. Since the tidal rectification mechanism operates regardless of season, wind direction or freshwater runoff, it is an important transport mechanism. However, much stronger mean flows appear to have been present.

The locations where tidal rectification will be most pronounced are over Learmonth Bank and along the very steep slope between Hecate Strait and Dixon Entrance where "overfalls" are noted on the chart. Lacking direct current measurements in the region, we can only estimate the residual flows which could be generated. Using a cross-isobath flow of 50 cm s^{-1} (30% of the value indicated on the nautical chart) and assuming conservatively that R = 0, rectified flows of 30 to 40 cm s^{-1} are predicted eastward along the drop-off between Hecate Strait and Dixon Entrance and clockwise around Learmonth Bank. Current measurements in these areas would permit definitive evaluation of the rectification mechanism in Dixon Entrance.

4.2 THERMOHALINE FLOW - FRESH WATER DISCHARGE

The combined discharge of the Nass and Skeena Rivers peaked in June 1984 at 4 x $10^3 m^3 s^{-1}$ (Dept. of Env., 1985). Using this mean June discharge figure, the induced estuarine flow in the upper layers of Dixon Entrance can be computed using salt and mass balances (Knudsen's relations). If Q_1 is the seaward near-surface flow in Dixon Entrance driven by fresh-water discharge, Q_2 is the deep return flow and Q_r the river discharge then

$$Q_2 = Q_1 - Q_r \tag{23}$$

in order to conserve mass. If S_1 and S_2 are the salinities associated with the upper and lower layers in Dixon Entrance, then

$$Q_1 S_1 = Q_2 S_2 \tag{24}$$

in order to conserve salt.

Table 4.1 Rectified Flows Predicted by Theory

Meter No.	M (cm s^{-1})	m (cm s^{-1})	θ (deg)	R	ϕ (deg)	Cross Isobath Tidal Amplitude U_o (cm s^{-1})	Cross Isobath Tidal Excursion L_e (km)	Topographic Length Scale L_h (km)	Non-Dimensional Rectified Current v	Dimensional Rectified Current $v' = vU_o$ (cm s^{-1})
					M_2 Currents from Current Meter Data					
D14	33.8	-4.2	0	8.0	+90	4.2	0.30	9.0	0.28	1.2
D13	34.0	-5.1	0	6.7	+90	5.1	0.37	38.0	0.07	0.4
QF2	37.4	-5.7	0	6.6	+90	5.7	0.41	7.2	0.40	2.3
D05	26.0	-5.1	0	5.1	+90	5.1	0.37	25.2	0.16	0.8
D06	17.9	+3.7	+35	1.3	-20	10.9	0.78	9.9	0.002	0.02
D01	52.5	-7.7	0	6.8	+90	7.7	0.55	6.0	0.66	5.1
D10	36.5	-10.4	+35	1.3	+26	23.4	1.68	42.0	0.04	0.9
QF1	42.8	-14.0	+40	1.1	+27	30.9	2.22	12.3	0.17	5.1
D04	29.0	-10.3	0	2.8	+90	10.3	0.74	54.0	0.04	0.5
					M_2 Currents from Drifter Data					
Drift No.	M (cm s^{-1})	m (cm s^{-1})	θ (deg)	R	ϕ (deg)	U_o (cm s^{-1})	L_e (km)	L_h (km)	v	$v' = vU_o$ (cm s^{-1})
1	30.6	+5.4	0	5.7	-90	5.4	0.39	7.4	-0.28	-1.5
2	52.4	-7.9	0	6.6	+90	7.9	0.56	42.0	+0.09	0.7
3	37.7	-12.3	45	0.9	+57	29.4	2.1	25.9	+0.09	2.8
4	52.0	-21.4	0	2.4	+90	21.4	1.5	13.9	+0.31	6.5
5	27.8	-9.8	0	2.8	+90	9.8	0.7	11.1	+0.20	2.0
6	19.2	+7.4	90	0.4	-	19.2	1.4	5.0	+0.12	2.3
7	34.2	-9.5	0	3.6	+90	9.5	0.68	4.5	+0.61	5.8
9	26.3	-2.2	0	12.0	+90	2.2	0.16	10.8	+0.18	0.4
10	53.4	-26.3	90	0.5	-	53.4	3.8	20.0	+0.08	4.3

Combining (23) and (24) and solving for Q_1:

$$Q_1 = \frac{Q_r S_2}{S_2 - S_1}$$

Using $S_2 = 33$, $S_1 = 31$ and $Q_r = 4 \times 10^3$ m^3 s^{-1}

$$Q_1 = 6.6 \times 10^4 \text{ m}^3 \text{ s}^{-1}$$

or about 0.07 Sverdrups.

The extent of the seaward estuarine flow can be very roughly estimated from Figures 3.8 and 3.9 which show a plume of about 10 km width. If a depth of 50 m is assumed then a mean velocity of roughly 13 cm s^{-1} along the assumed plume trajectory of Figures 3.8 and 3.9 arises.

The numbers are very rough but the conclusion is clearly that the freshwater discharge in June is capable of producing flow speeds due to estuarine circulation in excess of 10 cm s^{-1}.

4.3 WIND-DRIVEN FLOW

A general impression of the effect of wind stress on the circulation can be formed by scrutinizing the two week period of the drift measurements (June 1984).

Between 12 June and 20 June in Dixon Entrance the wind was northwesterly at about 10 to 20 knots. In the evening of 21 June a southeasterly gale (about 30 knots) began which continued through the end of the survey on 25 June. Thus there were nine days of measurement during which northwesterly winds prevailed and about four days during which southeasterly winds were dominant. The differences in the measured Eulerian and Lagrangian currents during these two periods can provide an estimate of the strength of wind-driven flows.

Figure 3.2 shows the daily averaged currents at the moored instruments at less than 50 m depth. The velocity vectors have been contoured to show isotachs (not streamlines). Early in the survey the anticyclonic gyre over Learmonth Banks displayed maximum currents of about 20 cm s^{-1} while the cyclonic Rose Spit gyre had maximum speeds of about 10 cm s^{-1}. After the onset of the southeasterly gale on 21 June both gyres appear to weaken. From these data one may conclude that northwesterly winds tend to enhance both gyres to depths of a least 50 m.

The mean drifter trajectories, Figure 3.1, also show the effect of the reversal in wind stress. Both drifters deployed on 21 June were advected primarily toward the northwest indicating that flow at 10 m depth was strongly affected by the gale.

4.4 ANALYSIS OF THE COMPONENTS OF FLOW

The processes which contributed to the circulation in Dixon Entrance in mid-June 1984 were tidal rectification, freshwater discharge and wind stress. The approximate sizes and senses of the contributions from each of these effects (in cm s^{-1} current speed) are shown in Figures 4.1, 4.2 and 4.3 respectively. Figure 4.4 shows the sum of the contributions and represents the impression of the circulation gained during the course of this study.

The three mechanisms are very different in character. The tidal rectification mechanism will vary in strength over the fortnightly cycle (Butman et al., 1983) but the monthly mean flow from tidal rectification is nearly constant. The contribution from freshwater discharge peaks in June and July and decreases by more than a factor of 10 in February. The wind-driven flow has summer (northwesterly winds) and winter (southeasterly winds) modes. The winter mode is probably about twice the strength of the summer mode and persists for a greater part of the year.

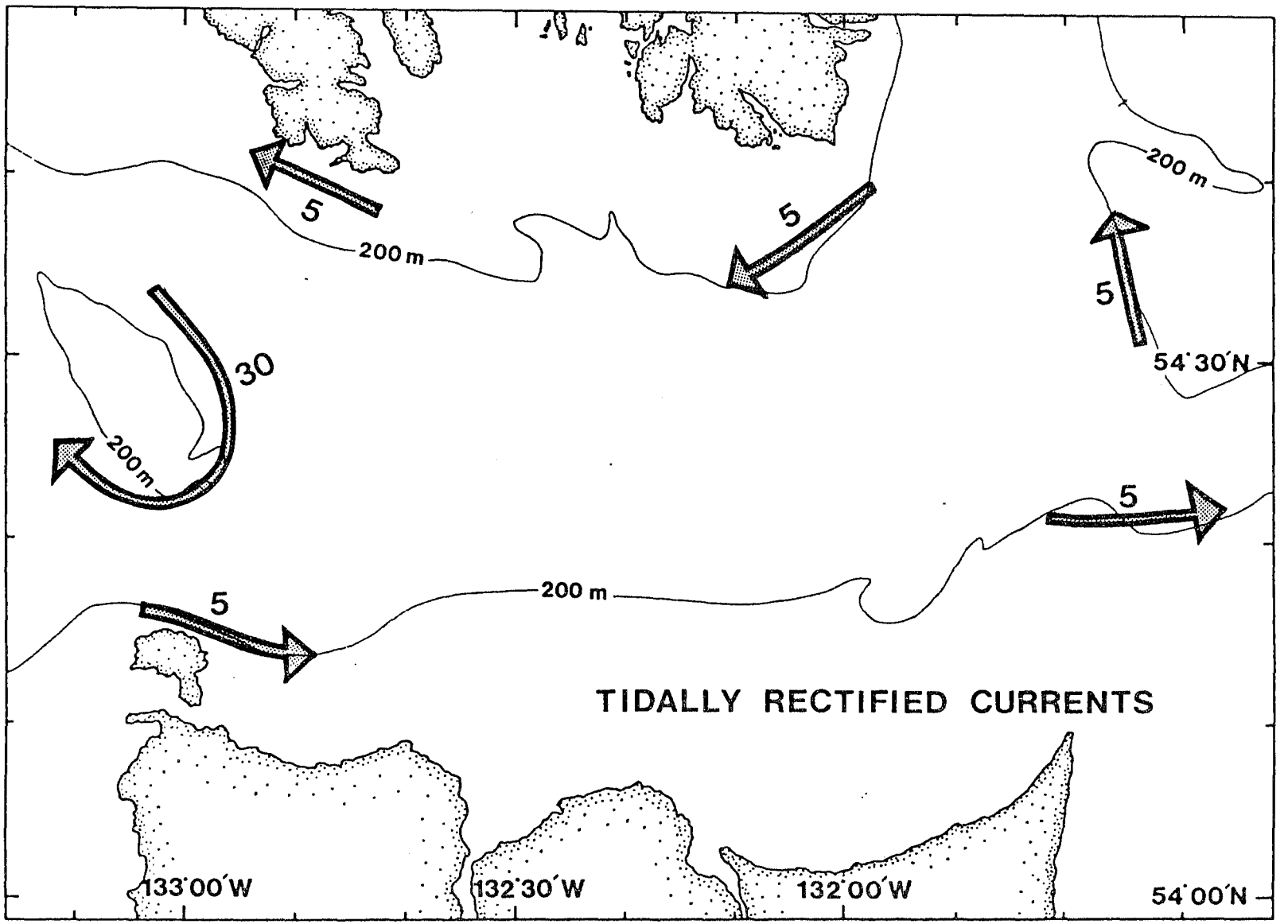

Figure 4.1 Schematic of the approximate contribution to the total near-surface flow due to tidal rectification (numbers indicate speeds in cm s^{-1}).

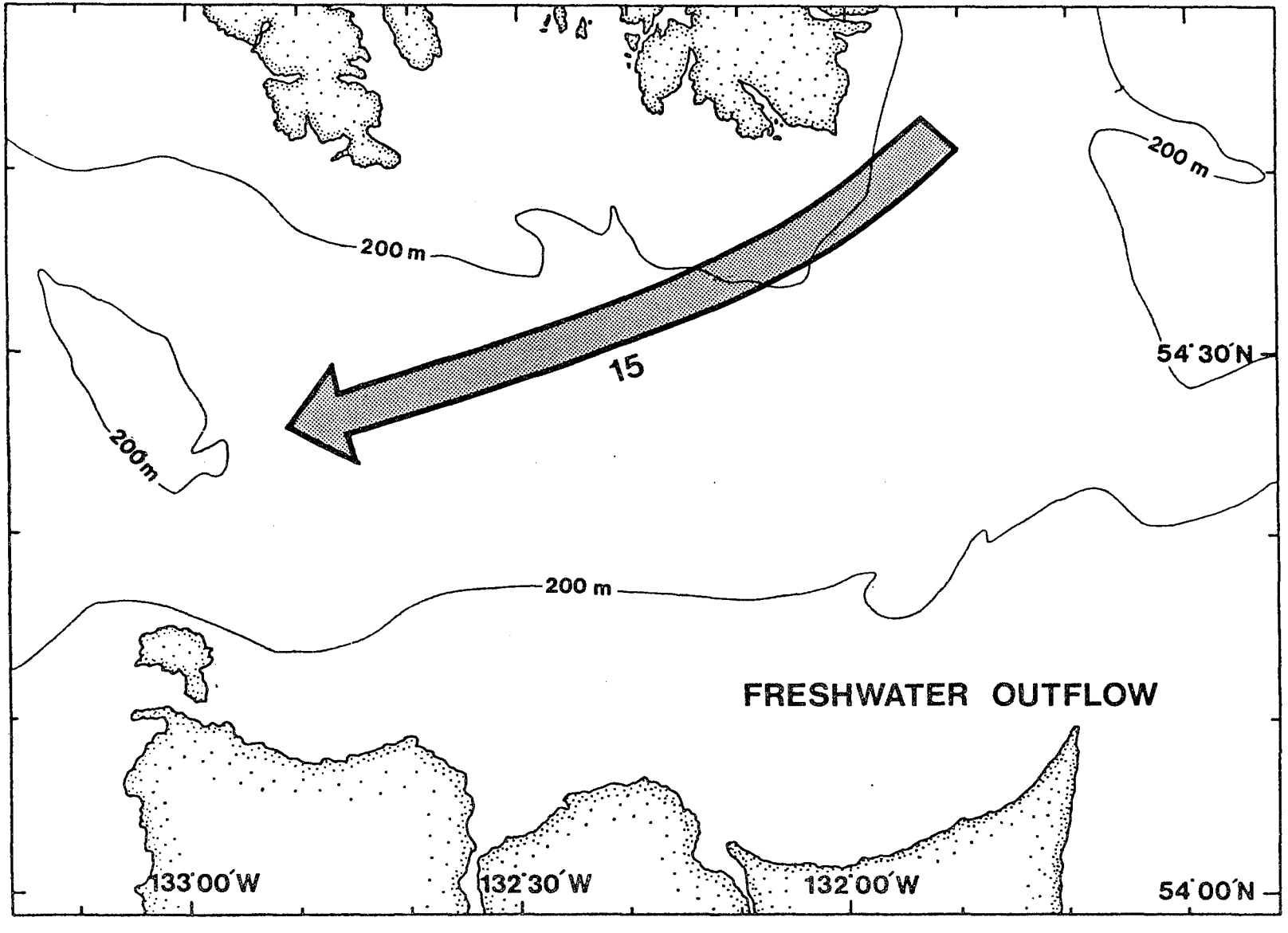

Figure 4.2 Schematic of the approximate contribution of freshwater discharge (cm s^{-1}).

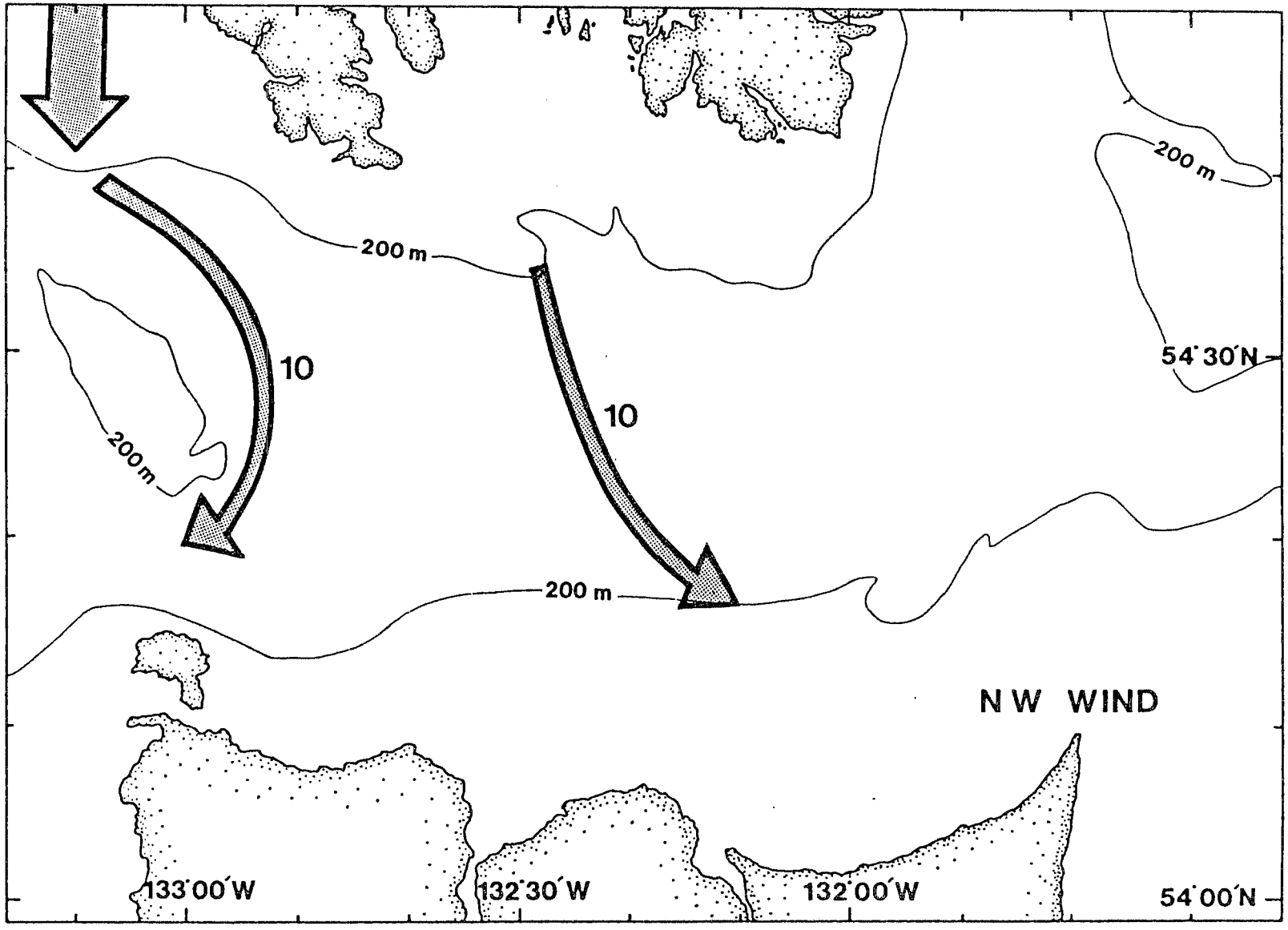

Figure 4.3 Schematic of the approximate contribution of moderate northwest wind stress, cm s^{-1}.

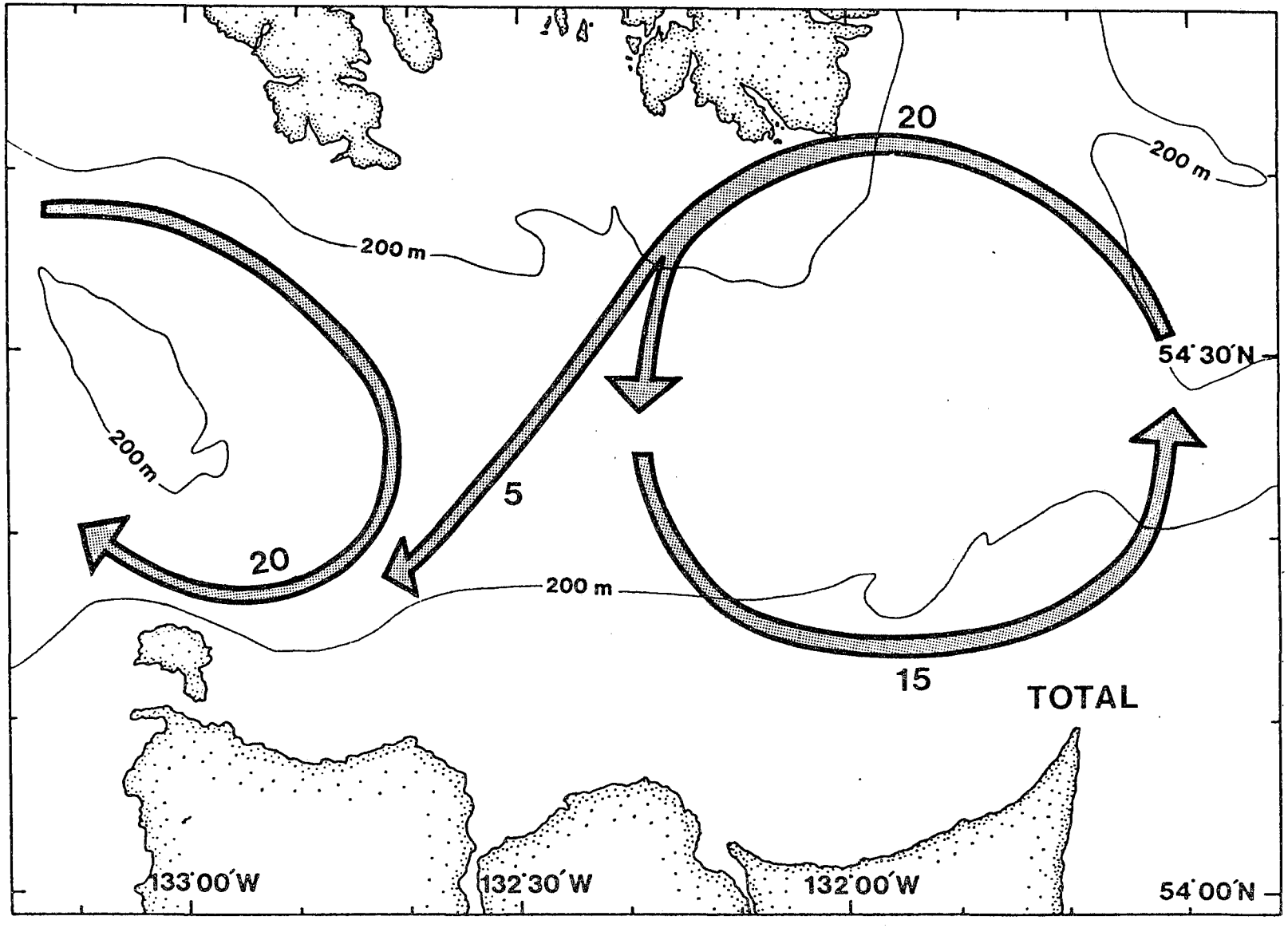

Figure 4.4 The sum of the effects shown in Figures 4.1, 4.2 and 4.3: tidal rectification + freshwater discharge + wind stress (cm s^{-1}).

Further quantification of the contributions from each mechanism to the circulation in Dixon Entrance will probably be possible upon examination of the long time series of Eulerian currents which now (October, 1985) exist. However the strong tidally rectified currents around Learmonth Bank will not be resolved by the data now available and further drifter studies will be required.

5.0 CONCLUSIONS

The mean surface currents in Dixon Entrance are driven by three processes: tidal rectification, freshwater discharge and wind stress.

Throughout Dixon Entrance the tidally rectified flows are directed with the shallow water to the right. Above most of the slopes, rectified currents are about 5 cm s^{-1}; however, over the steep slopes around Learmonth Bank and between Hecate Strait and Dixon Entrance, rectified tidal currents in excess of 30 cm s^{-1} are present. The importance of the tidal rectification mechanism is more in its persistence than in its magnitude. Tidally rectified flows are deterministic, present regardless of season and thus are the major factor in driving the annual average circulation. The cyclonic Rose Spit gyre, observed in both model and field studies, is driven by tidal rectification.

The freshwater discharge from the Nass and Skeena Rivers peaks in June every year. In this respect its influence is deterministic. However, the river discharges are dependent upon the total snow pack so that their effect varies in importance among years. It is likely that the most pronounced estuarine effects due to river discharge are present in Dixon Entrance in June and July. Westward flowing freshened surface currents may reach speeds of up to 15 cm s^{-1} due solely to river discharge and entrainment. Our survey indicated that the freshwater plume appears to hug the northern shore at Cape Chacon, then traverse Dixon Entrance from north to south (toward Wiah Point) and exit north of Langara Island.

The wind regime is the least deterministic of the local driving mechanisms for the mean flow. It is probable that surface currents are driven (as elsewhere) at about 3 per cent of the wind speed. During most of our survey in June 1984, the mean wind speed was in the range of 2 to 10 m s^{-1} from the northwest. Near the end of our survey a southeast gale began with winds exceeding 15 m s^{-1}. The behaviour of the drifters suggests that during the prevailing northwest winds of summer, wind-driven flows at 10 m depth are about 10 cm s^{-1}.

6.0 REFERENCES

Bell, W.H. and N. Boston, 1962. The Hecate Model. Fish. Res. Bd. Canada, MS Rept. Ser. (Oceanogr. Limnol.). No. 110, 35p.

Bell, W.H., 1963. Surface current studies in the Hecate Model. Fish. Res. Bd. Canada, MS Rept. Ser. (Oceanogr. Limnol.). No. 159, 27p.

Bell, W.H. and N. Boston, 1963. Tidal calibration of the Hecate Model. J. Fish. Res. Bd. Canada 20 (5): 1197-1212.

Butman, B., M. Noble, D.C. Chapman and R.C. Beardsley, 1983. An upper bound for the tidally rectified current at one location on the southern flank of Georges Bank. Journ. Phy. Ocean. 13: 1452-1460.

Crean, P.B., 1967. Physical oceanography of Dixon Entrance, British Columbia. Bulletin 156, Fisheries Research Board of Canada. 66p.

Department of Environment, 1985. Surface water data, 1984. Inland Waters Directorate, Water Survey of Canada, Department of the Environment.

Foreman, M.G.G., 1978. Manual for tidal currents analysis and prediction. Pacific Marine Science Report 78-6. Institute of Ocean Sciences, Patricia Bay, B.C.

Greisman, P., 1985. Data Report, Dixon Entrance Loran-C drifter and CTD study June 1984. Unpublished Report prepared for Tides and Currents, CHS, IOS, Sidney, B.C. 121p.

Huthnace, J.M., 1973. Tidal current asymmetries over the Norfolk Sandbanks. Est. Coastal Mar. Sci. 1: 89-99.

Loder, J.W., 1980. Topographic rectification of tidal currents on the sides of Georges Bank. J. Phys. Oceanog. 10: 1399-1416.

Wright, D.G. and J.W. Loder, 1985. A depth-dependent study of the topographic rectification of tidal currents. Geophys. Astrophys. Fluid Dynamics. 31: 169-220.

THIS PAGE IS BLANK

Cross Sections S, T, σ_t June 1984

Appendix 1

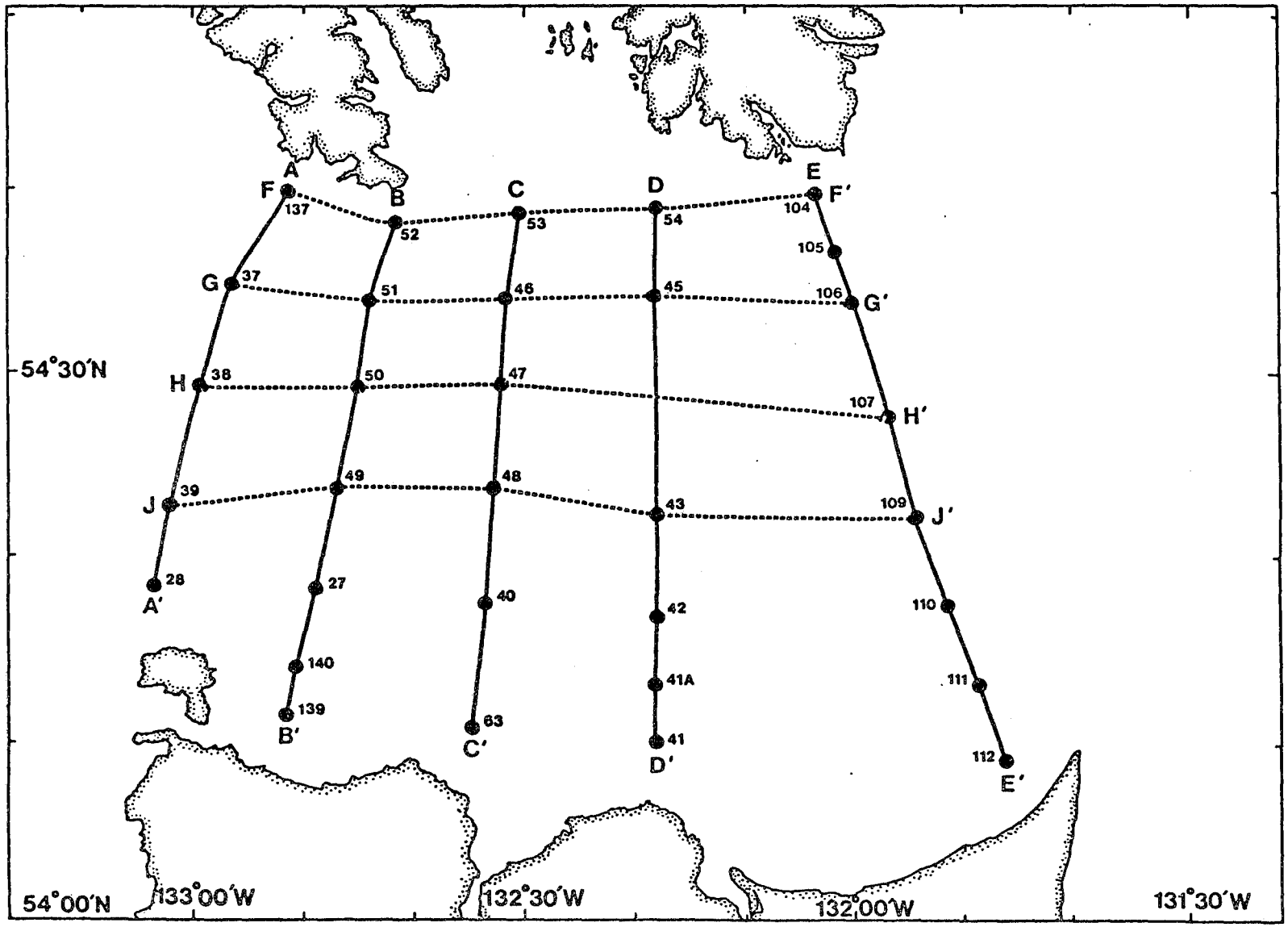

DOBROCKY SEATECH

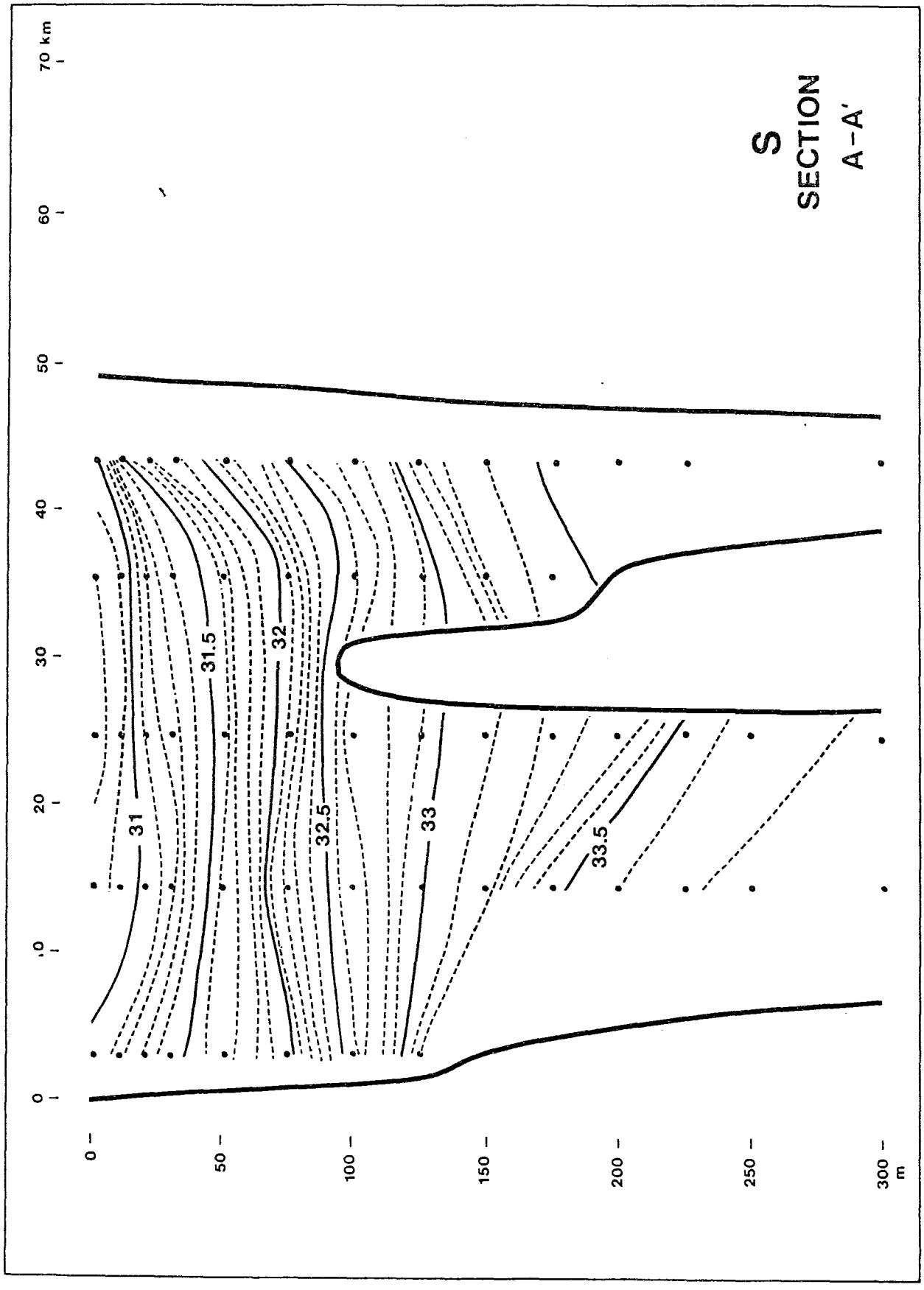

DOBROCKY
SEATECH

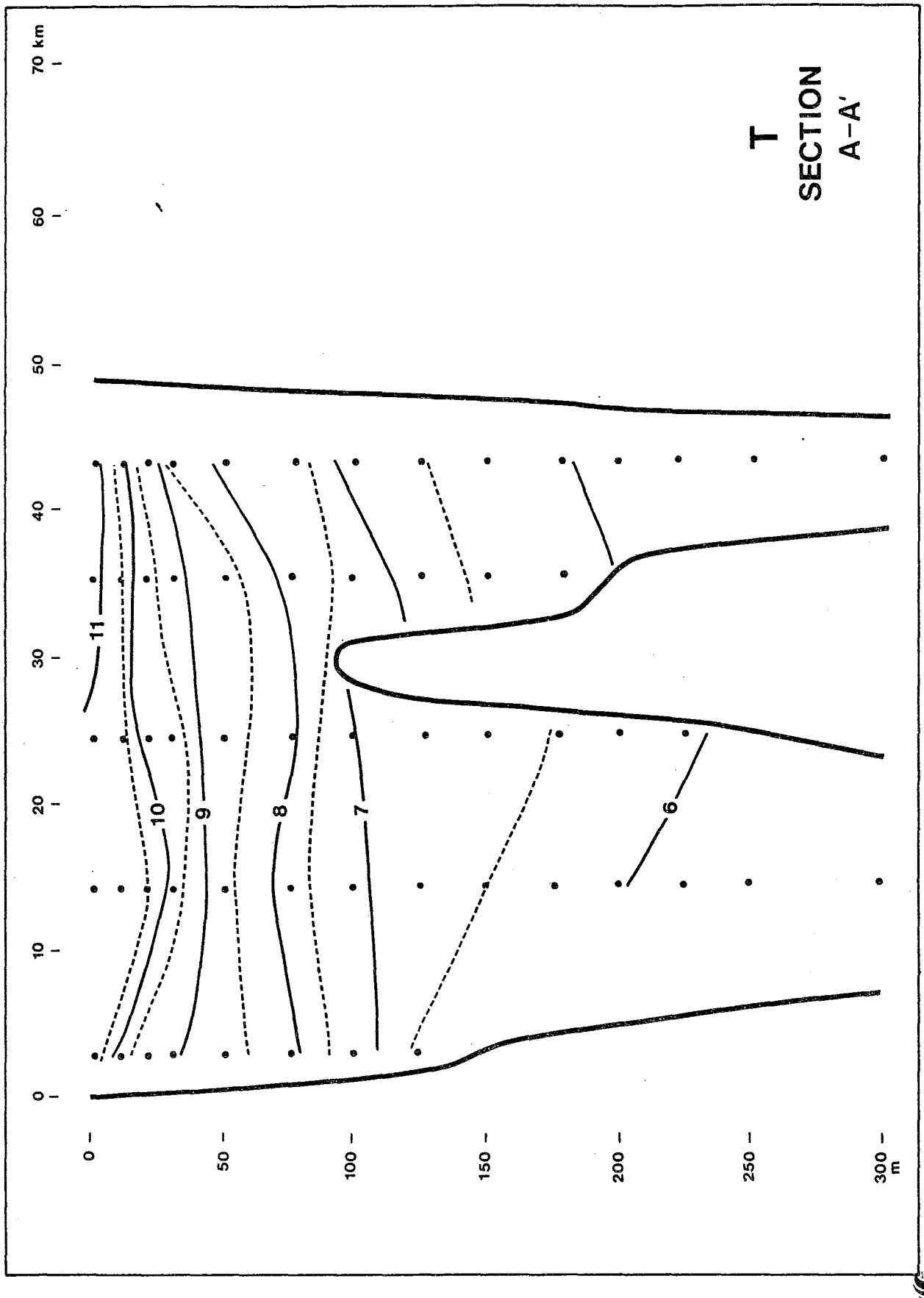

DOBROCKY
SEATECH

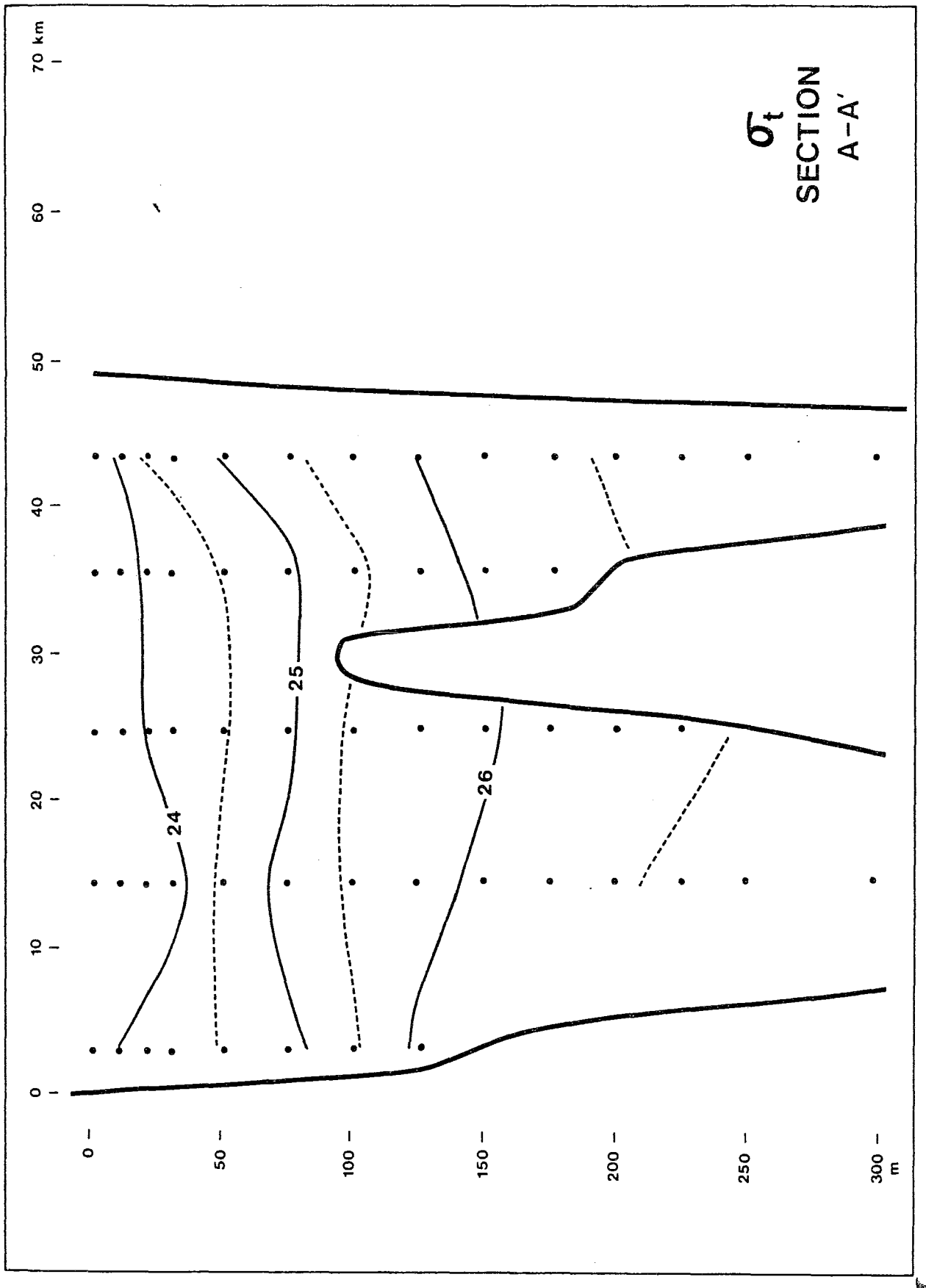

DOBROCKY
SEATECH

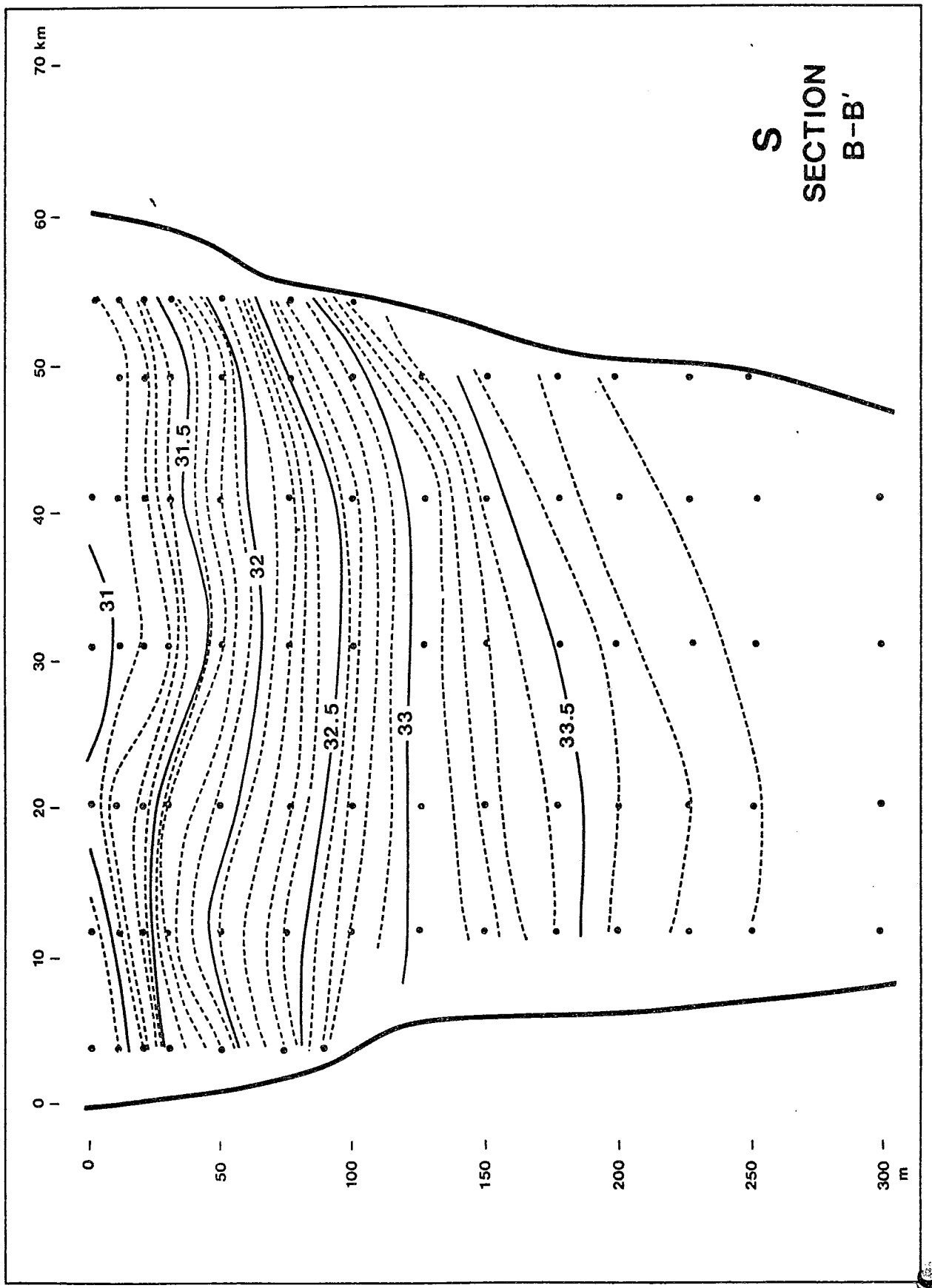

DOBROCKY
SEATECH

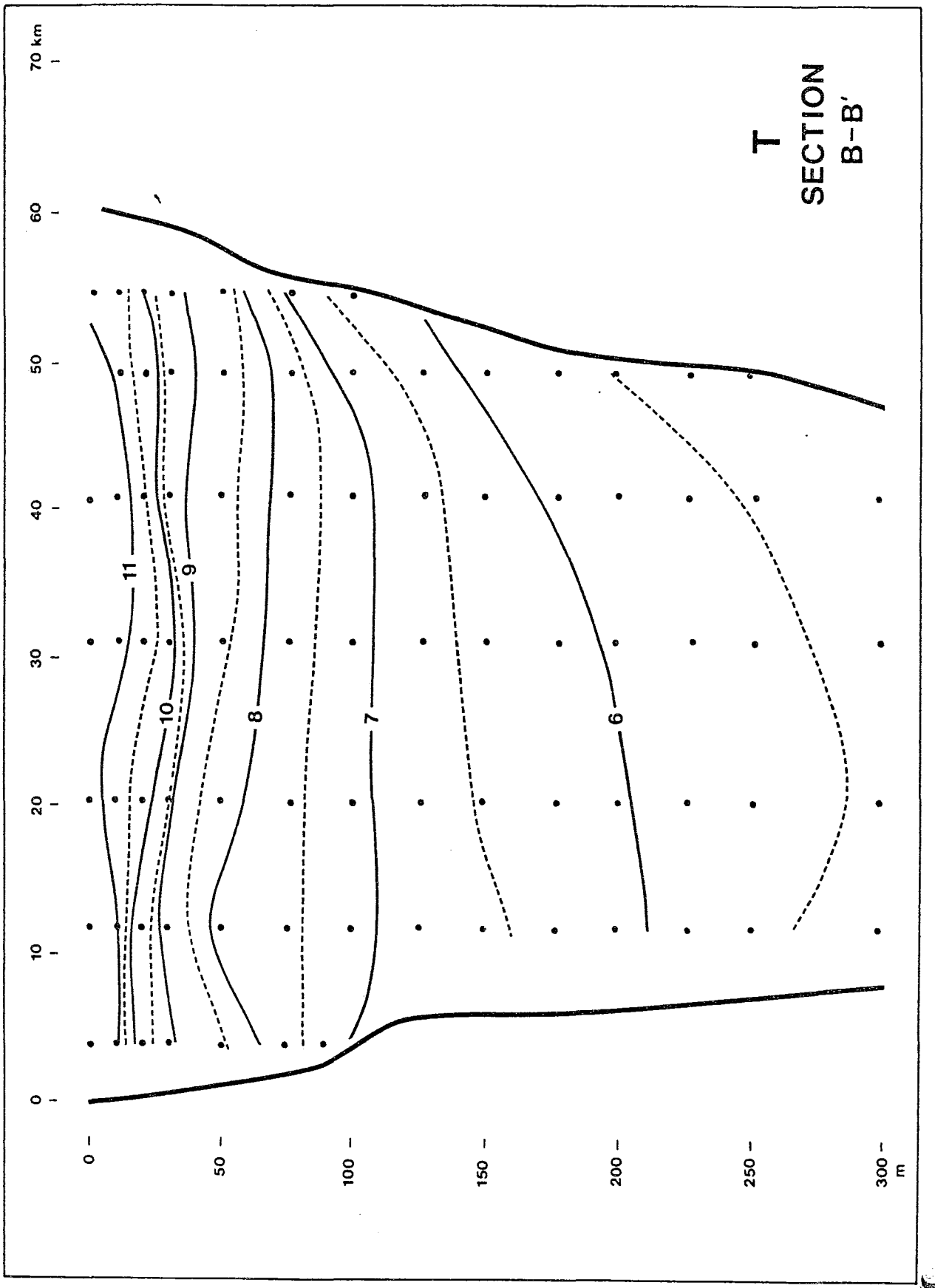

DOBROCKY
SEATECH

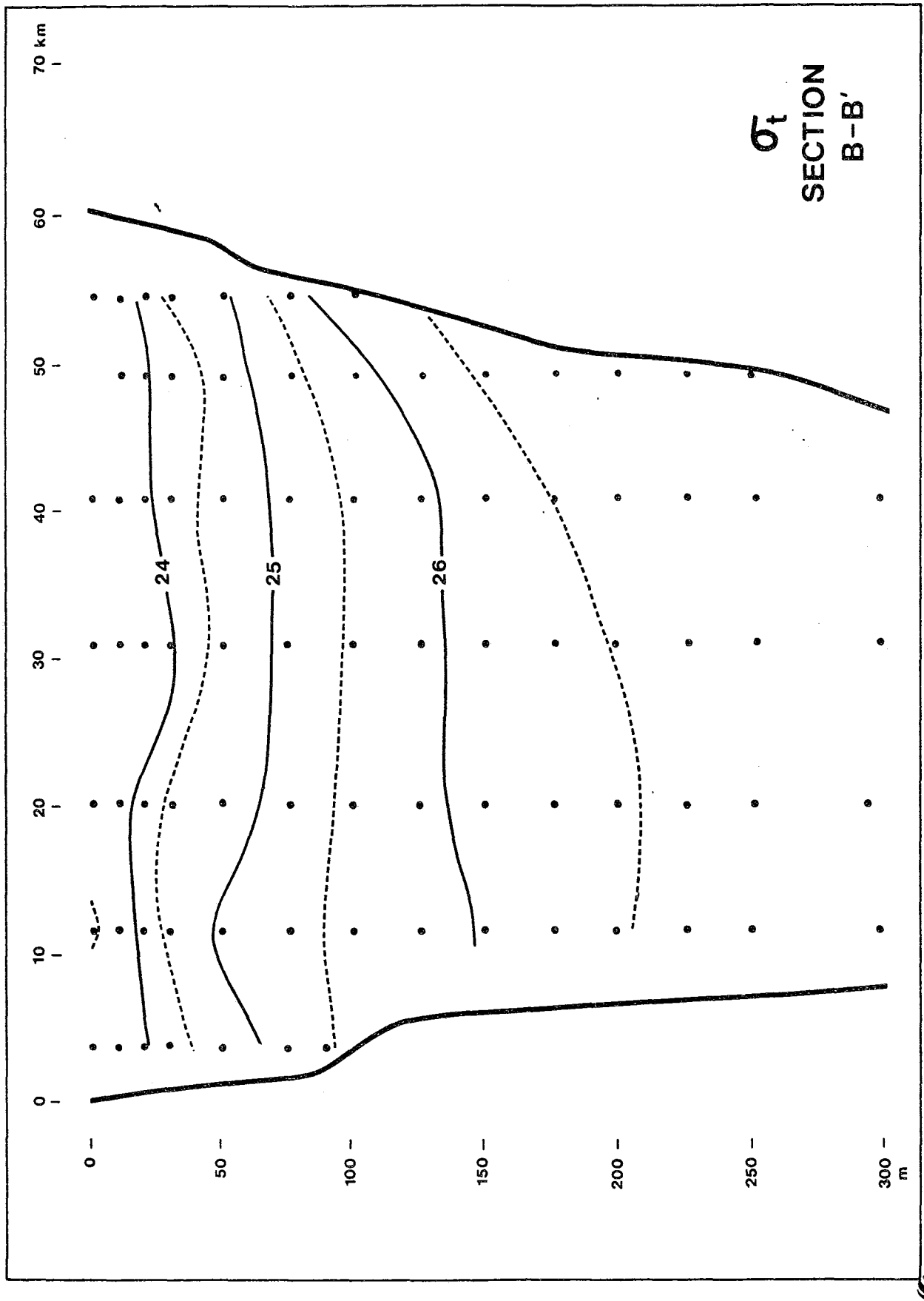

DOBROCKY
SEATECH

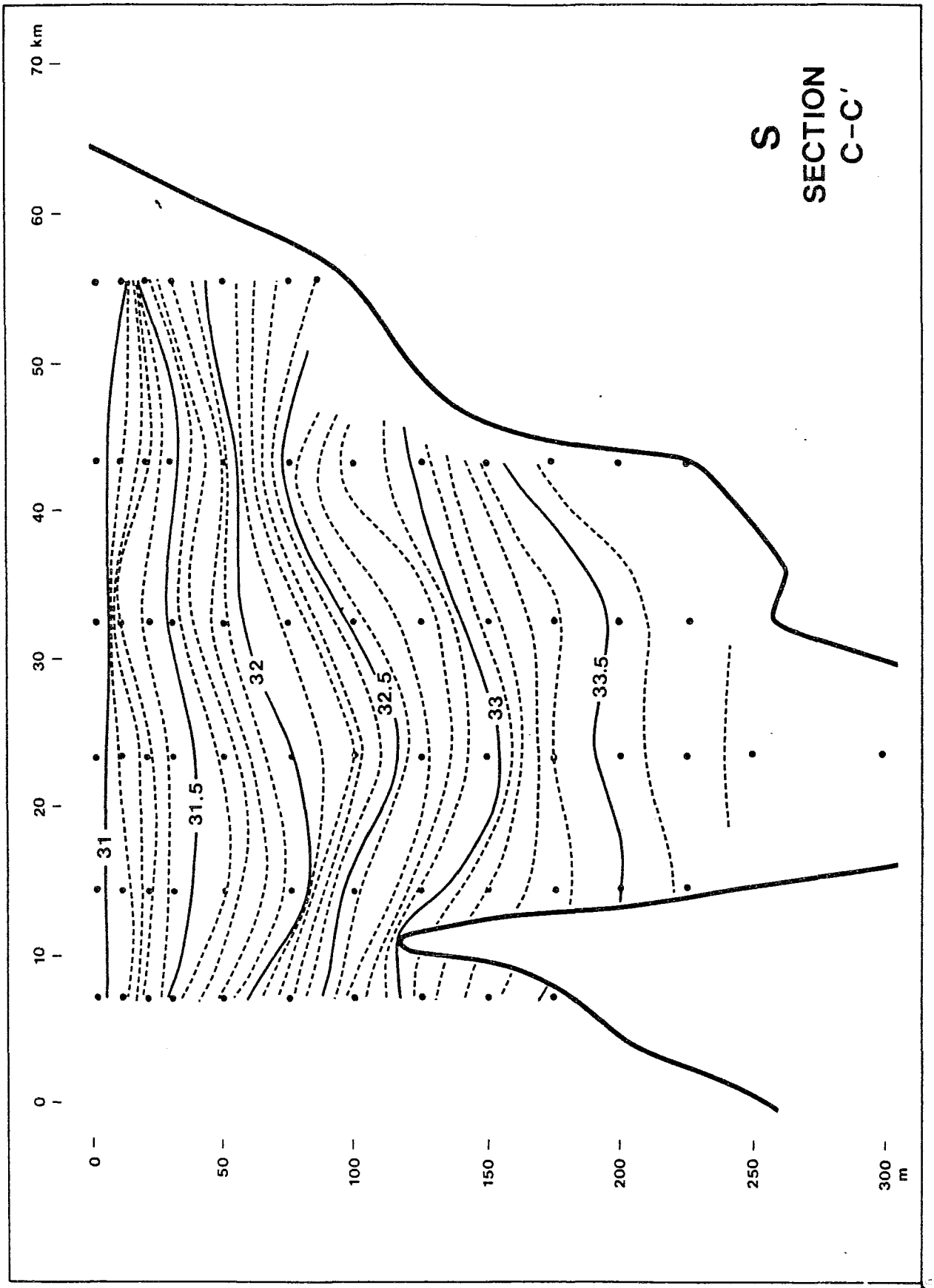

DOBROCKY
SEATECH

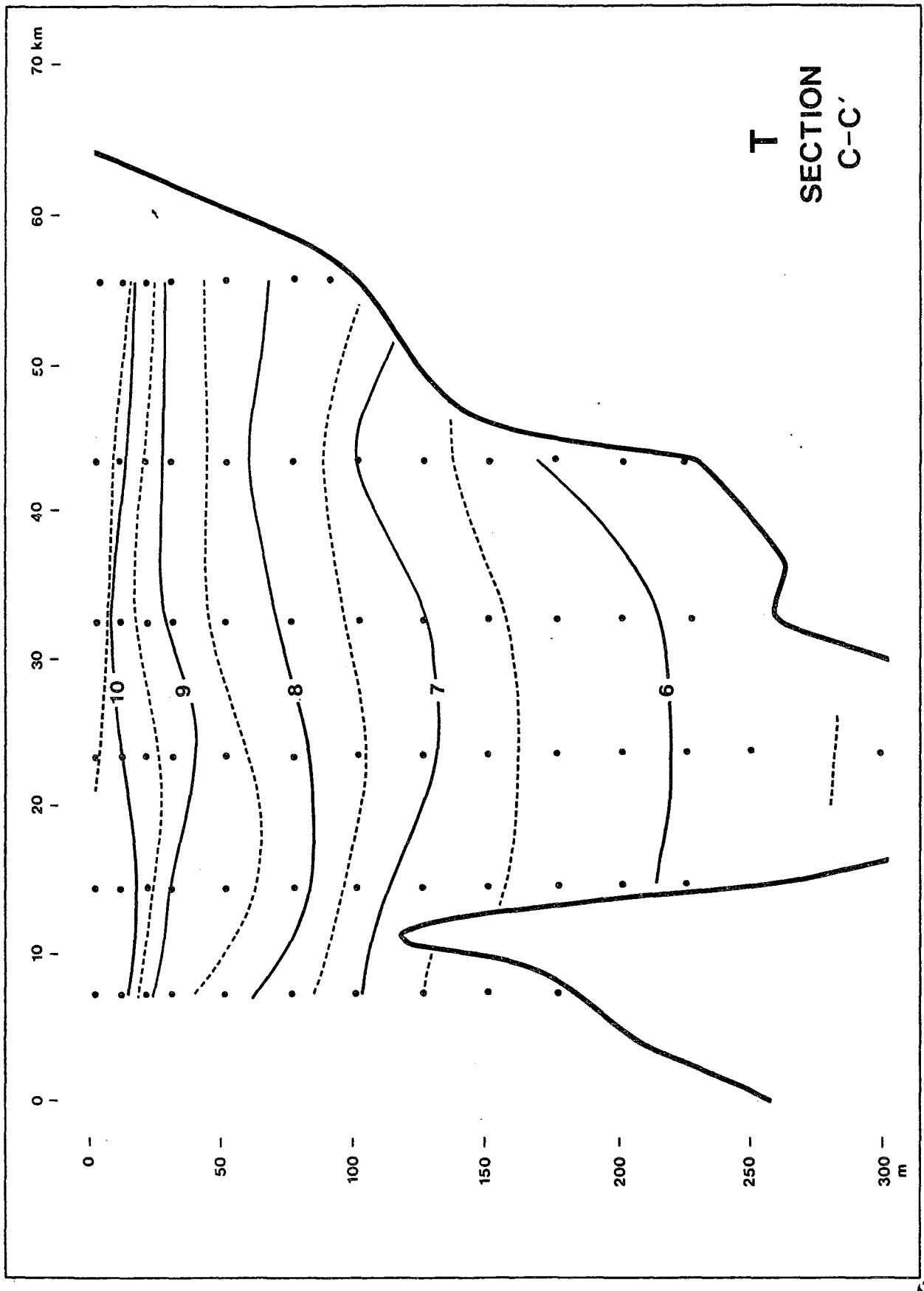

DOBROCKY
SEATECH

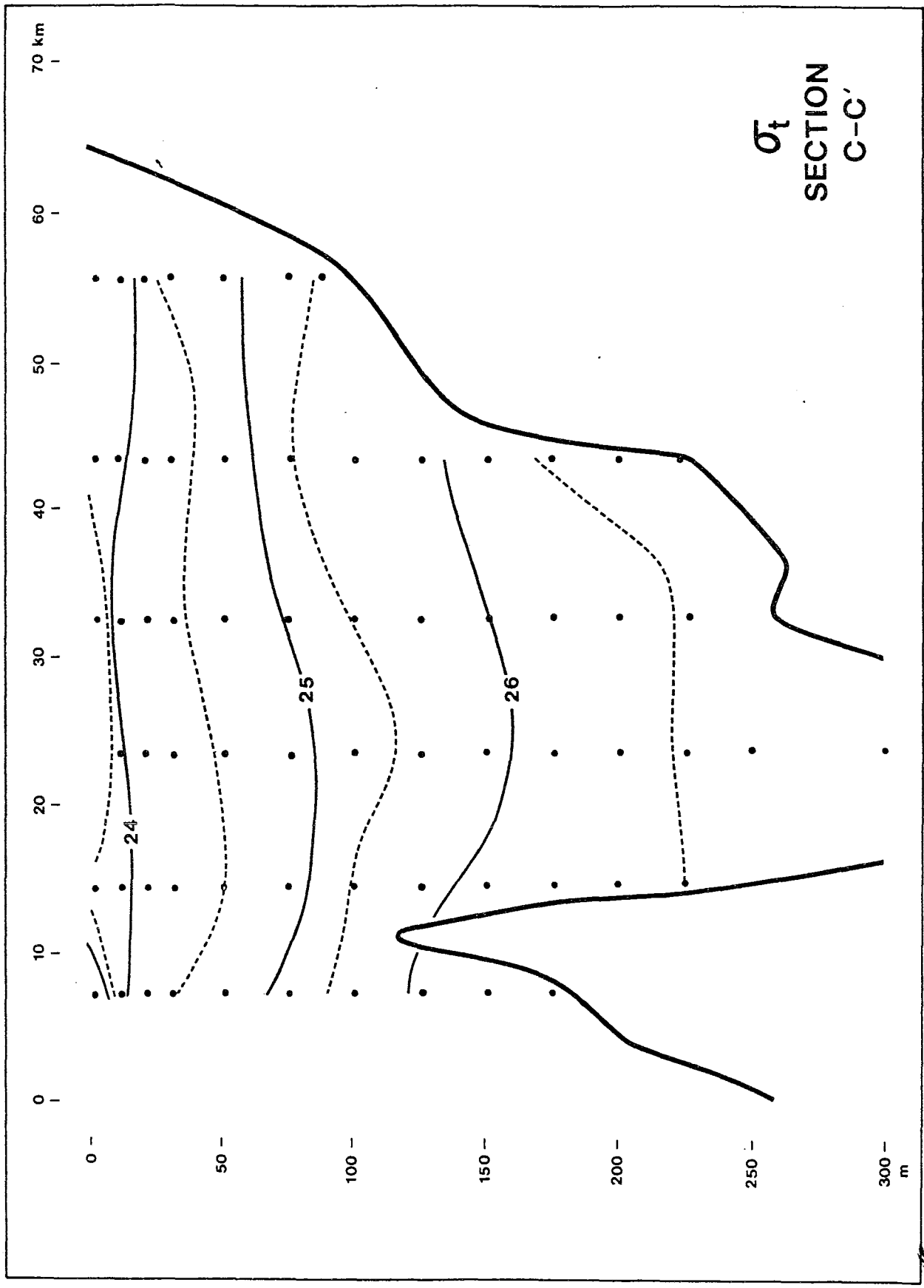

DOBROCKY SEATECH

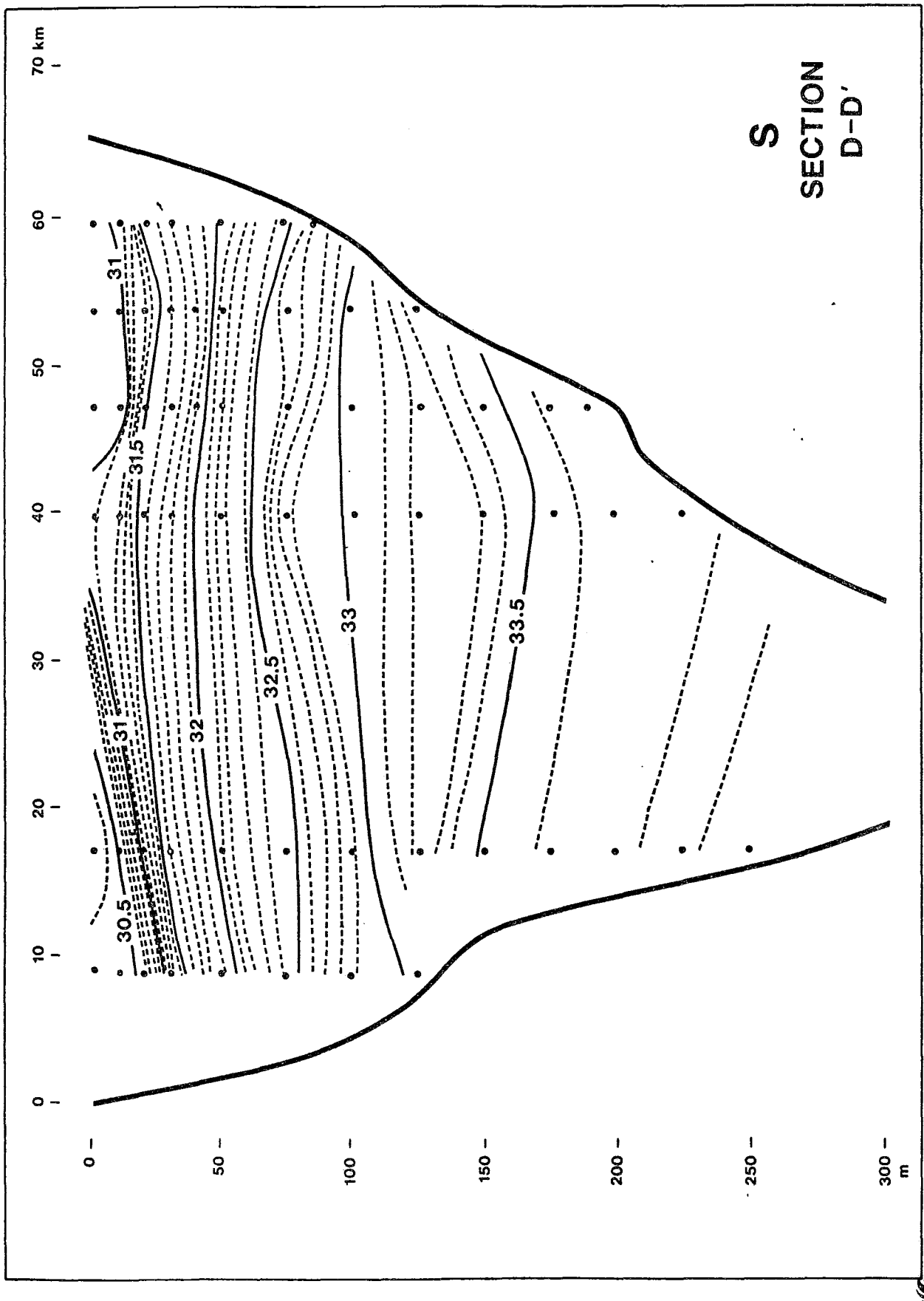

DOBROCKY SEATECH

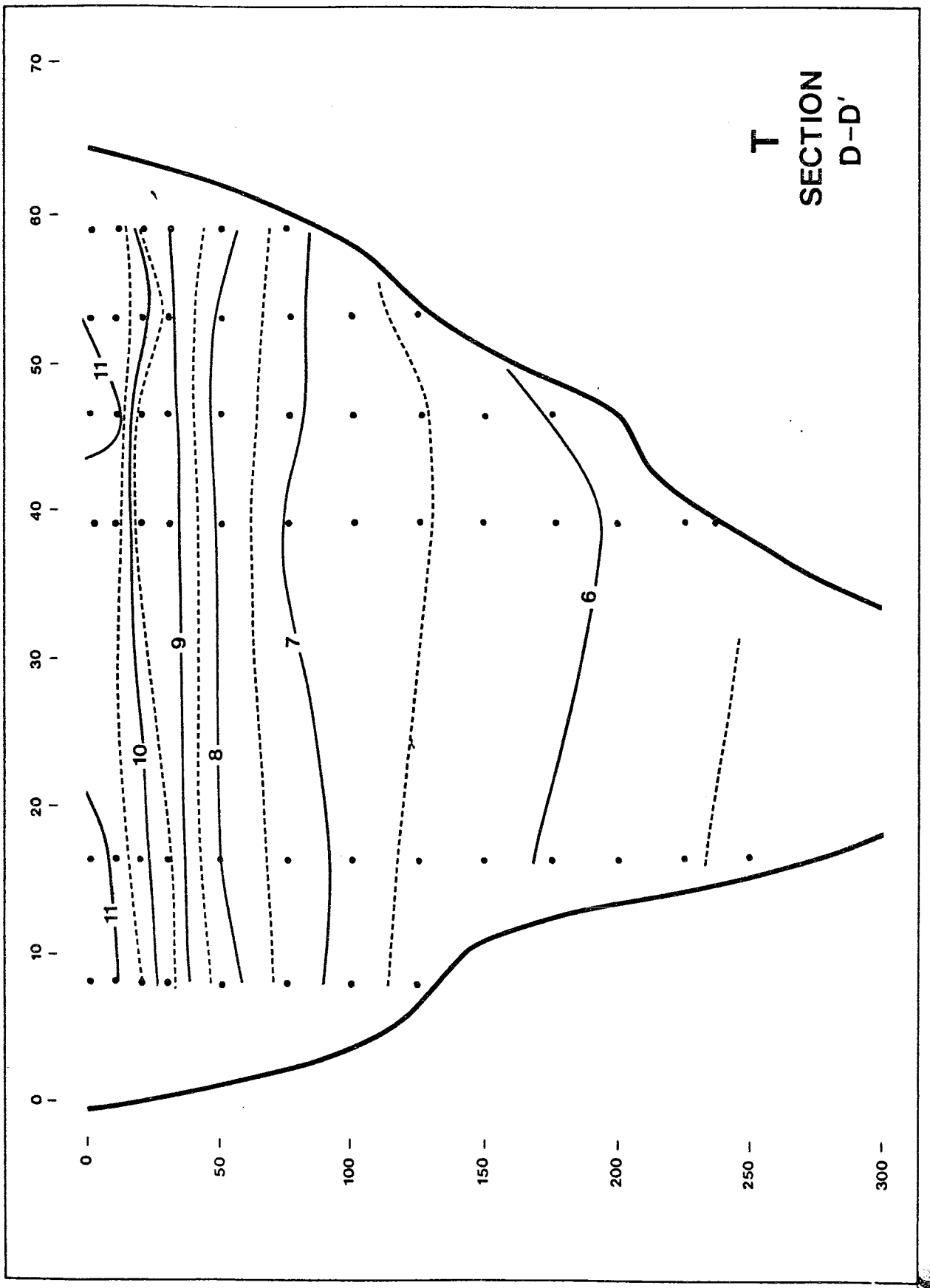

DOBROCKY
SEATECH

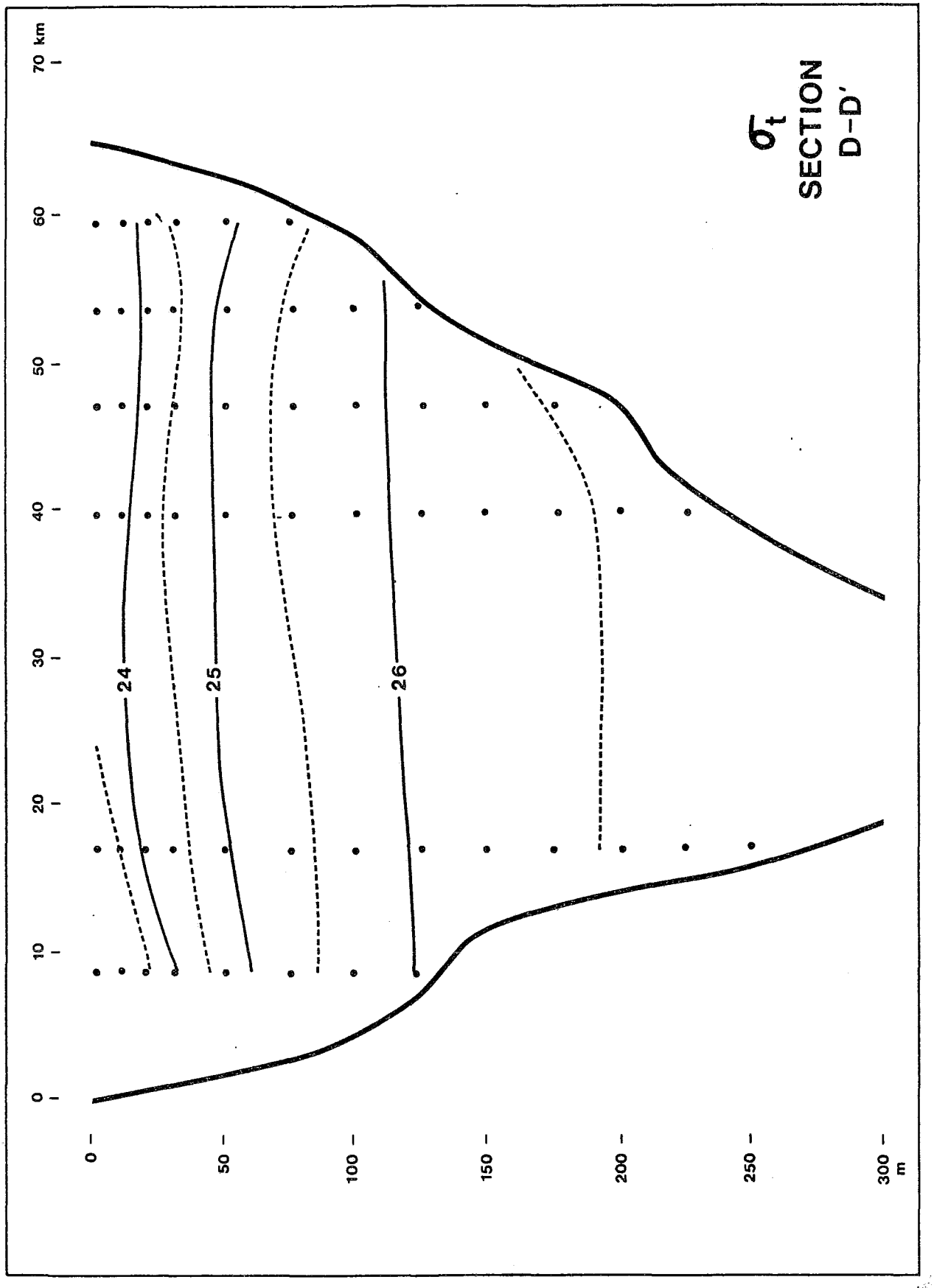

DOBROCKY
SEATECH

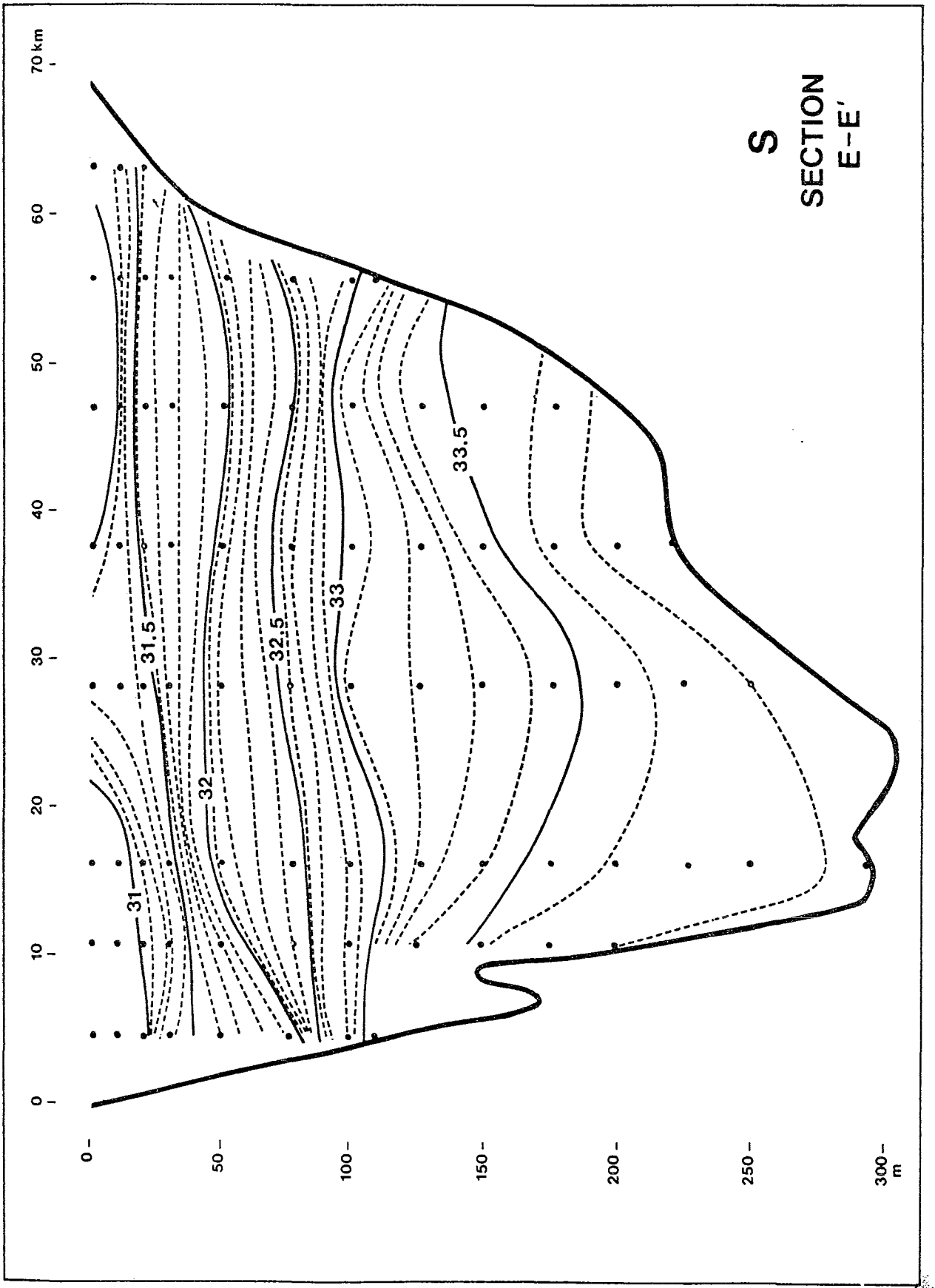

DOBROCKY
SEATECH

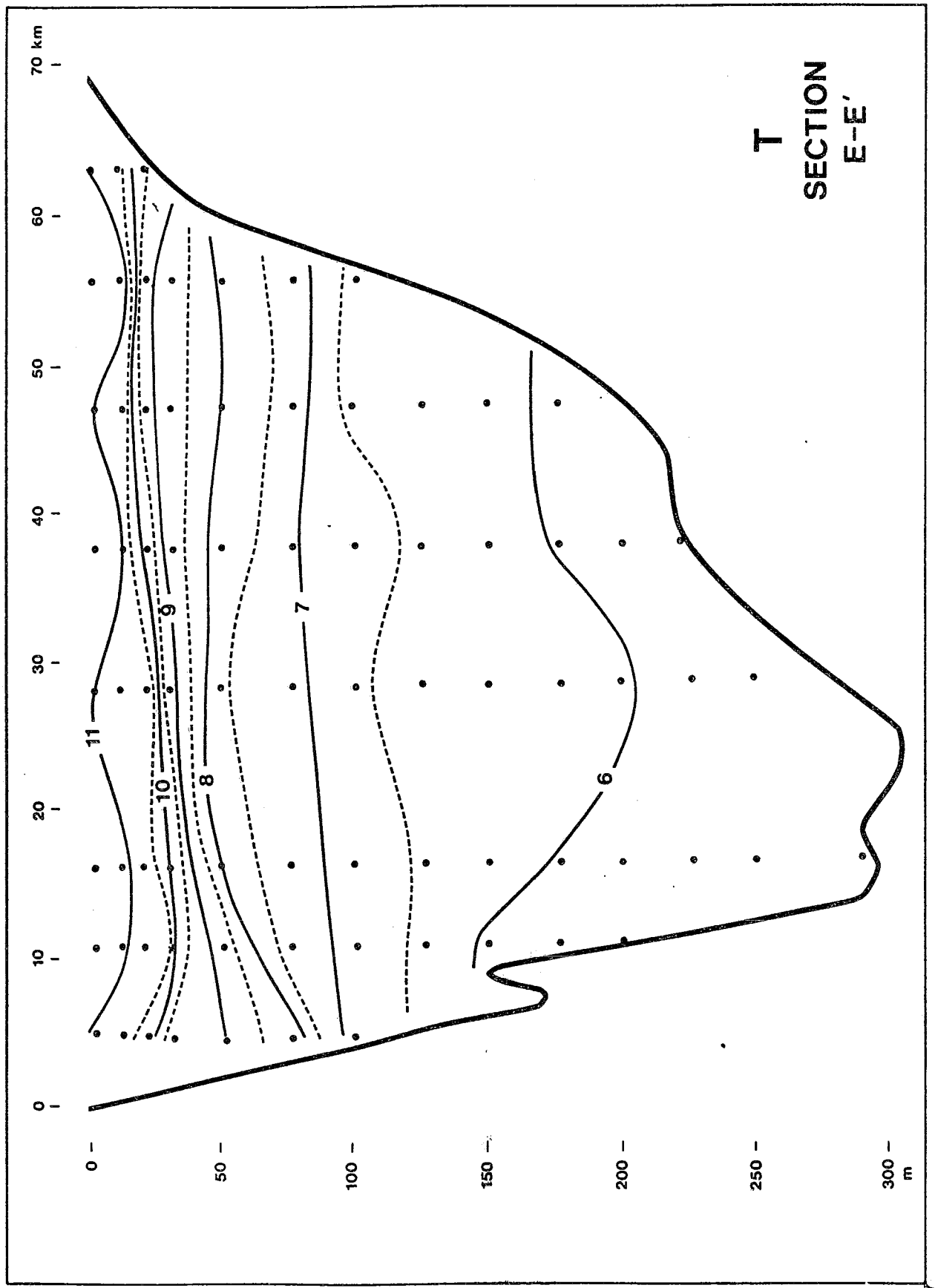

DOBROCKY
SEATECH

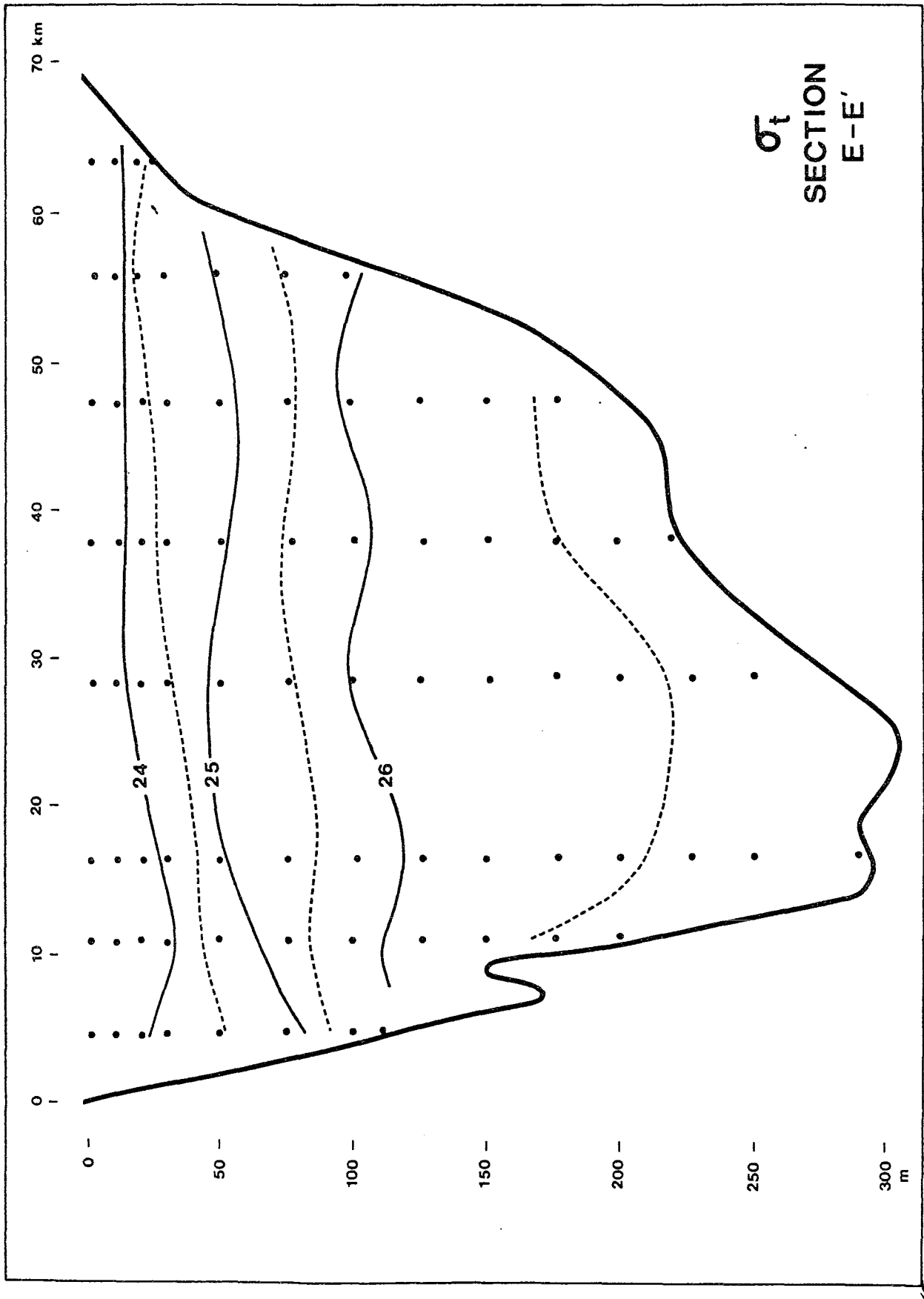

DOBROCKY SEATECH

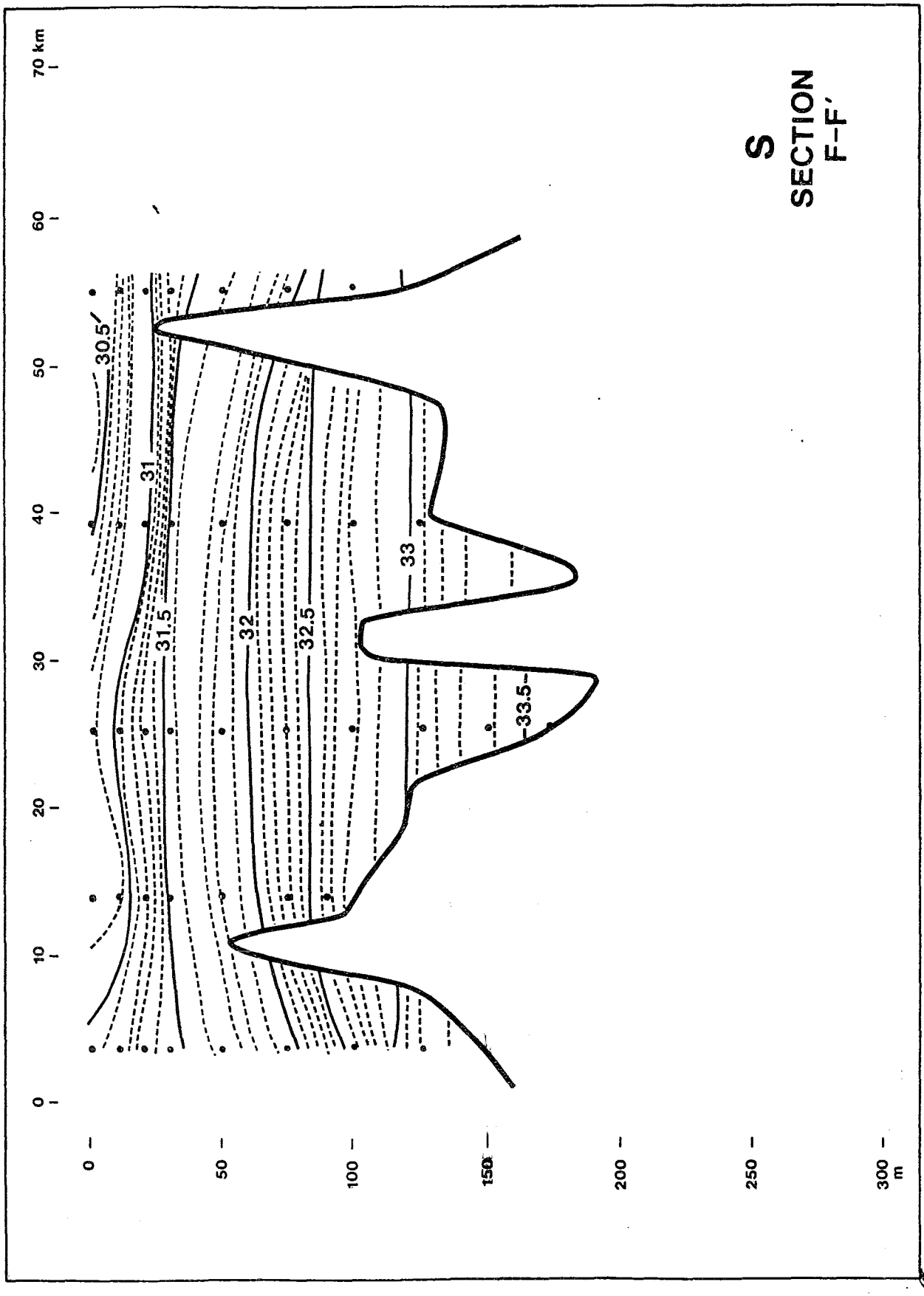

DOBROCKY
SEATECH

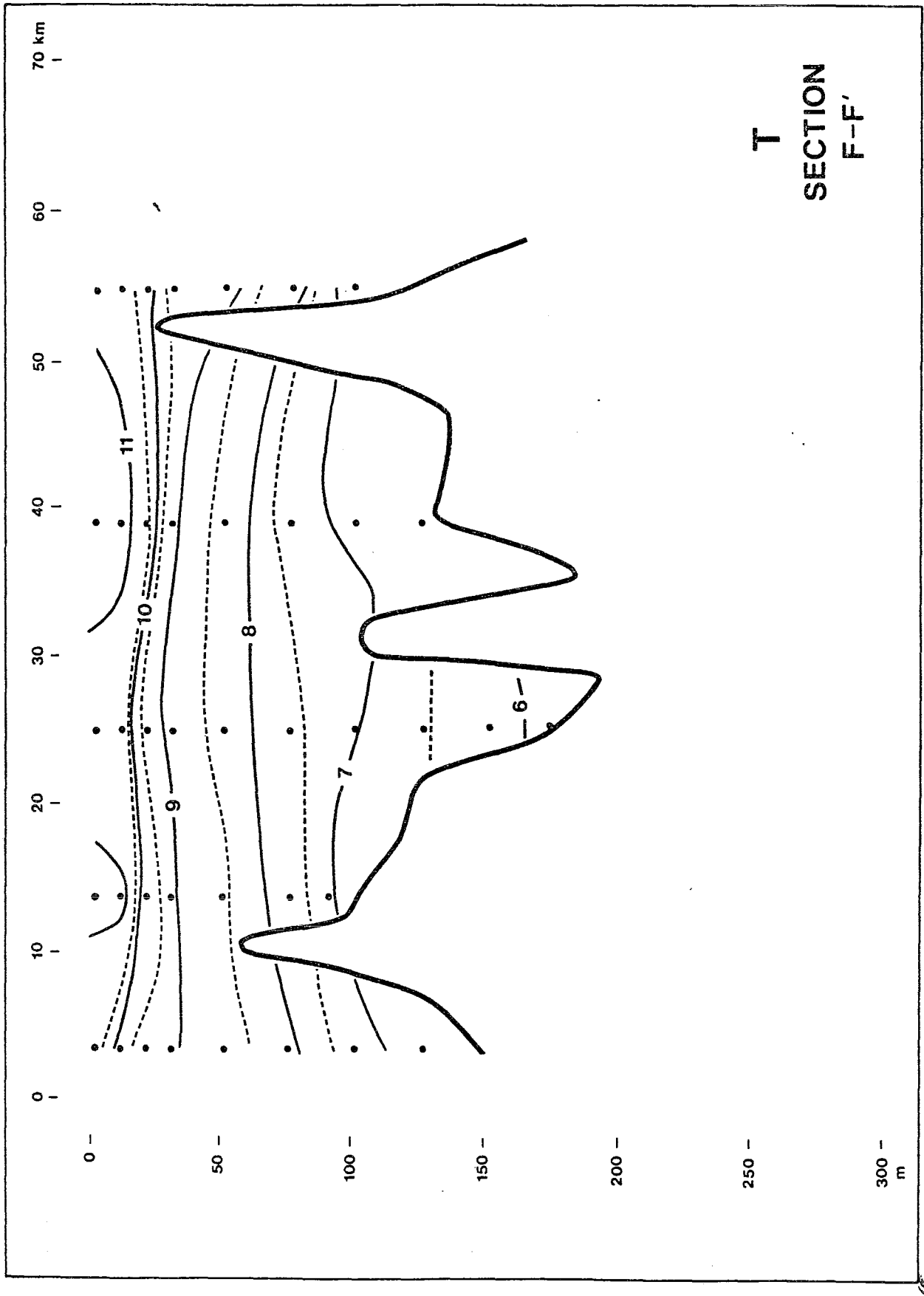

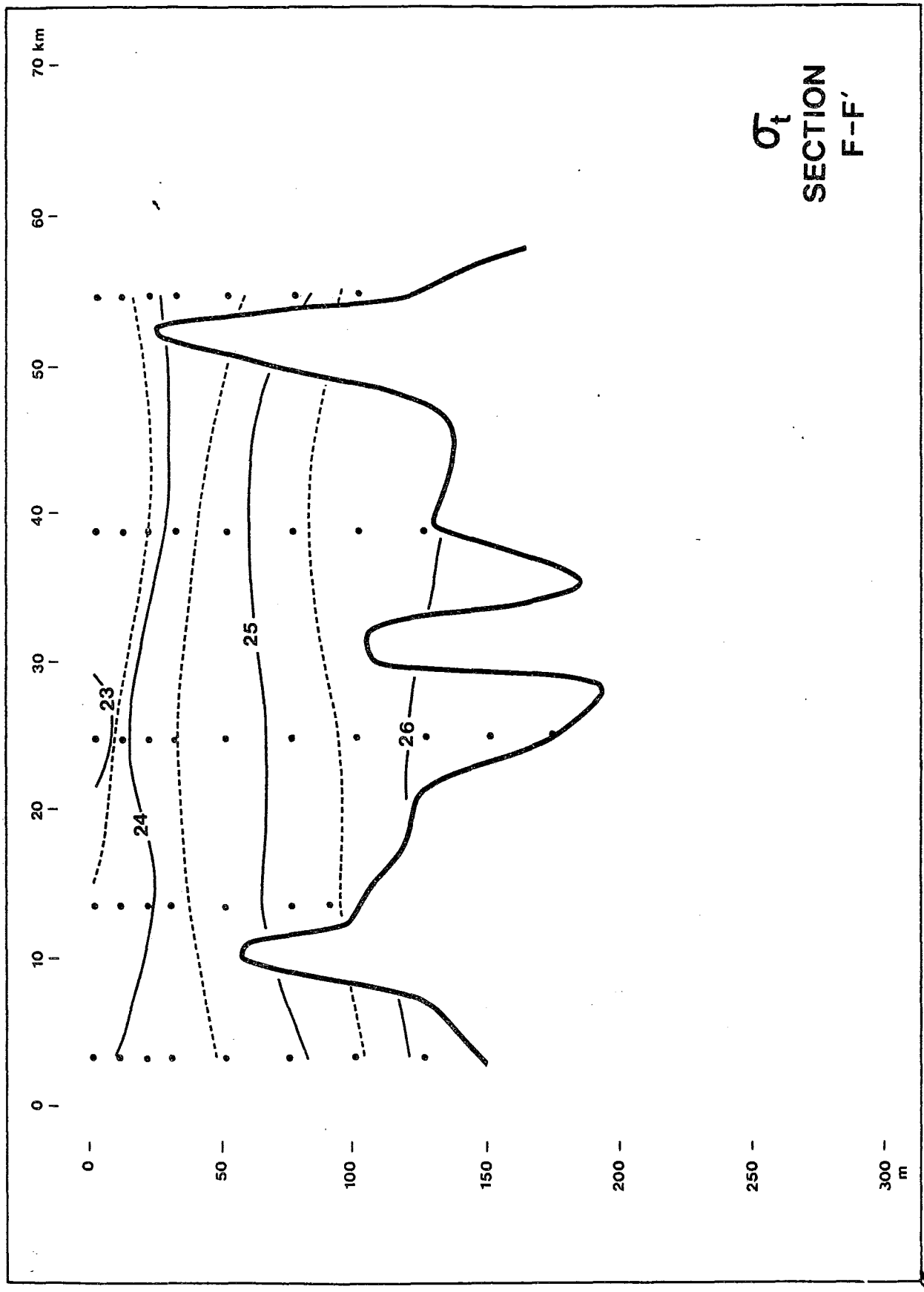

DOBROCKY
SEATECH

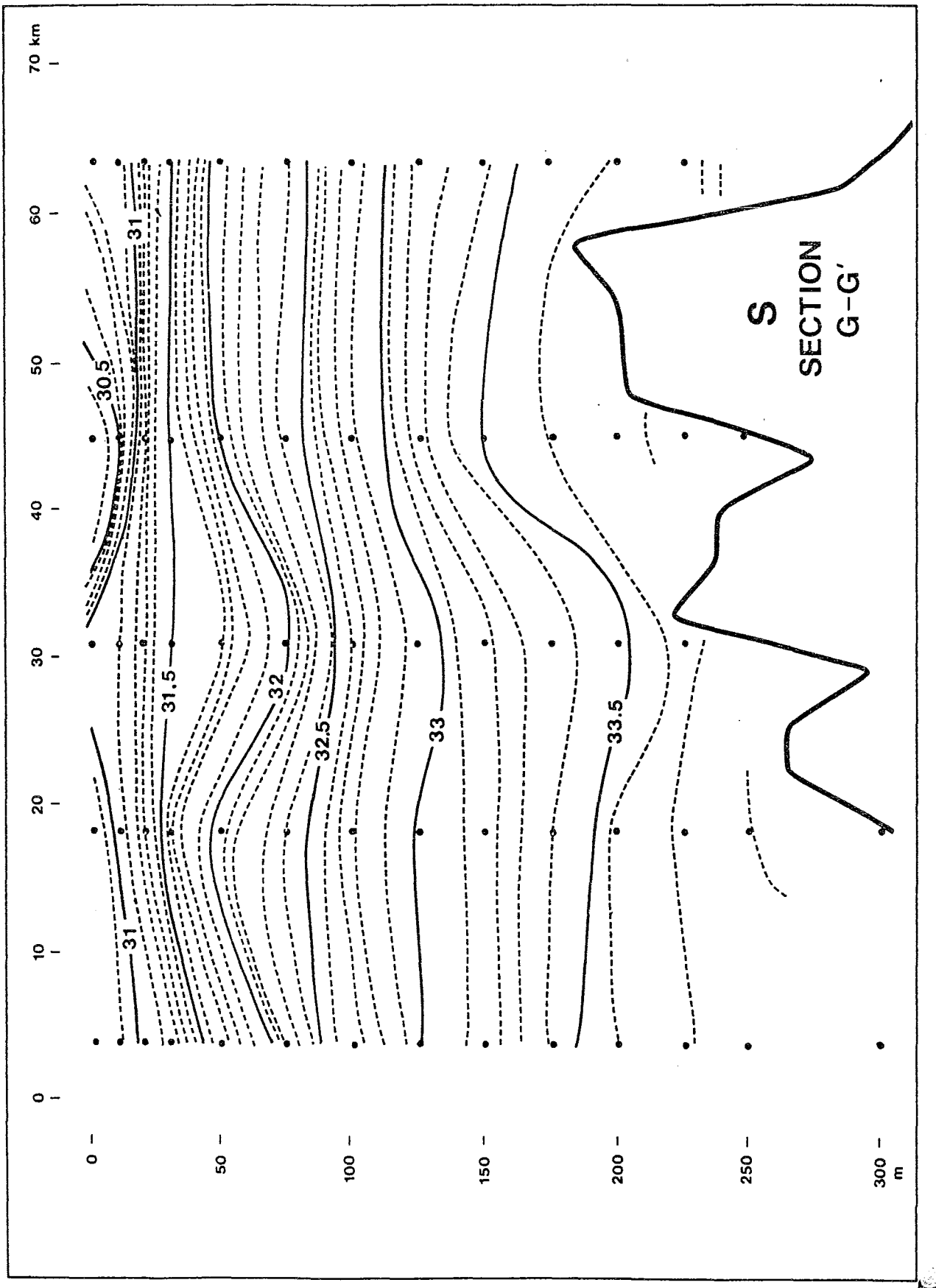

DOBROCKY
SEATECH

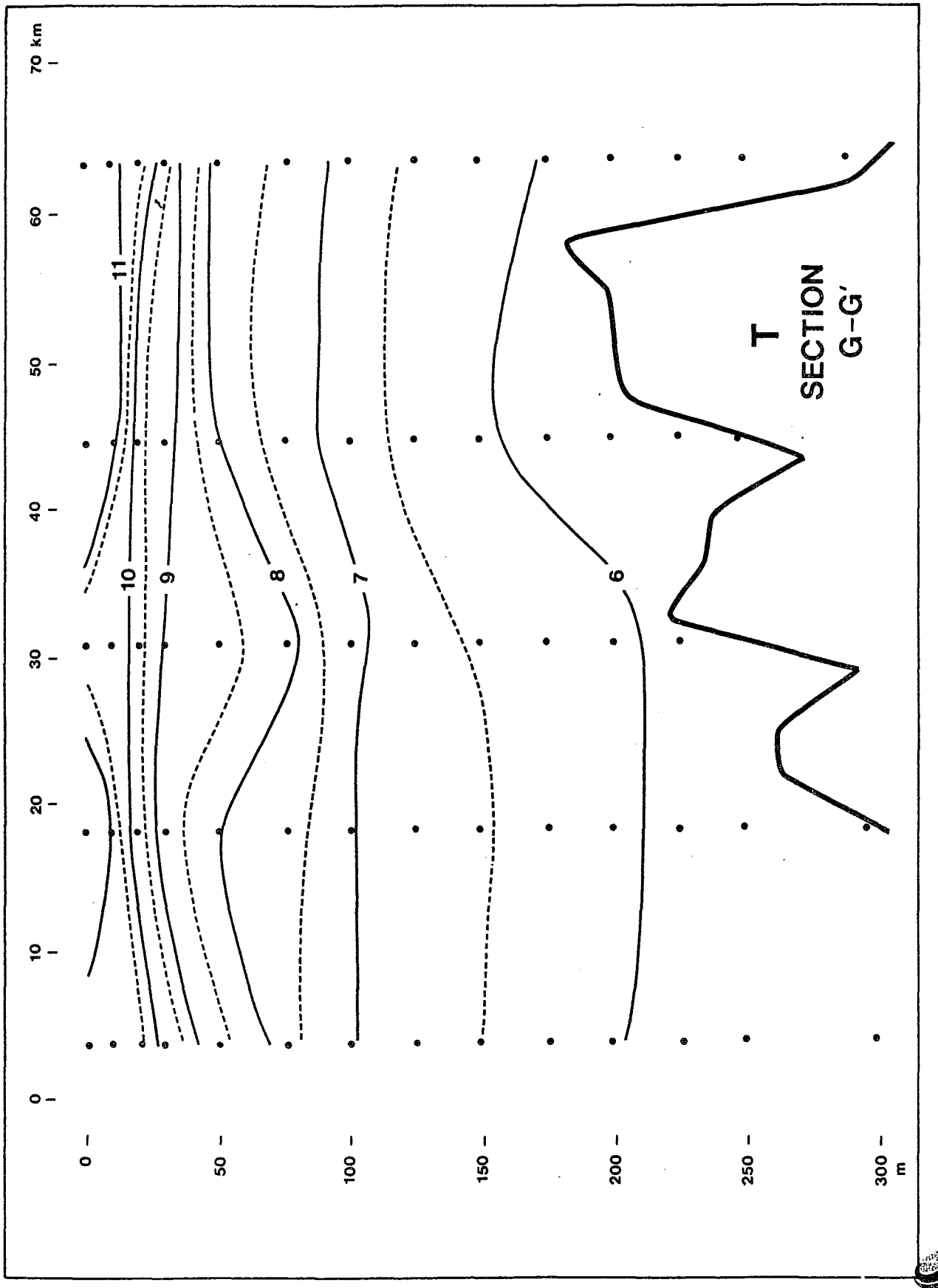

DOBROCKY
SEATECH

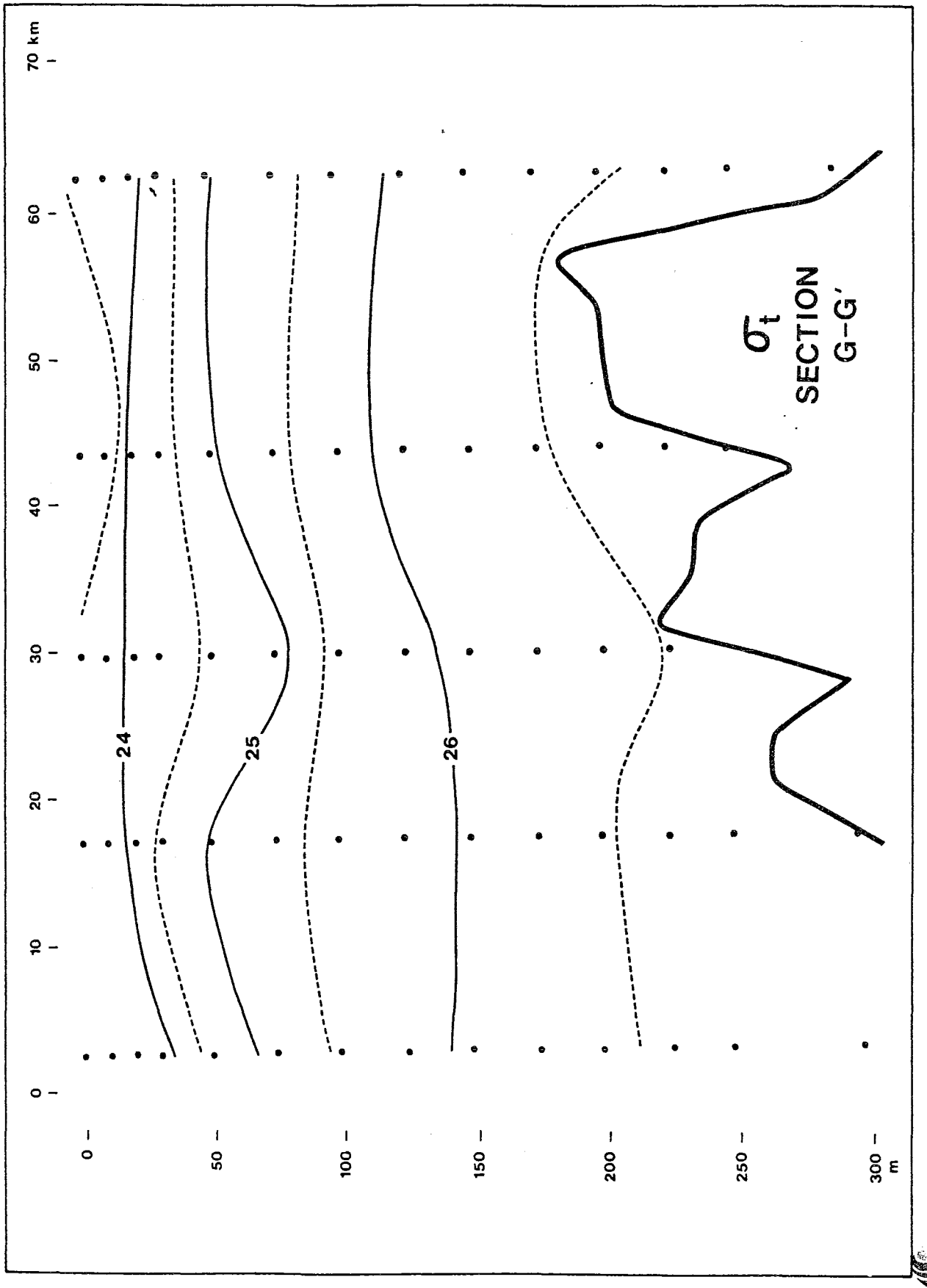

DOBROCKY
SEATECH

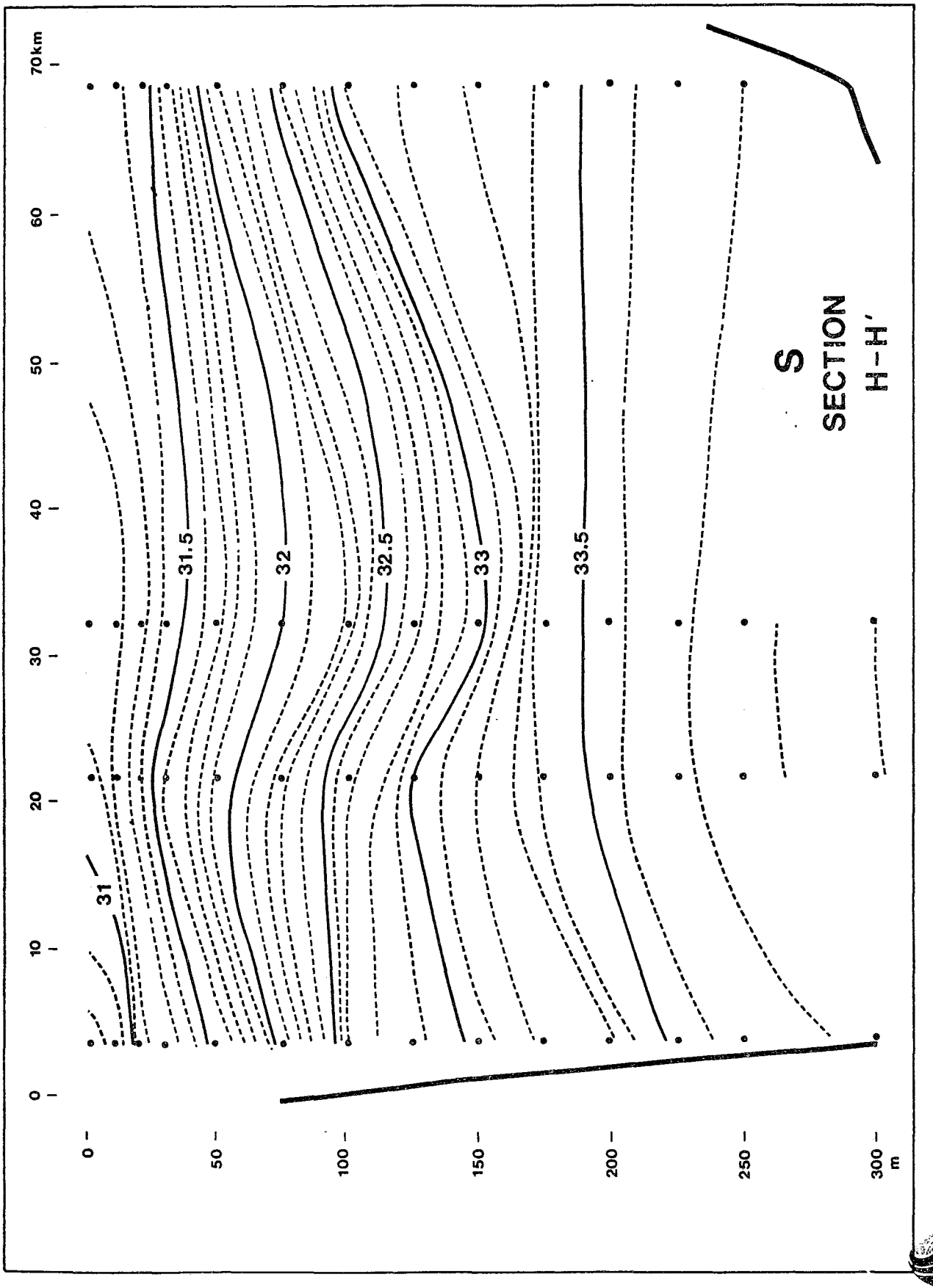

DOBROCKY
SEATECH

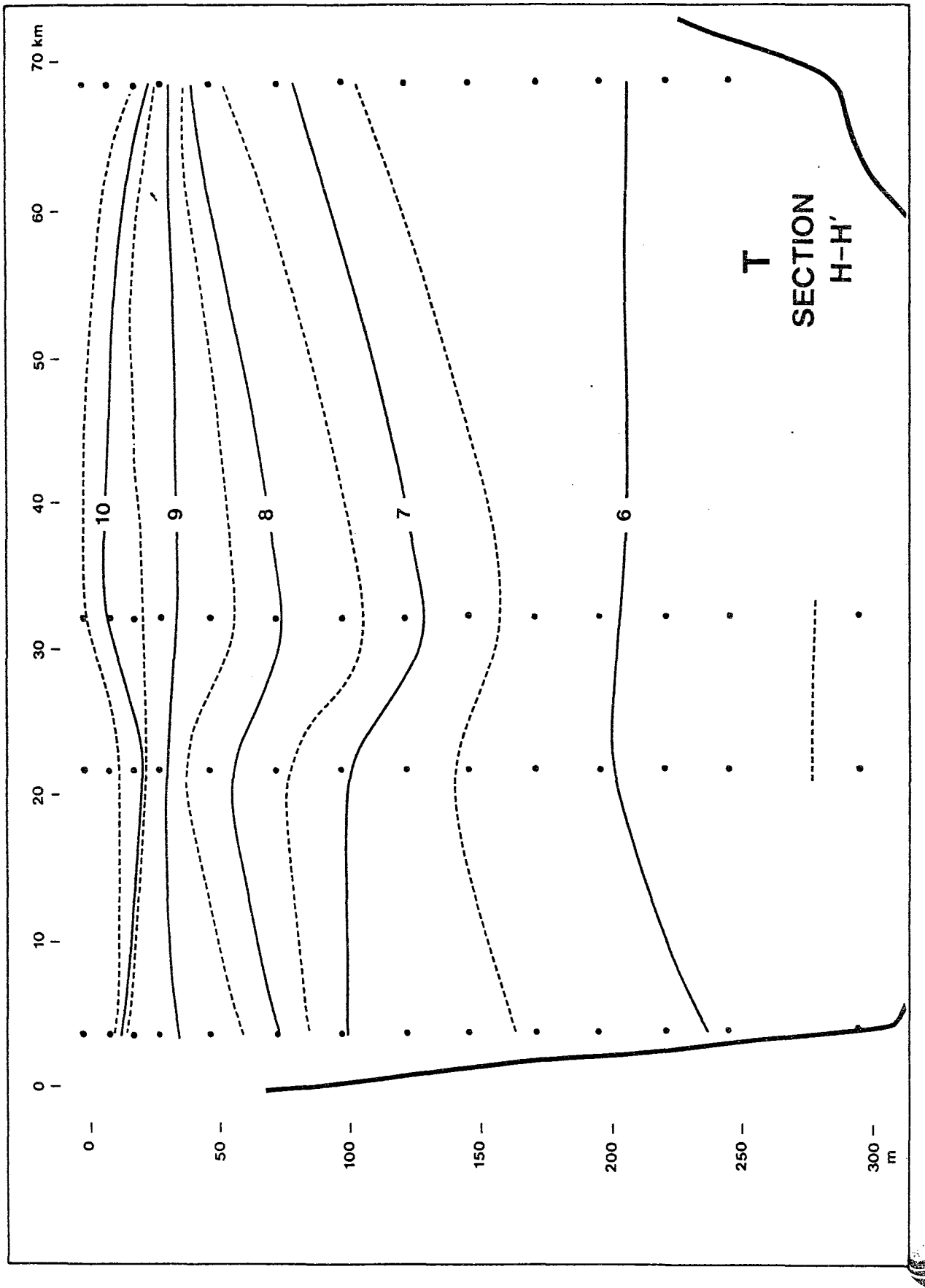

DOBROCKY
SEATECH

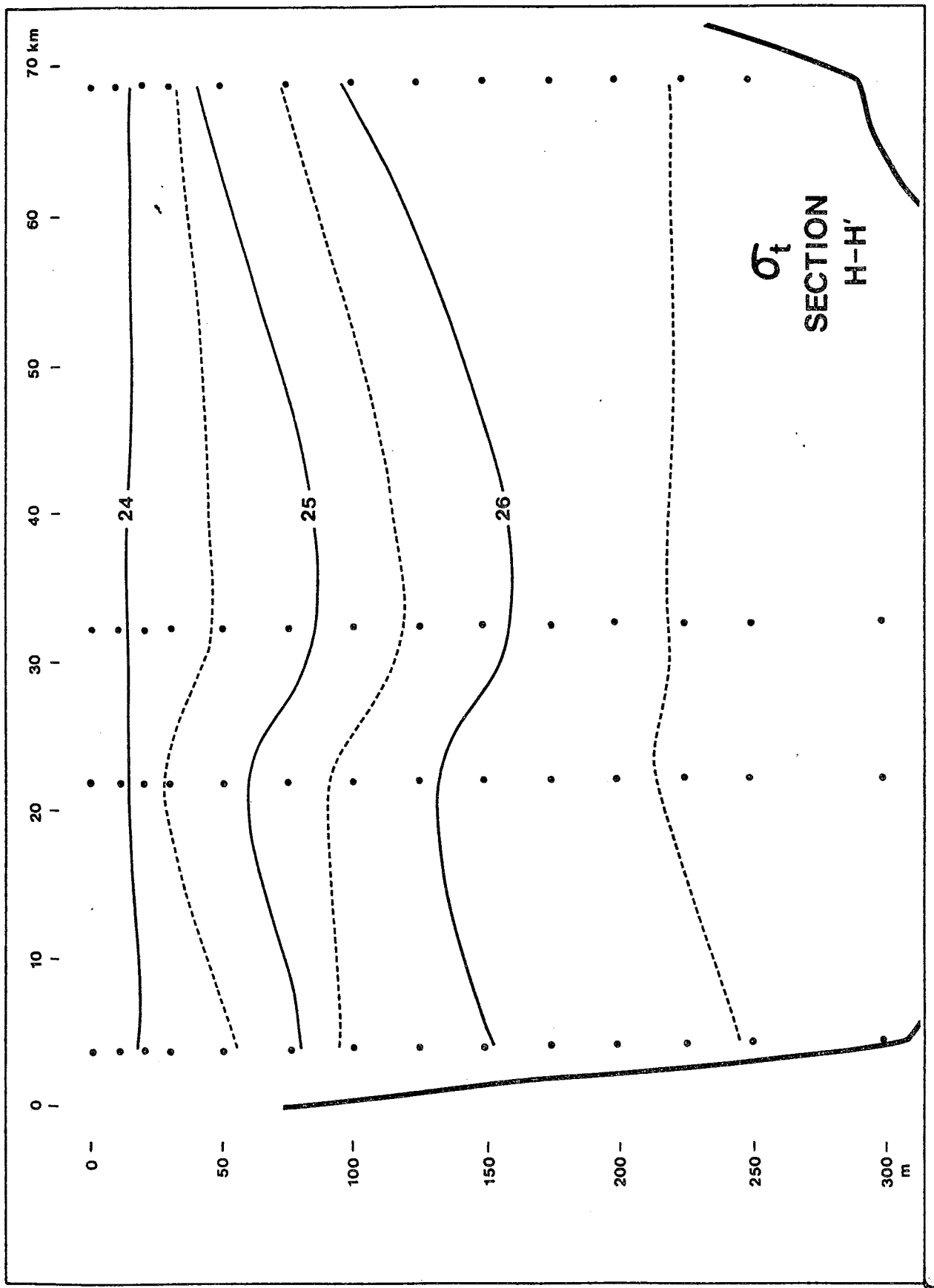

DOBROCKY
SEATECH

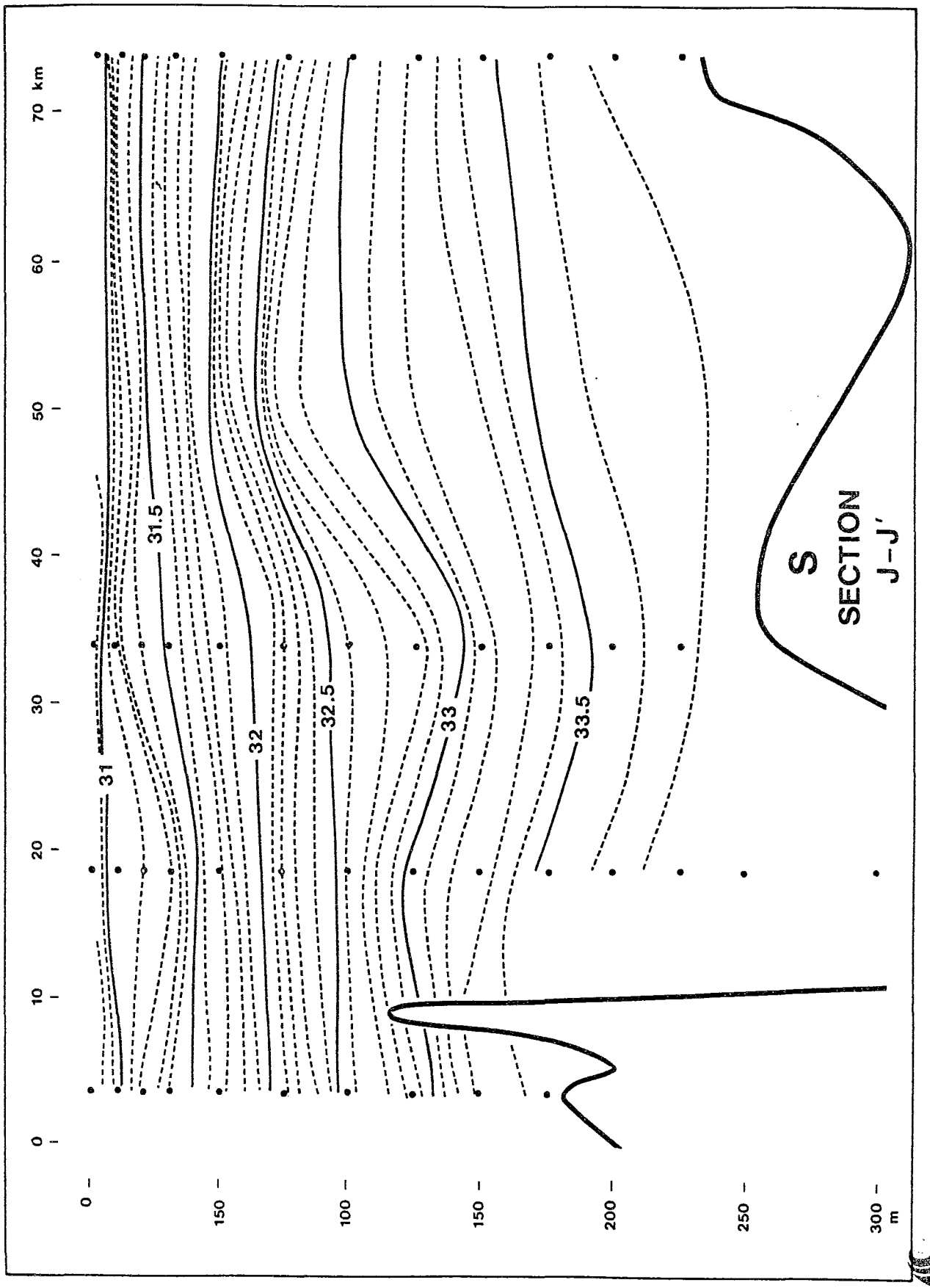

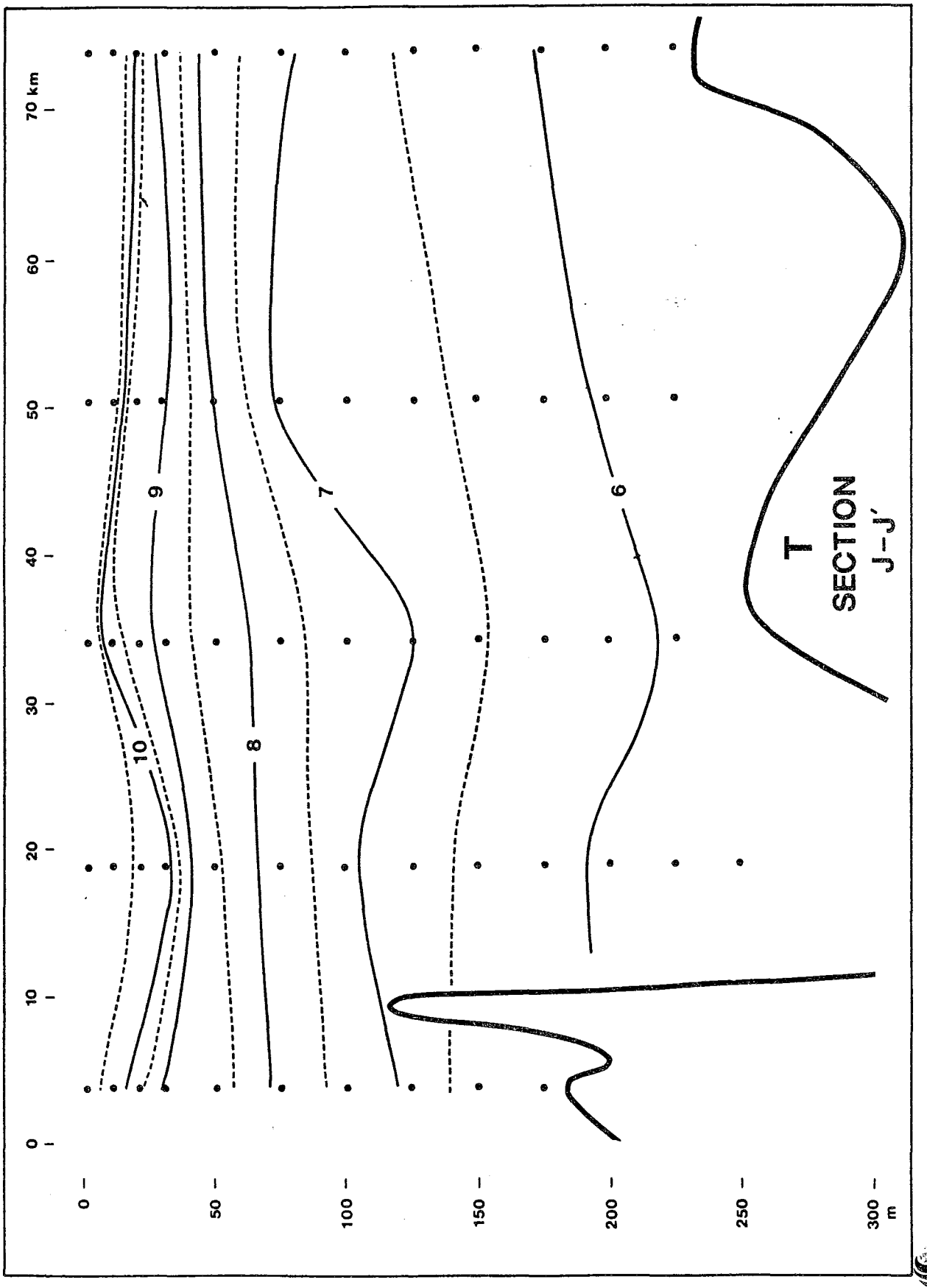

DOBROCKY
SEATECH

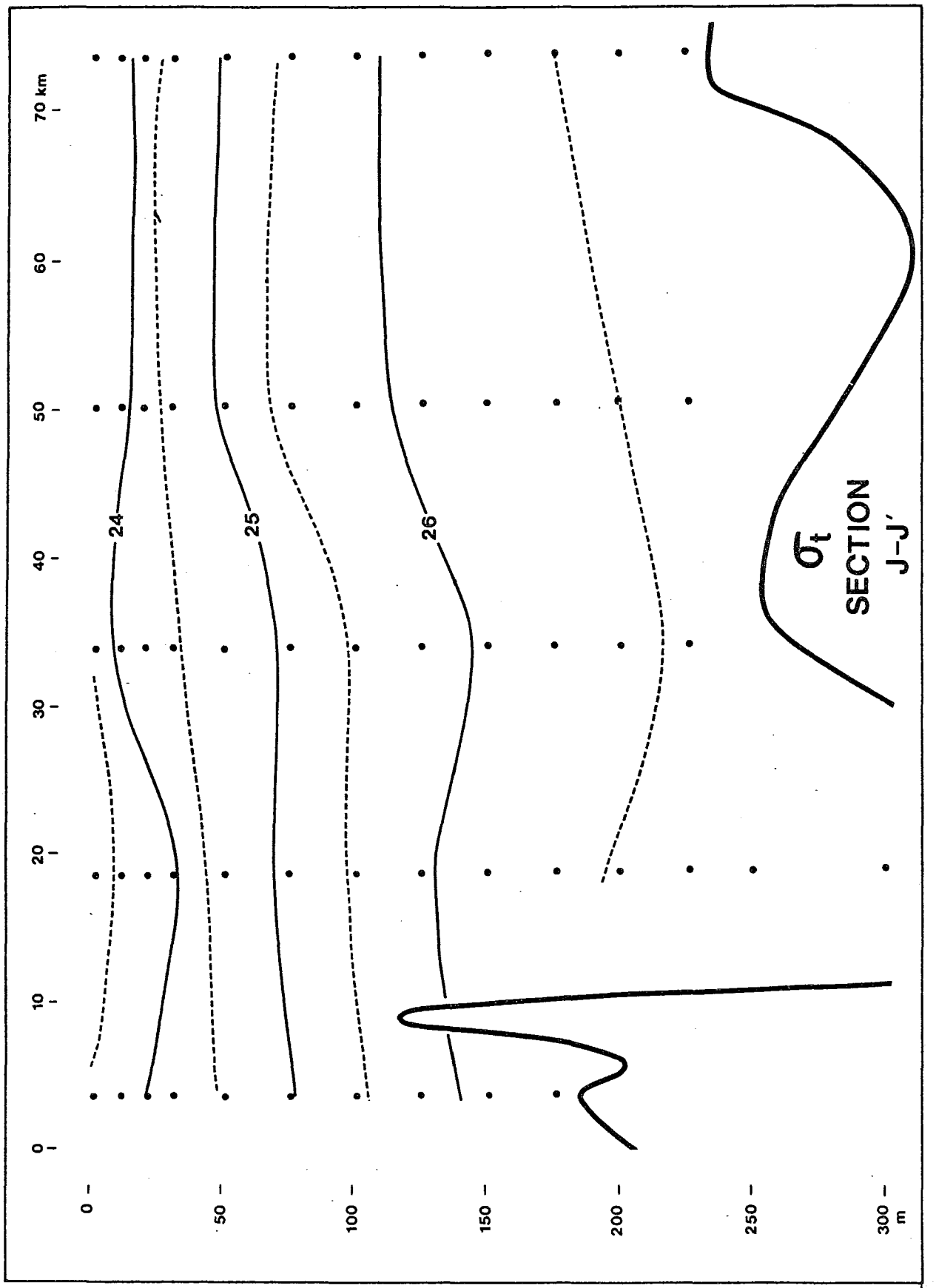

DOBROCKY
SEATECH

THIS PAGE IS BLANK

Tidal Stream Analyses, Drifters

Appendix 2

ANALYSIS RESULTS IN CURRENT ELLIPSE FORM
DATA IS ASSUMED TO BE UNFILTERED

STN: TRACK#1 LAT: 54 30 0.0 N
DEPTH: 0 M LONG: 132 30 0.0 W
START: 2300Z 12/ 6/84 END: 600Z 14/ 6/84

	NAME	FREQUENCY (CY/HR)	MAJOR (CM/S)	MINOR (CM/S)	INC	G	G+	G-	
1	Z0	0.00000000	25.792	0.000	0.7	180.0	179.3	180.7	
2	O1	0.03873065	2.528	-0.418	44.2	171.0	126.8	215.2	INF FR K1
3	K1	0.04178075	4.213	-0.697	44.2	179.0	134.8	223.2	
4	M2	0.08051139	30.631	5.395	30.0	116.9	86.9	147.0	
5	S2	0.08333331	9.802	1.726	30.0	140.9	110.9	171.0	INF FR M2
6	M3	0.12076712	7.523	-0.940	95.4	70.6	335.2	166.0	
7	M4	0.16102278	5.652	0.147	87.6	333.1	245.5	60.6	
8	2MK5	0.20280355	1.886	-0.554	156.8	271.0	114.2	67.9	
9	M6	0.24153417	3.160	0.857	30.7	192.4	161.8	223.1	
10	3MK7	0.28331494	2.234	0.079	156.4	16.8	220.4	173.2	
11	M8	0.32204562	2.210	-0.635	83.4	60.6	337.2	144.0	

DOBROCKY
SEATECH

ANALYSIS RESULTS IN CURRENT ELLIPSE FORM
DATA IS ASSUMED TO BE UNFILTERED

STN: TRACK#2 LAT: 54 30 0.0 N
DEPTH: 0 M LONG: 132 30 0.0 W
START: 2200Z 12/ 6/84 END: 1300Z 16/ 6/84

	NAME	FREQUENCY (CY/HR)	MAJOR (CM/S)	MINOR (CM/S)	INC	G	G+	G-	
1	Z0	0.00000000	7.562	0.000	45.6	180.0	134.4	225.6	
2	O1	0.03873065	6.343	-0.329	14.0	95.4	81.5	109.4	INF FR K1
3	K1	0.04178075	10.572	-0.549	14.0	103.4	89.5	117.4	
4	M2	0.08051139	52.437	-7.916	9.8	110.0	100.2	119.8	
5	S2	0.08333331	16.780	-2.533	9.8	134.0	124.2	143.8	INF FR M2
6	M3	0.12076712	2.154	-0.978	93.5	236.7	143.2	330.2	
7	M4	0.16102278	1.747	-1.068	15.6	137.2	121.6	152.8	
8	2MK5	0.20280355	1.259	-0.555	91.0	68.5	337.5	159.5	
9	M6	0.24153417	3.417	-0.318	9.7	149.8	140.0	159.5	
10	3MK7	0.28331494	1.311	-0.257	27.9	219.6	191.8	247.5	
11	M8	0.32204562	2.355	-0.587	167.8	207.0	39.2	14.8	

ANALYSIS RESULTS IN CURRENT ELLIPSE FORM
DATA IS ASSUMED TO BE UNFILTERED

STN: TRACK#3 LAT: 54 30 0.0 N
DEPTH: 0 M LONG: 132 30 0.0 W
START: 600Z 14/ 6/84 END: 2100Z 15/ 6/84

	NAME	FREQUENCY (CY/HR)	MAJOR (CM/S)	MINOR (CM/S)	INC	G	G+	G-	
1	Z0	0.00000000	11.721	0.000	73.1	180.0	106.9	253.1	
2	O1	0.03873065	4.986	-1.069	177.5	253.1	75.6	70.6	INF FR K1
3	K1	0.04178075	8.310	-1.782	177.5	261.1	83.6	78.6	
4	M2	0.08051139	37.691	-12.295	43.1	130.8	87.7	173.9	
5	S2	0.08333331	12.061	-3.934	43.1	154.8	111.7	197.9	INF FR M2
6	M3	0.12076712	6.694	-1.216	132.7	83.5	310.8	216.2	
7	M4	0.16102278	4.143	1.363	66.0	316.6	250.6	22.6	
8	2MK5	0.20280355	4.007	-1.017	121.9	109.4	347.5	231.4	
9	M6	0.24153417	2.437	-0.773	10.0	237.8	227.8	247.7	
10	3MK7	0.28331494	2.972	0.147	134.5	289.7	155.2	64.2	
11	M8	0.32204562	2.014	0.700	73.1	39.6	326.5	112.8	

DOBROCKY
SEATECH

ANALYSIS RESULTS IN CURRENT ELLIPSE FORM
DATA IS ASSUMED TO BE UNFILTERED

STN: TRACK#4 LAT: 54 30 0.0 N
DEPTH: 0 M LONG: 132 30 0.0 W
START: 2300Z 14/ 6/84 END: 2000Z 16/ 6/84

	NAME	FREQUENCY (CY/HR)	MAJOR (CM/S)	MINOR (CM/S)	INC	G	G+	G-	
1	Z0	0.00000000	20.939	0.000	72.5	180.0	107.5	252.5	
2	O1	0.03873065	3.229	1.304	122.0	287.6	165.6	49.6	INF FR K1
3	K1	0.04178075	5.382	2.174	122.0	295.6	173.6	57.6	
4	M2	0.08051139	51.999	-21.406	26.0	113.0	87.0	139.0	
5	S2	0.08333331	16.640	-6.850	26.0	137.0	111.0	163.0	INF FR M2
6	M3	0.12076712	2.998	-0.361	158.5	259.5	101.0	58.1	
7	M4	0.16102278	3.473	0.081	44.6	72.7	28.1	117.3	
8	2MK5	0.20280355	4.950	-0.571	14.2	142.7	128.5	156.9	
9	M6	0.24153417	5.114	1.080	168.1	8.1	200.0	176.2	
10	3MK7	0.28331494	2.287	0.800	6.6	278.0	271.4	284.7	
11	M8	0.32204562	1.347	0.455	56.1	13.7	317.6	69.7	

ANALYSIS RESULTS IN CURRENT ELLIPSE FORM
DATA IS ASSUMED TO BE UNFILTERED

STN: TRACK#5 LAT: 54 30 0.0 N
DEPTH: 0 M LONG: 132 30 0.0 W
START: 200Z 15/ 6/84 END: 300Z 18/ 6/84

	NAME	FREQUENCY (CY/HR)	MAJOR (CM/S)	MINOR (CM/S)	INC	G	G+	G-	
1	Z0	0.00000000	8.716	0.000	125.6	180.0	54.4	305.6	
2	O1	0.03873065	4.350	-0.218	9.7	113.7	104.0	123.4	INF FR K1
3	K1	0.04178075	7.250	-0.363	9.7	121.7	112.0	131.4	
4	M2	0.08051139	27.821	-9.834	49.0	134.4	85.4	183.4	
5	S2	0.08333331	8.903	-3.147	49.0	158.4	109.4	207.4	INF FR M2
6	M3	0.12076712	2.728	0.217	36.6	254.2	217.6	290.8	
7	M4	0.16102278	2.204	1.235	59.1	247.2	188.1	306.3	
8	2MK5	0.20280355	1.598	0.120	137.5	68.5	291.0	206.0	
9	M6	0.24153417	1.326	-0.178	68.4	225.2	156.8	293.6	
10	3MK7	0.28331494	1.199	-0.882	89.6	58.3	328.7	147.9	
11	M8	0.32204562	1.683	-0.606	100.8	204.9	104.0	305.7	

ANALYSIS RESULTS IN CURRENT ELLIPSE FORM
DATA IS ASSUMED TO BE UNFILTERED

STN: TRACK#6 LAT: 54 30 0.0 N
DEPTH: 0 M LONG: 132 30 0.0 W
START: 1200Z 16/ 6/84 END: 1300Z 18/ 6/84

	NAME	FREQUENCY (CY/HR)	MAJOR (CM/S)	MINOR (CM/S)	INC	G	G+	G-	
1	Z0	0.00000000	9.622	0.000	16.2	360.0	343.8	16.2	
2	O1	0.03873065	3.739	-0.591	168.5	310.4	141.9	118.9	INF FR K1
3	K1	0.04178075	6.232	-0.985	168.5	318.4	149.9	126.9	
4	M2	0.08051139	19.233	7.367	163.8	255.9	92.1	59.7	
5	S2	0.08333331	6.155	2.357	163.8	279.9	116.1	83.7	INF FR M2
6	M3	0.12076712	6.368	-2.345	94.3	294.6	200.3	28.9	
7	M4	0.16102278	1.858	-1.491	81.9	34.4	312.5	116.4	
8	2MK5	0.20280355	1.642	0.144	45.7	78.2	32.5	123.8	
9	M6	0.24153417	2.665	0.013	78.5	343.6	265.1	62.1	
10	3MK7	0.28331494	1.042	0.384	35.8	348.0	312.2	23.8	
11	M8	0.32204562	1.485	-0.648	60.0	257.6	197.6	317.6	

ANALYSIS RESULTS IN CURRENT ELLIPSE FORM
DATA IS ASSUMED TO BE UNFILTERED

STN: TRACK#7 LAT: 54 30 0.0 N
DEPTH: 0 M LONG: 132 30 0.0 W
START: 200Z 16/ 6/84 END: 1000Z 17/ 6/84

	NAME	FREQUENCY (CY/HR)	MAJOR (CM/S)	MINOR (CM/S)	INC	G	G+	G-	
1	Z0	0.00000000	19.611	0.000	165.6	360.0	194.4	165.6	
2	O1	0.03873065	6.439	-2.284	157.3	276.9	119.7	74.2	INF FR K1
3	K1	0.04178075	10.732	-3.806	157.3	284.9	127.7	82.2	
4	M2	0.08051139	34.201	-9.493	173.2	262.8	89.6	76.0	
5	S2	0.08333331	10.944	-3.038	173.2	286.8	113.6	100.0	INF FR M2
6	M3	0.12076712	4.255	0.326	16.9	295.5	278.6	312.3	
7	M4	0.16102278	2.284	-0.349	153.6	259.5	105.9	53.1	
8	2MK5	0.20280355	2.717	-0.699	148.4	129.7	341.3	278.0	
9	M6	0.24153417	1.553	-0.489	58.3	341.7	283.4	40.0	
10	3MK7	0.28331494	1.939	0.494	166.1	74.4	268.4	240.5	
11	M8	0.32204562	1.774	-0.623	176.5	244.9	68.4	61.4	

DOBROCKY SEATECH

ANALYSIS RESULTS IN CURRENT ELLIPSE FORM
DATA IS ASSUMED TO BE UNFILTERED

STN: TRACK#9 LAT: 54 30 0.0 N
DEPTH: 0 M LONG: 132 30 0.0 W
START: 2200Z 18/ 6/84 END: 1400Z 22/ 6/84

	NAME	FREQUENCY (CY/HR)	MAJOR (CM/S)	MINOR (CM/S)	INC	G	G+	G-	
1	Z0	0.00000000	13.120	0.000	4.7	180.0	175.3	184.7	
2	O1	0.03873065	2.138	-0.381	28.9	52.6	23.7	81.5	INF FR K1
3	K1	0.04178075	3.563	-0.635	28.9	60.6	31.7	89.5	
4	M2	0.08051139	26.261	-2.150	12.2	111.9	99.7	124.1	
5	S2	0.08333331	8.403	-0.688	12.2	135.9	123.7	148.1	INF FR M2
6	M3	0.12076712	1.877	-0.349	131.4	210.1	78.7	341.4	
7	M4	0.16102278	2.437	-0.782	134.8	30.3	255.5	165.0	
8	2MK5	0.20280355	1.071	0.257	142.8	174.2	31.4	317.0	
9	M6	0.24153417	1.769	-0.712	133.5	229.7	96.2	3.2	
10	3MK7	0.28331494	0.547	-0.068	66.0	43.5	337.5	109.5	
11	M8	0.32204562	1.078	-0.794	49.5	138.2	88.7	187.7	

DOBROCKY
SEATECH

ANALYSIS RESULTS IN CURRENT ELLIPSE FORM
DATA IS ASSUMED TO BE UNFILTERED

STN: TRACK#10 LAT: 54 30 0.0 N
DEPTH: 0 M LONG: 132 30 0.0 W
START: 200Z 20/ 6/84 END: 1800Z 22/ 6/84

	NAME	FREQUENCY (CY/HR)	MAJOR (CM/S)	MINOR (CM/S)	INC	G	G+	G-	
1	Z0	0.00000000	12.478	0.000	90.3	180.0	89.7	270.3	
2	O1	0.03873065	5.777	-2.303	174.5	304.7	130.2	119.2	INF FR K1
3	K1	0.04178075	9.629	-3.839	174.5	312.7	138.2	127.2	
4	M2	0.08051139	53.362	-26.276	4.1	101.8	97.7	105.8	
5	S2	0.08333331	17.076	-8.408	4.1	125.8	121.7	129.8	INF FR M2
6	M3	0.12076712	3.148	0.511	55.5	322.6	267.1	18.1	
7	M4	0.16102278	0.821	-0.278	152.7	69.6	276.9	222.4	
8	2MK5	0.20280355	1.580	-0.689	154.1	61.3	267.1	215.4	
9	M6	0.24153417	1.087	0.149	51.9	119.3	67.5	171.2	
10	3MK7	0.28331494	0.403	-0.231	115.3	349.4	234.2	104.7	
11	M8	0.32204562	1.059	0.121	119.8	355.1	235.3	114.9	

ANALYSIS RESULTS IN CURRENT ELLIPSE FORM
DATA IS ASSUMED TO BE UNFILTERED

STN: TRACK#11 LAT: 54 30 0.0 N
DEPTH: 0 M LONG: 132 30 0.0 W
START: 100Z 21/ 6/84 END: 1200Z 23/ 6/84

	NAME	FREQUENCY (CY/HR)	MAJOR (CM/S)	MINOR (CM/S)	INC	G	G+	G-	
1	Z0	0.00000000	17.021	0.000	158.0	360.0	202.0	158.0	
2	O1	0.03873065	6.976	-0.485	42.6	91.3	48.7	133.9	INF FR K1
3	K1	0.04178075	11.627	-0.809	42.6	99.3	56.7	141.9	
4	M2	0.08051139	29.614	-0.027	5.3	88.5	83.1	93.8	
5	S2	0.08333331	9.477	-0.009	5.3	112.5	107.1	117.8	INF FR M2
6	M3	0.12076712	2.429	-0.761	19.5	217.7	198.2	237.3	
7	M4	0.16102278	2.647	-0.624	92.2	277.2	185.1	9.4	
8	2MK5	0.20280355	1.449	-0.342	122.0	280.7	158.7	42.7	
9	M6	0.24153417	1.150	-0.743	28.5	187.5	159.0	216.0	
10	3MK7	0.28331494	1.152	-0.112	127.4	55.5	288.1	182.9	
11	M8	0.32204562	0.824	-0.110	36.2	33.8	357.5	70.0	

THIS PAGE IS BLANK

Tidal Stream Analyses, Current Meters

Appendix 3

ANALYSIS RESULTS IN CURRENT ELLIPSE FORM
DATA IS ASSUMED TO BE UNFILTERED

STN: QF1 LAT: 54 33 48.0 N
DEPTH: 57 M LONG: 132 55 0.0 W
START: 1700Z 12/ 6/84 END: 1600Z 25/ 6/84

	NAME	FREQUENCY (CY/HR)	MAJOR (CM/S)	MINOR (CM/S)	INC	G	G+	G-	
1	Z0	0.00000000	7.213	0.000	15.8	360.0	344.2	15.8	
2	O1	0.03873065	3.405	-0.288	166.1	89.5	283.5	255.6	INF FR K1
3	K1	0.04178075	5.675	-0.479	166.1	97.5	291.5	263.6	
4	M2	0.08051139	42.848	-13.956	2.8	99.5	96.8	102.3	
5	S2	0.08333331	13.711	-4.466	2.8	123.5	120.8	126.3	INF FR M2
6	M3	0.12076712	1.910	-1.624	113.4	218.1	104.7	331.5	
7	M4	0.16102278	3.536	-1.409	156.8	279.2	122.4	76.0	
8	2MK5	0.20280355	1.018	-0.305	94.1	9.7	275.6	103.8	
9	2SK5	0.20844740	0.639	-0.578	51.1	98.9	47.8	150.0	
10	M6	0.24153417	1.830	-0.793	24.4	45.7	21.4	70.1	
11	3MK7	0.28331494	0.870	-0.526	153.0	197.2	44.1	350.2	
12	M8	0.32204562	0.435	-0.111	45.8	139.8	94.0	185.6	

DOBROCKY
SEATECH

ANALYSIS RESULTS IN CURRENT ELLIPSE FORM
DATA IS ASSUMED TO BE UNFILTERED

STN: QF2 LAT: 54 19 18.0 N
DEPTH: 70 M LONG: 133 2 12.0 W
START: 1700Z 12/ 6/84 END: 1600Z 25/ 6/84

	NAME	FREQUENCY (CY/HR)	MAJOR (CM/S)	MINOR (CM/S)	INC	G	G+	G-	
1	Z0	0.00000000	11.212	0.000	139.9	360.0	220.1	139.9	
2	O1	0.03873065	5.994	-1.504	154.6	110.3	315.7	265.0	INF FR K1
3	K1	0.04178075	9.991	-2.506	154.6	118.3	323.7	273.0	
4	M2	0.08051139	37.400	-5.712	6.6	105.4	98.7	112.0	
5	S2	0.08333331	11.968	-1.828	6.6	129.4	122.7	136.0	INF FR M2
6	M3	0.12076712	2.733	-2.346	124.0	146.5	22.5	270.4	
7	M4	0.16102278	1.788	-0.019	7.1	70.8	63.7	77.8	
8	2MK5	0.20280355	2.224	-0.832	152.5	314.6	162.1	107.1	
9	2SK5	0.20844740	1.126	-0.836	71.6	36.5	324.9	108.0	
10	M6	0.24153417	1.919	0.076	99.0	78.6	339.6	177.6	
11	3MK7	0.28331494	1.176	-0.451	97.4	284.2	186.7	21.6	
12	M8	0.32204562	1.063	0.418	39.4	56.1	16.7	95.5	

DOBROCKY
SEATECH

ANALYSIS RESULTS IN CURRENT ELLIPSE FORM
DATA IS ASSUMED TO BE UNFILTERED

STN: D01 LAT: 54 38 24.0 N
DEPTH: 18 M LONG: 132 5 42.0 W
START: 1700Z 12/ 6/84 END: 1600Z 24/ 6/84

	NAME	FREQUENCY (CY/HR)	MAJOR (CM/S)	MINOR (CM/S)	INC	G	G+	G-	
1	Z0	0.00000000	22.580	0.000	179.3	360.0	180.7	179.3	
2	O1	0.03873065	6.911	-0.179	8.5	250.2	241.7	258.7	INF FR K1
3	K1	0.04178075	11.519	-0.298	8.5	258.2	249.7	266.7	
4	M2	0.08051139	52.549	-7.671	178.9	234.0	55.1	53.0	
5	S2	0.08333331	16.816	-2.455	178.9	258.0	79.1	77.0	INF FR M2
6	M3	0.12076712	3.358	-1.236	149.5	336.8	187.3	126.4	
7	M4	0.16102278	2.809	0.616	95.5	5.9	270.4	101.4	
8	2MK5	0.20280355	1.170	-0.962	112.4	111.2	358.7	223.6	
9	2SK5	0.20844740	0.831	-0.528	173.7	318.2	144.5	132.0	
10	M6	0.24153417	2.247	0.430	45.1	249.1	204.0	294.2	
11	3MK7	0.28331494	1.731	0.221	48.0	221.7	173.8	269.7	
12	M8	0.32204562	2.136	-0.901	19.8	19.6	359.7	39.4	

DOBROCKY
SEATECH

ANALYSIS RESULTS IN CURRENT ELLIPSE FORM
DATA IS ASSUMED TO BE UNFILTERED

STN: D04 LAT: 54 26 42.0 N
DEPTH: 52 M LONG: 132 0 30.0 W
START: 1700Z 12/ 6/84 END: 1600Z 24/ 6/84

	NAME	FREQUENCY (CY/HR)	MAJOR (CM/S)	MINOR (CM/S)	INC	G	G+	G-	
1	Z0	0.00000000	5.657	0.000	177.3	360.0	182.7	177.3	
2	O1	0.03873065	3.698	0.100	1.0	269.4	268.3	270.4	INF FR K1
3	K1	0.04178075	6.163	0.167	1.0	277.4	276.3	278.4	
4	M2	0.08051139	28.981	-10.329	38.7	108.1	69.3	146.8	
5	S2	0.08333331	9.274	-3.305	38.7	132.1	93.3	170.8	INF FR M2
6	M3	0.12076712	2.446	-1.738	134.2	310.2	176.0	84.4	
7	M4	0.16102278	1.974	-0.382	145.1	141.5	356.4	286.5	
8	2MK5	0.20280355	1.685	-0.166	2.6	157.5	154.9	160.0	
9	2SK5	0.20844740	0.548	0.126	0.1	344.9	344.8	345.0	
10	M6	0.24153417	3.171	-2.521	157.4	230.2	72.8	27.7	
11	3MK7	0.28331494	1.116	-0.833	51.1	52.3	1.2	103.5	
12	M8	0.32204562	1.382	-0.639	9.9	160.2	150.2	170.1	

DOBROCKY
SEATECH

ANALYSIS RESULTS IN CURRENT ELLIPSE FORM
DATA IS ASSUMED TO BE UNFILTERED

STN: D05 LAT: 54 16 18.0 N
DEPTH: 50 M LONG: 131 55 0.0 W
START: 1700Z 12/ 6/84 END: 1600Z 24/ 6/84

	NAME	FREQUENCY (CY/HR)	MAJOR (CM/S)	MINOR (CM/S)	INC	G	G+	G-	
1	Z0	0.00000000	2.791	0.000	166.2	180.0	13.8	346.2	
2	O1	0.03873065	1.772	-0.201	18.5	284.1	265.6	302.7	INF FR K1
3	K1	0.04178075	2.953	-0.335	18.5	292.1	273.6	310.7	
4	M2	0.08051139	25.994	-5.142	47.3	109.3	62.0	156.6	
5	S2	0.08333331	8.318	-1.645	47.3	133.3	86.0	180.6	INF FR M2
6	M3	0.12076712	0.938	-0.112	63.6	259.5	195.8	323.1	
7	M4	0.16102278	1.876	-0.759	49.5	233.1	183.5	282.6	
8	2MK5	0.20280355	0.416	-0.093	171.7	111.2	299.4	282.9	
9	2SK5	0.20844740	0.525	0.147	31.5	199.1	167.6	230.6	
10	M6	0.24153417	0.676	-0.130	72.4	327.7	255.4	40.1	
11	3MK7	0.28331494	0.645	-0.524	59.8	308.6	248.8	8.4	
12	M8	0.32204562	0.724	-0.124	56.9	130.4	73.5	187.2	

DOBROCKY SEATECH

ANALYSIS RESULTS IN CURRENT ELLIPSE FORM
DATA IS ASSUMED TO BE UNFILTERED

STN: D06 LAT: 54 12 12.0 N
DEPTH: 53 M LONG: 131 57 0.0 W
START: 1700Z 12/ 6/84 END: 1600Z 24/ 6/84

	NAME	FREQUENCY (CY/HR)	MAJOR (CM/S)	MINOR (CM/S)	INC	G	G+	G-	
1	Z0	0.00000000	6.468	0.000	15.5	360.0	344.5	15.5	
2	O1	0.03873065	1.073	-0.355	0.4	239.7	239.3	240.2	INF FR K1
3	K1	0.04178075	1.789	-0.592	0.4	247.7	247.3	248.2	
4	M2	0.08051139	17.914	3.715	31.4	96.9	65.4	128.3	
5	S2	0.08333331	5.732	1.189	31.4	120.9	89.4	152.3	INF FR M2
6	M3	0.12076712	1.421	-0.508	136.6	359.1	222.6	135.7	
7	M4	0.16102278	1.117	-0.556	23.5	132.3	108.8	155.8	
8	2MK5	0.20280355	1.314	0.036	124.3	74.3	310.0	198.6	
9	2SK5	0.20844740	0.647	-0.045	86.5	258.5	172.0	344.9	
10	M6	0.24153417	0.779	0.088	43.1	39.3	356.1	82.4	
11	3MK7	0.28331494	0.143	-0.095	49.5	91.0	41.5	140.6	
12	M8	0.32204562	0.263	-0.190	135.6	351.6	216.0	127.2	

DOBROCKY
SEATECH

ANALYSIS RESULTS IN CURRENT ELLIPSE FORM
DATA IS ASSUMED TO BE UNFILTERED

STN: D10 LAT: 54 27 0.0 N
DEPTH: 50 M LONG: 132 17 0.0 W
START: 1700Z 12/ 6/84 END: 1600Z 24/ 6/84

	NAME	FREQUENCY (CY/HR)	MAJOR (CM/S)	MINOR (CM/S)	INC	G	G+	G-	
1	Z0	0.00000000	5.106	0.000	118.4	180.0	61.6	298.4	
2	O1	0.03873065	3.507	-0.255	10.7	291.8	281.1	302.4	INF FR K1
3	K1	0.04178075	5.845	-0.425	10.7	299.8	289.1	310.4	
4	M2	0.08051139	36.487	-10.431	32.4	101.7	69.3	134.1	
5	S2	0.08333331	11.676	-3.338	32.4	125.7	93.3	158.1	INF FR M2
6	M3	0.12076712	2.498	-1.900	94.2	204.1	110.0	298.3	
7	M4	0.16102278	3.321	-3.027	99.9	272.7	172.7	12.6	
8	2MK5	0.20280355	0.863	-0.352	1.1	65.6	64.5	66.6	
9	2SK5	0.20844740	0.766	-0.338	58.8	323.1	264.3	21.9	
10	M6	0.24153417	0.944	-0.287	105.3	96.0	350.7	201.3	
11	3MK7	0.28331494	1.045	-0.159	9.2	131.9	122.7	141.0	
12	M8	0.32204562	1.572	-0.868	95.1	294.3	199.2	29.4	

ANALYSIS RESULTS IN CURRENT ELLIPSE FORM
DATA IS ASSUMED TO BE UNFILTERED

STN: D13 LAT: 54 21 54.0 N
DEPTH: 45 M LONG: 132 34 36.0 W
START: 1700Z 12/ 6/84 END: 1600Z 24/ 6/84

	NAME	FREQUENCY (CY/HR)	MAJOR (CM/S)	MINOR (CM/S)	INC	G	G+	G-	
1	Z0	0.00000000	17.712	0.000	53.0	180.0	127.0	233.0	
2	O1	0.03873065	4.157	-0.325	179.7	108.1	288.3	287.8	INF FR K1
3	K1	0.04178075	6.929	-0.542	179.7	116.1	296.3	295.8	
4	M2	0.08051139	33.981	-5.141	19.7	86.0	66.3	105.8	
5	S2	0.08333331	10.874	-1.645	19.7	110.0	90.3	129.8	INF FR M2
6	M3	0.12076712	3.843	-1.694	98.6	83.4	344.8	182.0	
7	M4	0.16102278	7.389	-4.275	89.9	125.4	35.5	215.3	
8	2MK5	0.20280355	1.058	0.426	171.6	242.9	71.2	54.5	
9	2SK5	0.20844740	0.346	0.014	161.2	219.8	58.5	21.0	
10	M6	0.24153417	1.419	-0.103	50.8	222.3	171.5	273.2	
11	3MK7	0.28931494	0.961	0.548	133.3	124.4	351.0	257.7	
12	M8	0.32204562	0.775	0.329	52.0	163.2	111.2	215.2	

DOBROCKY
SEATECH

ANALYSIS RESULTS IN CURRENT ELLIPSE FORM
DATA IS ASSUMED TO BE UNFILTERED

STN: D14 LAT: 54 13 0.0 N
DEPTH: 59 M LONG: 132 30 0.0 W
START: 1700Z 12/ 6/84 END: 1600Z 24/ 6/84

	NAME	FREQUENCY (CY/HR)	MAJOR (CM/S)	MINOR (CM/S)	INC	G	G+	G-	
1	Z0	0.00000000	9.517	0.000	38.9	180.0	141.1	218.9	
2	01	0.03873065	4.611	-0.785	133.9	55.5	281.5	189.4	INF FR K1
3	K1	0.04178075	7.685	-1.308	133.9	63.5	289.5	197.4	
4	M2	0.08051139	33.805	-4.230	170.2	254.1	83.9	64.3	
5	S2	0.08333331	10.818	-1.354	170.2	278.1	107.9	88.3	INF FR M2
6	M3	0.12076712	0.910	-0.200	71.8	10.9	299.1	82.6	
7	M4	0.16102278	3.731	-2.223	178.0	10.9	192.9	188.9	
8	2MK5	0.20280355	1.687	-1.134	87.2	269.5	182.3	356.8	
9	2SK5	0.20844740	0.885	0.120	94.6	98.6	4.0	193.2	
10	M6	0.24153417	1.429	-0.473	9.0	279.0	270.1	288.0	
11	3MK7	0.28331494	1.301	-0.462	169.1	356.4	187.3	165.5	
12	M8	0.32204562	0.648	-0.040	175.5	167.3	351.9	342.8	

DOBROCKY
SEATECH

ANALYSIS RESULTS IN CURRENT ELLIPSE FORM
DATA IS ASSUMED TO BE UNFILTERED

STN: D15T
DEPTH: 22 M
START: 1700Z 12/ 6/84

LAT: 54 33 6.0 N
LONG: 131 21 18.0 W
END: 1600Z 24/ 6/84

	NAME	FREQUENCY (CY/HR)	MAJOR (CM/S)	MINOR (CM/S)	INC	G	G+	G-	
1	Z0	0.00000000	8.494	0.000	169.7	360.0	190.3	169.7	
2	O1	0.03873065	2.813	0.239	11.1	275.2	264.1	286.3	INF FR K1
3	K1	0.04178075	4.688	0.398	11.1	283.2	272.1	294.3	
4	M2	0.08051139	29.660	-12.805	23.8	92.4	68.5	116.2	
5	S2	0.08333331	9.491	-4.098	23.8	116.4	92.5	140.2	INF FR M2
6	M3	0.12076712	2.781	-0.612	127.4	327.2	199.8	94.6	
7	M4	0.16102278	2.781	-0.462	91.5	253.3	161.7	344.8	
8	2MK5	0.20280355	1.718	-0.150	173.0	289.8	116.8	102.8	
9	2SK5	0.20844740	1.185	-0.397	42.3	42.5	0.2	84.8	
10	M6	0.24153417	0.888	0.082	53.2	212.9	159.7	266.1	
11	3MK7	0.28331494	1.149	-0.365	127.7	155.3	27.6	282.9	
12	M8	0.32204562	0.580	0.559	51.4	5.6	314.3	57.0	

DOBROCKY
SEATECH

ANALYSIS RESULTS IN CURRENT ELLIPSE FORM
DATA IS ASSUMED TO BE UNFILTERED

STN: D15B LAT: 54 33 6.0 N
DEPTH: 52 M LONG: 131 21 18.0 W
START: 1700Z 12/ 6/84 END: 1600Z 24/ 6/84

	NAME	FREQUENCY (CY/HR)	MAJOR (CM/S)	MINOR (CM/S)	INC	G	G+	G-	
1	Z0	0.00000000	3.868	0.000	24.9	180.0	155.1	204.9	
2	O1	0.03873065	2.460	-0.935	42.0	269.5	227.5	311.6	INF FR K1
3	K1	0.04178075	4.100	-1.559	42.0	277.5	235.5	319.6	
4	M2	0.08051139	25.150	-7.885	42.4	84.0	41.6	126.4	
5	S2	0.08333331	8.048	-2.523	42.4	108.0	65.6	150.4	INF FR M2
6	M3	0.12076712	2.147	-1.285	22.5	179.1	156.5	201.6	
7	M4	0.16102278	1.133	0.063	82.2	214.4	132.2	296.6	
8	2MK5	0.20280355	0.726	-0.562	7.4	293.6	286.2	301.0	
9	2SK5	0.20844740	0.368	-0.187	132.4	183.5	51.2	315.9	
10	M6	0.24153417	1.732	-0.352	98.0	18.2	280.2	116.1	
11	3MK7	0.28331494	0.363	0.157	94.6	309.5	214.9	44.1	
12	M8	0.32204562	0.797	-0.055	70.7	185.7	115.0	256.4	